University of Warsaw
Faculty of Mathematics, Informatics and Mechanics

Mikołaj Rybiński

Modelling networks of biochemical reactions

PhD dissertation

Supervisor

dr hab. Anna Gambin

Institute of Informatics
University of Warsaw

June 2012

Author's declaration:
aware of legal responsibility I hereby declare that I have written this dissertation myself and all the contents of the dissertation have been obtained by legal means.

June 14, 2012 .....

date *Mikołaj Rybiński*

Supervisor's declaration:
the dissertation is ready to be reviewed

June 14, 2012 .....

date *dr hab. Anna Gambin*

Thesis supervisor: dr hab. Anna Gambin Mikołaj Rybiński

Modelling networks of biochemical reactions

Abstract

The process in which a mathematical model of a molecular biological system is formulated and refined helps to articulate hypotheses and thereby supports the design of experiments to validate these hypotheses and the model itself. Once the model is validated it is used to speculate about mechanisms underlying a cell function of interest. In this dissertation we describe and apply methods valid in a general framework of spatially homogeneous models of biochemical reactions networks. However, our focus is set specifically on practical applications to models of intracellular signalling pathways.

We start with selecting the most plausible variant of a JAK-STAT pathway activation mechanism. Solution of this model selection task is based solely on a deterministic mathematical framework, represented by the ordinary differential equations. Moreover, here we exert a concept of robustness based on the sensitivity analysis. Next, we extend the range of mathematical models of biochemical reactions network to a spatially homogeneous stochastic variant, represented by the continuous-time Markov process. To that end, we apply the probabilistic model checking technique to a simple enzymatic reaction model, exploring an idea of a property-specific sensitivity analysis. On this occasion, we have developed a supporting open source software named Tav4SB, used for scientific cloud computing. Finally, we exploit both deterministic and stochastic methods in a case study based on the heat-shock response model. We investigate the thermotolerance phenomenon and the effect of a combined hyperthermia and a drug therapy of cancer.

In principle, our results demonstrate feasibility and practical potential of techniques such as the sensitivity analysis and probabilistic model checking, as well as potential of a standardised, easily-accessible software, in the context of analysis of kinetic models of biological systems.

Keywords: signalling pathway, model selection, sensitivity analysis, model checking, cloud computing
ACM Classification: J.3, C.2.4

Promotor rozprawy: dr hab. Anna Gambin Mikołaj Rybiński

Modelowanie układów reakcji biochemicznych

Streszczenie

Proces tworzenia i udoskonalania modelu pomaga formułować hipotezy i tym samym sugeruje projekt eksperymentu, który sprawdzi zarówno te hipotezy jak i sam model. Potwierdzony eksperymentalnie model jest wykorzystywany do wnioskowania na temat mechanizmów leżących u podstaw badanej funkcji komórki. W tej rozprawie opisujemy i stosujemy metody poprawne dla jednorodnych w przestrzeni modeli układów reakcji biochemicznych. Jednak skupimy się przede wszystkim na praktycznych zastosowaniach dla modeli wewnątrzkomórkowych szlaków sygnałowych.

Zaczynamy wybierając najbardziej wiarygodny wariant aktywacji szlaku sygnałowego JAK-STAT. Rozwiązanie tego zadania selekcji modelu jest oparte wyłącznie na deterministycznym opisie, reprezentowanym przez równania różniczkowe zwyczajne. Co więcej, wykorzystujemy tu koncepcję krzepkości opartą na analizie wrażliwości. Następnie poszerzamy zakres matematycznych modeli układów reakcji biochemicznych do jednorodnego w przestrzeni wariantu stochastycznego, reprezentowanego przez proces Markowa z czasem ciągłym. W tym celu wykorzystujemy technikę probabilistycznej weryfikacji modelowej do analizy prostego modelu reakcji enzymatycznej, obrazując ideę analizy wrażliwości specyficznej dla badanej własności. Przy tej okazji zbudowaliśmy wspierające, otwarte narzędzia programistyczne zwane Tav4SB, służące do naukowych obliczeń "w chmurze". W końcu, wykorzystujemy zarówno deterministyczne jak i stochastyczne metody w studium przypadku modelu odpowiedzi na szok termiczny. Badamy zjawisko termotolerancji i efekt łączonej terapii hipertermią oraz lekami przeciwnowotworowymi.

Nasze wyniki przedstawiają możliwości praktycznego zastosowania oraz potencjał technik takich jak analiza wrażliwości czy weryfikacja modelowa, jak również zestandaryzowanego, łatwo-dostępnego oprogramowania, w kontekście analizy kinetycznych modeli systemów biologicznych.

Słowa kluczowe: szlak sygnałowy, selekcja modelu, analiza wrażliwości, weryfikacja modelowa, chmura obliczeniowa
Klasyfikacja tematyczna ACM: J.3, C.2.4

Contents

Listing of figures

List of Tables

Dedicated to Olga and Janek.

Acknowledgements

This work would not have been done without the enormous help of many benevolent people and institutions. First of all, I would like to thank to my supervisor Anna Gambin for pushing me forward and for providing constant support throughout my whole struggle with the PhD idea.

I appreciate collaboration that helps to overcome a lot of adversities, which in computational biology can be particularly difficult because of its interdisciplinary character. Many thanks to my co-authors, especially, Anna Gambin, Sławomir Lasota, Zuzanna Szymańska and Michał Lula.

I would also like to thank to all those with whom I had many fruitful discussions and who shared their helpful comments on my research. Among these are people not directly involved in my work, such as Bogdan Lesyng, Haluk Resat, and Andrzej Mizera, as well as many of past and current members of the computational biology group at the Faculty of Mathematics, Informatics and Mechanics, University of Warsaw, in particular, Bartosz Wilczyński, Maciej Sykulski, and Bogusław Kluge.

My work would not have been possible without financial support by Polish Ministry of Science and Higher Education/National Science Center grants, the Biocentrum Ochota project, and by the scholarship within the Human Capital Operational Programme financed by European Social Fund and the state budget.

Most importantly, I wish to express gratitude to my loved ones for their presence and support, especially to my steadfast wife Olga and to our unconsciously motivating son. I would also like to thank sincerely to my parents who encouraged me throughout these many years of my scientific education. Last but not least, many thanks to my parents-in-law for their constant willingness to help, that I often benefited from.

Share your knowledge. It is a way to achieve immortality.

Dalai Lama XIV

1 Introduction

Mathematical modelling of dynamic behaviour of molecular biological systems complements experimental technologies, which are used to identify and comprehend a role of system components. The process in which a model is formulated and refined helps to articulate hypotheses and thereby supports the design of experiments to validate these hypotheses and the model itself. Once the model is validated it is used to speculate about mechanisms underlying, e.g., a cell function of interest.

The construction and analysis of mechanistic models of molecular biological systems is a part of recently established, highly interdisciplinary fields of systems and computational biology. Modelling encompasses gene regulatory networks (Alon, 2007), signal transduction and metabolic pathways (Wolkenhauer et al., 2008; Klipp et al., 2009). In this dissertation we describe and apply methods valid in a general framework of spatially homogeneous models of biochemical reactions networks. However, our fo-

cus is set specifically on practical applications to models of intracellular signalling pathways.

Our contribution regards multiple aspects of analysis of biochemical reactions networks. Summary of the relevant subjects and their relations, as presented in this work, is depicted in Figure 1.

Figure 1: Dissertation mind map presenting biological systems and methods under consideration. For a context an unexploited concept of spatial models (i.e. models accounting explicitly for a spatial heterogeneity) is also presented. Arrows represent relations between different concepts as presented in this work. Arrow labels and directions depict a character of a relation. For instance, in this work, the JAK-STAT signalling pathway has only a deterministic version of a model, or the TAV4SB project provides the multi-parameter sensitivity analysis method. All unlabelled arrows from a biological systems to numerical or analysis methods denote which of these methods are used in a case study relevant to the indicated biological system. Similarly, all unlabelled arrows from analysis methods indicate a relation of being based on, or, in case of dashed arrows, of a possibility of being based on. For example, model selection may be based on numerical optimisation. Indeed, if goodness of fit criterion is considered as a selection method then it uses numerical optimisation method, but, for instance, the Bayesian model selection method doesn't require numerical optimisation. Note that all analysis in this work is based on numerical simulations suitable to a mathematical model.

Figure on the next page.

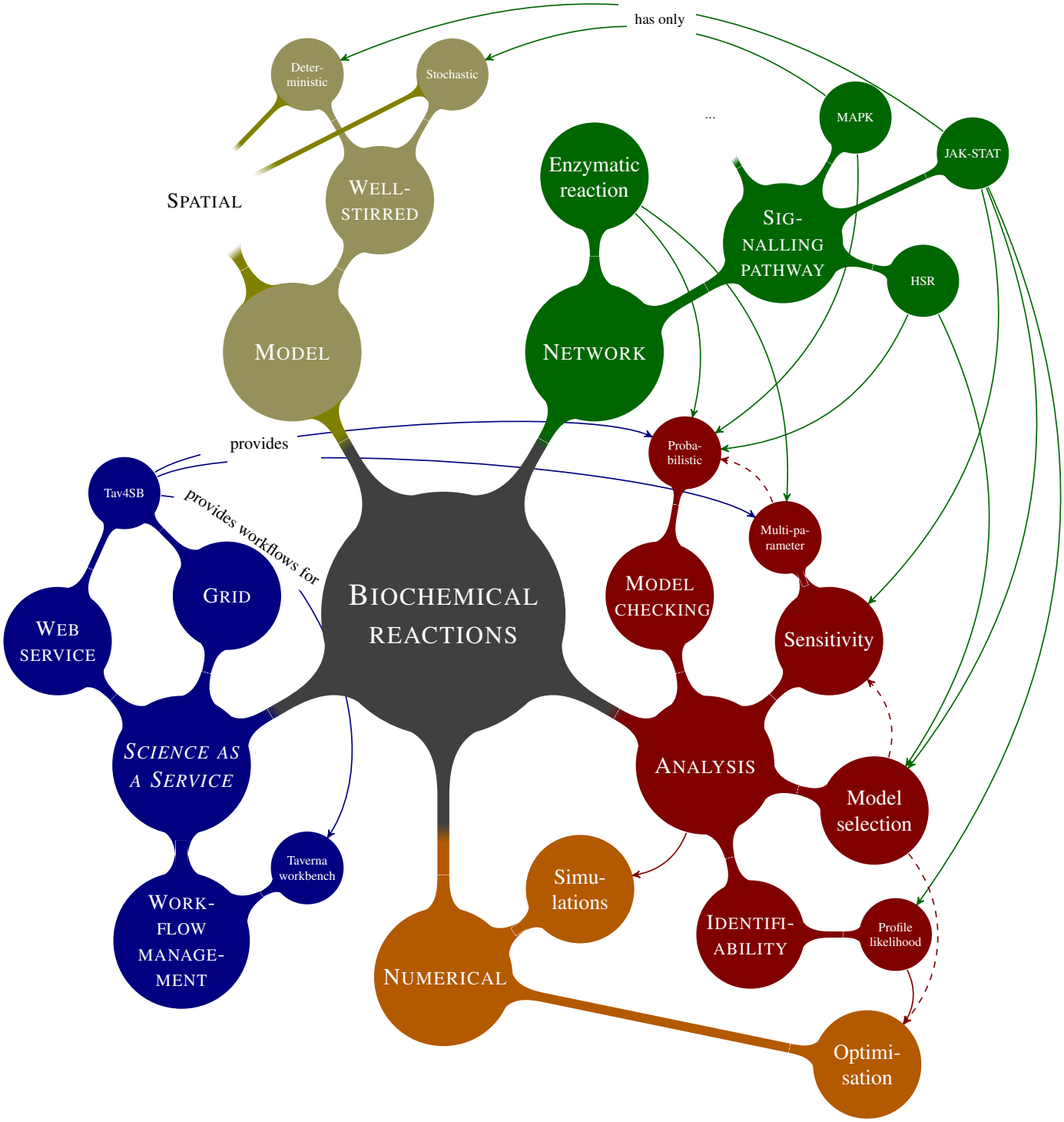
has only
Deter-
ministic
Stochastic
...
MAPK
JAK-STAT
Enzymatic
reaction
SPATIAL
WELL-
STIRRED
SIG-
NALLING
PATHWAY
HSR
MODEL
NETWORK
provides
Proba-
bilistic
Tav4SB
provides workflows for
Multi-pa-
rameter
GRID
BIOCHEMICAL
REACTIONS
MODEL
CHECKING
Sensitivity
WEB
SERVICE
SCIENCE AS
A SERVICE
ANALYSIS
Model
selection
Taverna
workbench
Simu-
lations
WORK-
FLOW
MANAGE-
MENT
IDENTIFI-
ABILITY
Profile
likelihood
NUMERICAL
Optimi-
sation

1.1 Principles of intracellular signalling

Fundamental cell processes (growth, division, motility etc.) are driven by intracellular and intercellular communication (Alberts et al., 2002). The latter is performed via direct contact between cells or soluble factors like hormones or cytokines. Environmental signals are received by on–membrane parts of receptors, which induce cascade of biochemical reactions in cell's cytoplasm and nucleus. In effect, one or more target proteins influence behaviour of the cell, usually by altering the expression level of target genes (change via gene regulatory proteins). Signal transduction can also affect cell shape or movement (change via cytoskeletal proteins) or metabolism (change via metabolic enzymes). Figure 1.1.1 depicts a simple scheme of how signal it transduced in the cell. Such signalling pathways, responsible for processing specific signals, are a part of a whole intracellular reactions network. In most cases activity of a signalling pathway is self–regulated by it's components, allowing cell to control transient response to external stimuli (e.g. internal signal is attenuated after it has been successfully processed as a change of target genes expression profile).

Most of reactions responsible for transducing a signal inside the cell are catalysed by enzymes which activate or deactivate subsequent proteins on the pathway. For instance, activation or deactivation can be executed by addition or removal of the phosphate groups, which are provided by donors such as ATP. Phosphate modification of a protein causes conformational changes in its structure and a change in it's free energy. These processes are called, respectively, *phosphorylation* and *dephosphorylation* (enzymes which catalyse these reactions are called *kinases* and *phosphatases*). In principle, enzymatic reactions are basic building blocks for complicated networks of intracellular signalling.

Activity of pathway components is a biological concept and should be identified with an efficiency of technological process that generates specific number of molecules. Therefore, it is correct to define activity in terms of an amount of a species. Nota bene, a number of one protein type molecules inside the cell usually ranges around 10^2–10^3.

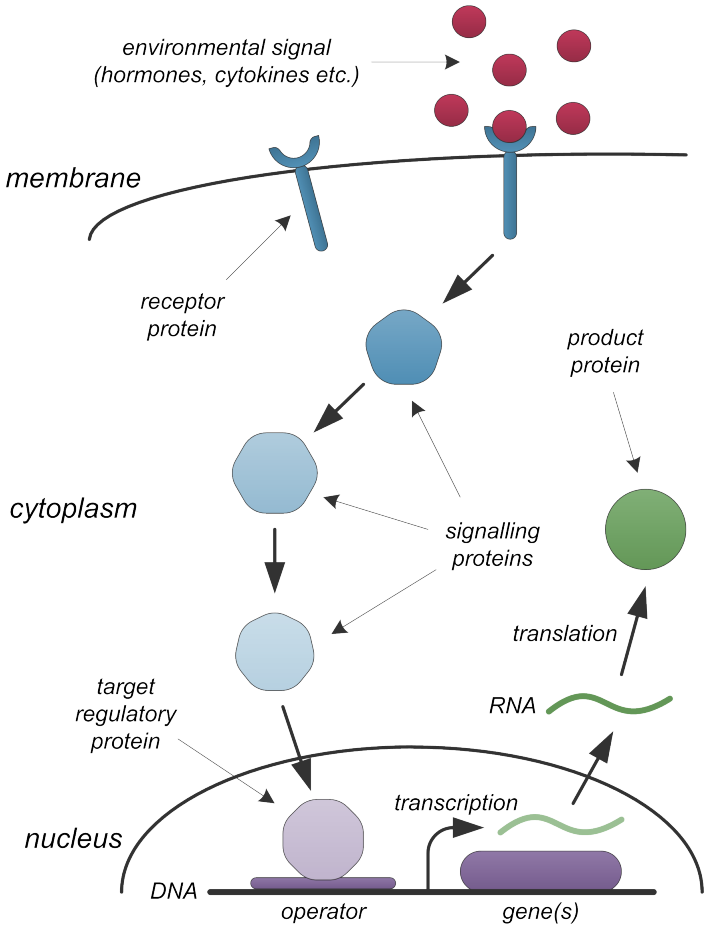

Figure 1.1.1: Generic scheme of processing of an intracellular signal. In a process of passing an extracellular signal (e.g. in form of a small environmental factors) receptors and cytoplasmic signalling proteins undergo state changes, form complexes or induce activity of subsequent proteins. Eventually, some form of the signalling proteins is imported to the nucleus where, directly or indirectly, it alters the genes expression profile. In effect, translated product proteins enter the intracellular environment to enable cell's actual response.

1.2 Modelling

Biochemical reactions take place in water, a physiological environment of the cell. For simplicity, we assume spatial homogeneity, i.e. that biomolecules are *well-stirred*, and diffusion effects are not taken into account. Moreover, we assume that a set of channels through which the reactions are occurring is fixed. This set of reaction channels together

with a set of species reacting in them is what we call a *biochemical reactions network*.

Time-dependent state of such a biochemical kinetic system can be described in terms of a state space of a number of molecules $\#\vec{S}$ of a vector of species $\vec{S}$. Unit of a quantitative description of molecules is *mole*, which approximately contains $N_{\mathrm{A}} \approx 6.022 \cdot 10^{23}$ mol^{-1} number of molecules (N_{A} is called the *Avogadro constant*). *Molar concentration* is defined as a number of moles of solute per solution V volume, i.e.

$$[S] = \frac{\#S}{N_{\mathrm{A}} \cdot |V|} \quad \mathrm{M}, \tag{1.1}$$

where $|\cdot|$ is a volume in litres and M, equal to $\mathrm{mol} \cdot \mathrm{dm}^{-3}$, denotes a molar concentration unit.

Mathematical modelling of complex biological systems can be carried out in a deterministic, a stochastic or a hybrid manner. First of which uses the classical differential equations theory and the second one is based on the stochastic processes or the theory of the stochastic differential equations. As mentioned before, both types of models are usually based on some simplifying assumptions. In particular, we assume that the diffusion process occurs immediately, which ensures an even distribution of a substance over a limited volume (well-stirred). Also, we assume that the parameters of a biochemical environment, such as the temperature, are roughly constant, which allows to consider the set of reactions and, more importantly, their kinetic parameters as fixed throughout the time evolution of the system.

Description of kinetics in most models results from the classical chemical law of mass action (see, e.g., Lund, 1965). Deterministic models describe changes in concentrations of reagents over time, and they do not include the effect of the fluctuations (which do occur in reality). It means that for given initial conditions, a deterministic model will always give the same results. This is an initial value problem for the first-order differential equations, which are a mathematical formulation of the deterministic model. Variables represent reacting species and the non-differentiable terms of the equations represent rates of reactions, usually yielding a set of highly non-linear equations. In the most common continuous-time, spatially ho-

mogeneous setting, without any delays incorporated, the deterministic biochemical model is represented by the *reaction rate equations* (RRE).

Stochastic models describe the state of the system at a given time point by a number of particles of each species. These models are most often expressed in form of the *chemical master equation* (CME), which is an alternative form of the Chapman-Kolmogorov equation. CME describes evolution of a distribution of a *continuous-time Markov process* (CTMC) over a set of all possible discrete states (Kampen, 2007).

1.3 Numerical methods

Both RRE and CME are first-order *ordinary differential equations* (ODE) and both RRE and, especially CME are analytically intractable in almost every but the simplest cases (cf. Laurenzi, 2000; Jahnke and Huisinga, 2007). It is due to a high non-linearity and a large number of variables and reactions' components or, respectively, due to a size of a state space which covers all possible arrangements of molecules in the system, reachable through a given set of reactions channels. The simplest way to address this analytic infirmity is to employ numerical methods.

Many numerical methods of both high and low precision are available for both the deterministic and the stochastic mathematical framework. The most fundamental type of methods are numerical simulations, either of the differential equations (see, e.g., Butcher, 2008) or the Markov process (the so called stochastic simulations; see, e.g., Gillespie, 2007; Pahle, 2009). These allow to simulate the evolution in time of reacting species, thus, constituting a numerical basis for further analysis of the model.

Simulated trajectories of the model, after transformation to what can be in fact observed in the data, are used to estimate parameters of the model. A common error function for the fitting to data task is the *sum of squared errors* (SSE), which yields the *non-linear least squares* optimisation problem (NLS). This well-known task can be solved by many deterministic, numerical algorithms (see, e.g., Nocedal and Wright, 1999), but their main pitfall are local minima, which in case of moderate-sized and larger models of signalling pathways are common (Moles et al., 2003;

Rodriguez-Fernandez et al., 2006). To address this issue it is recommended to use global Monte Carlo optimisation methods such as the *simulated annealing* (SA; Kirkpatrick et al., 1983; Černý, 1985). Main drawback of these type of algorithms is their running time.

1.4 Analysis

The mathematical framework determines a structure of a kinetic formulation for a given biochemical network model of a biological system. As already mentioned, the standard representations are RRE for the deterministic framework and CME or CTMC for the stochastic framework (Wolkenhauer et al., 2004; Aldridge et al., 2006; Goutsias, 2007). However, some of commonly used analysis methods are in principle model-independent. These include, for instance, some of sensitivity analysis or model selection methods.

A straightforward technique of a model comparison is a *goodness of fit* (GOF) criterion measure such as SSE, which results in the *chi-squared* test (χ^2). Arguably, GOF criterion is not good for assessing biological models due to theirs inherent uncertainty and, more importantly, due to the noisy data (Myung and Pitt, 2004). A good fit can be achieved by fitting to the noise instead of the regularity of the underlying phenomenon (the problem of overfitting). For that reason, model selection methods implement the Occam's Razor principle by including terms that penalise model complexity, thus, favouring the generalizability.

A well founded, methods implementing the generalizability principle are the *Akaike information criterion* (AIC; Akaike, 1974) and the *Bayesian information criterion* (BIC; Schwarz, 1978), as well as the state of the art *Bayesian model selection* (BMS) method and directly related *Bayes factor* (BF) — a gold standard of model comparison in Bayesian statistics (Kass and Raftery, 1995; Myung et al., 2009). The downside of BF, contrary to AIC and BIC, is the computational complexity. A more general limitation of the aforementioned measures of generalizability, is that they summarise relationship between model and data into a single number (Myung et al., 2009), which makes a nonsubstantial result of the models comparison

practically useless. We address this deficiency with an application of the sensitivity analysis in the model selection problem.

Sensitivity analysis investigates the relation between uncertain parameters of the model and a property of an observable output. Biochemical reaction networks yield models of a nonlinear nature for which *global sensitivity analysis* methods (GSA) are the most suitable (Saltelli et al., 2005). GSA examines range of input parameters values simultaneously as opposed to one-factor-at-a-time methods like derivatives of output with respect to parameters. An exemplary GSA method implementation is the *multi-parameter sensitivity analysis* (MPSA; Young et al., 1978; Hornberger and Spear, 1981). This is a Monte Carlo filtering method which maps parameters space into behavioural and non-behavioural output regions.

We use the sensitivity analysis-based concept of robustness of biological systems. Low sensitivities may indicate robustness, but also, in a too complex model, non-identifiability of parameters. To that end, we complement our analysis with the profile likelihood-based identifiability analysis (Raue et al., 2009). The *identifiability analysis* (IA) of parameters allows to account for a feasibility of experimental measurements which, in turn, may precisely identify a correct reaction network structure.

We exploit MPSA further by combining it with the *probabilistic model checking* (PMC; Rutten et al., 2004; Kwiatkowska et al., 2007). PMC is a technique of a formal verification of systems that exhibit a stochastic behaviour. For biological applications, CTMC is chosen as an underlying model (see, e.g., Heath et al., 2008; Kwiatkowska et al., 2008), and the examined properties are specified in the *continuous stochastic logic* (CSL; Aziz et al., 1996). We also employ PMC as a stand-alone method of analysis of models of biochemical reactions.

Finally, on a more technical note of analysis, we engage in the idea of "*Science as a Service*" (SaaS; Foster, 2005, 2011). It's an idea where any researcher can comfortably carry out complex analysis which may rely on large data sets or heavy computations. By comfortably we mean that the analysis can be done on a moderate personal computer, at a preferred location, without putting a significant technical effort in it. More importantly, availability of scientific services allows a much broader community

to participate in the research process, which conforms to the concept of open science. From a technical point of view SaaS fits into the concept of cloud computing.

More specific concepts behind SaaS include: workflow management systems, such as the Taverna Workbench (Hull et al., 2006), which allow for repeatable *in silico* experiments; publicly available *Web services* (WS; The World Wide Web Consortium, 2002), which provide required functionality; and computational grid environments, which enable a usage of a specialised, physically scattered hardware.

1.5 Results

We start with selecting the most plausible variant of a JAK-STAT pathway activation mechanism. Solution of this model selection task is based solely on a deterministic mathematical framework (ODE). Moreover, here we exert a concept of robustness based on sensitivity analysis. Next, we extend the range of mathematical models of biochemical reactions network to a spatially homogeneous, stochastic variant. To that end, we apply the PMC technique to a simple enzymatic reaction model, exploring an idea of a property-specific sensitivity analysis. On this occasion, we have developed a supporting state of the art software tools, under the name of the Tav4SB project. Finally, we exploit both deterministic and stochastic methods in a case study based on the heat-shock response model. In this case study we investigate the thermotolerance phenomenon and the effect of a combined hyperthermia and a drug therapy of cancer. A conceptual links between models related to and methods used within undertaken case studies is depicted in Figure 1.

In principle, our results demonstrate feasibility and practical potential of techniques such as the sensitivity analysis and probabilistic model checking, as well as of a standardised, easily-accessible software, in the context of analysis of kinetic models of molecular biological systems.

1.5.1 JAK-STAT pathway model selection

The *Janus Kinase* and *Signal Transducer and Activator of Transcription* pathway family (JAK-STAT) is a principal signalling mechanism in eukaryotic cells (Aaronson and Horvath, 2002). Evolutionary conserved roles of this mechanism include control over fundamental processes such as cell growth or apoptosis. Deregulation of the JAK-STAT signalling is frequently associated with cancerogenesis. JAK-STAT pathways become hyper-activated in many human tumours (Yu and Jove, 2004). Therefore, components of these pathways are an attractive target for drugs, which design requires as adequate models as possible. Although, in principle, JAK-STAT signalling is relatively simple, the ambiguities in a receptor activation prevent a clear explanation of the underlying molecular mechanism.

We compare four variants of a computational model of the JAK1/2-STAT1 signalling pathway. These variants capture known, basic discrepancies in the mechanism of activation of a cytokine receptor, in the context of all key components of the pathway. We carry out a comparative analysis using mass action kinetics. The investigated differences are so marginal that all models satisfy a GOF criterion to the extent that the state of the art BMS method also fails to significantly promote one model. Therefore, we comparatively investigate changes in a robustness of the JAK1/2-STAT1 pathway variants using GSA, complemented with IA. Both BMS and GSA are used to analyse the models for the varying parameter values. We found out that, both BMS and GSA, narrowed down to the receptor activation component, slightly promote the least complex model. Further, insightful, comprehensive GSA, motivated by the concept of robustness, allowed us to show that the precise order of reactions of a ligand binding and a receptor dimerization is not as important as the on-membrane pre-assembly of the dimers in absence of ligand.

Main results of the JAK-STAT pathway case study are:

- proposing rigorous models for different variants of activation mechanism of the JAK1/2-STAT1 pathway,

- evaluating model selection methods in a case study of *de novo* analysis of a large-scale pathway model,
- identifying the most robust design of the JAK1/2-STAT1 pathway receptor activation mechanism.

1.5.2 Property-specific sensitivity analysis

Consider the simple, enzymatic reaction model of three reactions:

$$\begin{aligned} R_1: &\quad E + S \xrightarrow{k_1} ES, \\ R_2: &\quad ES \xrightarrow{k_2} E + S, \\ R_3: &\quad ES \xrightarrow{k_3} P + E, \end{aligned}$$

where species names S, E, ES and P stand for substrate, enzyme, enzyme-substrate complex and product, respectively. The task is to asses which of the two forward reactions: the complex formation reaction R_1 or the substrate conversion reaction R_3, is more influential in terms of the system's behaviour? We want to show that the answer to this question, in some extent, depends on the property which describes the system's behaviour.

MPSA has been applied to deterministic models of signalling pathways with an error function based on the RRE variables trajectories. In our task, a straightforward approach is to asses importance of parameters of the above-mentioned reactions using SSE of the RRE trajectory of the product P, for currently examined parameters values, with respect to the reference values. In such MPSA setting, the k_3 parameter significantly dominates the k_1 parameter. It is an expected outcome.

Now, consider the following question: how many times, on average, the enzyme-substrate complex association reaction R_1 has to occur before the amount of product P reaches 50% of its limit? This can be expressed as a reward-based CSL formula:

$$\mathrm{R}_{\{\#R_1=?\}}\left(\Diamond\left(P > 0.5 \cdot \lim_{t\to\infty} P(t)\right)\right).$$

With system's behaviour defined by such property of interest, focused on

efficiency of enzymes, we use the PMC for the MPSA error calculation with respect to the stochastic variant of the reference model. In this setting, one observes that k_1 parameter is more influential than the k_3 parameter, although, the domination is not as definite as in the previous setting.

1.5.3 Efficacy of hyperthermia treatment

Multimodal oncological strategies which combine chemotherapy or radiotherapy with hyperthermia (i.e. raising the temperature of a region of the body affected by cancer) have a potential of improving the efficacy of the non-surgical methods of cancer treatment (Hildebrandt et al., 2002; Neznanov et al., 2011; Wust et al., 2002). Hyperthermia engages the *heat-shock response* mechanism (HSR), which main component (the *heat-shock proteins*; HSP) is known to directly prevent the intended apoptosis of cancer cells. Moreover, cancer cells can have an already partially activated HSR, thereby hyperthermia may be more toxic to them relative to normal cells (Neznanov et al., 2011). However, HSR triggers thermotolerance, i.e. the hyperthermia treated cells show an impairment in their susceptibility to a subsequent heat-induced stress (Wust et al., 2002). For that reason, the application of the combined hyperthermia therapy should be carefully examined.

We adapt the Szymańska and Żylicz (2009) model and propose its stochastic extension, which we then analyse using the *approximate probabilistic model checking* techniques (APMC; Nimal, 2010). We estimate a global function of a level of protein denaturation and derive a correct protein denaturation rate. Next, we formalise the notion of the thermotolerance and compute the size and the duration of the HSR-induced thermotolerance. Finally, we quantify the effect of a combined therapy of hyperthermia and a cytotoxic inhibition of denatured proteins refolding. By mechanistic modelling of HSR we are able to support the common belief that the combination of different non-surgical cancer treatment strategies increases therapy efficacy.

1.5.4 Tav4SB project

Progress in the modelling of biological systems strongly relies on the availability of specialised computer-aided tools. To that end, the Taverna Workbench eases integration of software tools for life science research and provides a common workflow-based framework for computational experiments in Biology.

The open source *Taverna services for Systems Biology* (Tav4SB) project provides a set of new Web service operations, which extend the functionality of the Taverna Workbench in a domain of systems biology. Tav4SB operations allow you to perform numerical simulations or model checking of, respectively, deterministic or stochastic semantics of biological models. On top of this functionality, Tav4SB enables the construction of high-level experiments. As an illustration of possibilities offered by our project we apply MPSA. To visualise the results of model analysis a flexible plotting operation is provided as well.

Tav4SB operations are executed in a simple grid environment, integrating heterogeneous software such as Mathematica (Wolfram Research, Inc., 2008), PRISM (Hinton et al., 2006) and SBML ODE Solver (Machné et al., 2006). The source code, user guide, contact information, full documentation of available Web service operations, workflows and other additional resources can be found at the Tav4SB project's Web page: `http://bioputer.mimuw.edu.pl/tav4sb/`.

1.6 Organisation of dissertation

This dissertation is organised into four chapters, first of which is currently ready introduction, and last of which are overall and case study-specific conclusions.

In between, in Chapter 2 we review both state of the art and our original methods that we have applied in our research (cf. Figure 1). Namely, we introduce deterministic and stochastic mathematical models of biochemical reactions network and briefly review basic, appropriate methods

of numerical simulation and optimisation. Afterwards, we describe methods of analysis suited to our research problems. These include overview of model selection and sensitivity analysis methods, with an emphasis on global methods in the latter case. We also give a brief overview of profile likelihood-based identifiability analysis and probabilistic model checking techniques. Finally, we describe context, features and technical aspects of the Tav4SB original project.

Chapter 3 contains three sections with description and results of analysis of three biochemical reactions networks: JAK-STAT pathway (Section 3.1), enzymatic reaction (Section 3.2) and heat-shock response pathway (Section 3.3). Each section contains a statement of the investigated problem, a model description, presentation of results and a discussion, followed by a brief summary of applied software tools and setting for methods. In the case studies containing models of signalling pathways, we also provide biological background and related modelling research overview.

1.7 Articles and co-authors

Most of the results presented in this dissertation comes from peer reviewed articles. Descriptions of mathematical modelling frameworks and sensitivity analysis can be found in Charzyńska et al. (2012, cf. Sections 2.1 and 2.3.2). The JAK-STAT pathway case study (Section 3.1) is extensively described in Rybiński and Gambin (2012) article, where from majority of the text on that subject is taken (see also Rybiński and Gambin, 2007, 2009). Description of the Tav4SB project (Section 2.4.2) was first published by Rybiński et al. (2011). An extended version, with the property specific sensitivity analysis case study (Section 3.2), was published in Rybiński et al. (2012) article, co-written with Sławomir Lasota and Anna Gambin. Software was a joint work of Mikołaj Rybiński, Paweł Banasik (Banasik, 2008) and Michał Lula (Lula, 2009). The unpublished results are based on the drafts of two publications, co-created by Mikołaj Rybiński, Zuzanna Szymańska, Sławomir Lasota and Anna Gambin. These results regard the heat shock response mechanism and its connotations with hyperthermia and thermotolerance (Section 3.3).

I have come to believe that one's knowledge of any dynamical system is deficient unless one knows a valid way to numerically simulate that system on a computer.

Daniel T. Gillespie

2 Methods

Here we review methods that we have applied in our research. First, we introduce deterministic and stochastic mathematical models of biochemical reactions network and briefly review basic, appropriate methods of numerical simulation and optimisation. Next, we describe methods of analysis suited to our research problems. These include overview of model selection and sensitivity analysis methods, with an emphasis on global methods in the latter case. Both of these methods are extensively used in the JAK-STAT model selection case study (Section 3.1). Also both of these methods are selectively used in, respectively, efficacy of the hyperthermia treatment (Section 3.3) and property-specific sensitivity analysis (Section 3.2) case studies.

We also give a brief overview of profile likelihood-based identifiability analysis, used for the analysis of the JAK-STAT pathway model, and probabilistic model checking techniques, used in property-specific sensitivity analysis and in investigation of the hyperthermia treatment efficacy.

Finally, we describe context, features and technical aspects of the original TAV4SB project, which constitutes a software base for our property-specific sensitivity analysis.

2.1 MATHEMATICAL MODELS

The biochemical reactions network consists of M reaction channels $\{R_1 \ldots R_M\}$ occurring between N species $\{S_1 \ldots S_N\}$. Each *reaction channel* (in short, reaction) is usually, uniquely presented as:

$$R_m\colon \quad \underline{\nu}_{1m}S_1 + \cdots + \underline{\nu}_{Nm}S_N \quad \to \quad \overline{\nu}_{1m}S_1 + \cdots + \overline{\nu}_{Nm}S_N$$

where $\underline{\nu}_{nm}$ and $\overline{\nu}_{nm}$ denote amounts of molecules of n-th substance that are, respectively, consumed and produced in m-th reaction. We assume that all reaction channels are non-degenerate, i.e. that for each R_m there exists n such that $\underline{\nu}_{nm} \neq \overline{\nu}_{nm}$. We say that S_n is reaction R_m: *substrate* iff $\underline{\nu}_{nm} > 0$; *product* iff $\overline{\nu}_{nm} > 0$; *reactant* iff S_n is either substrate or product of reaction R_m; *catalyst* iff S_n is a reactant of reaction R_m and $\underline{\nu}_{nm} = \overline{\nu}_{nm}$. The total net effect of production of a species S_n in reaction R_m, i.e. $\nu_{nm} := \overline{\nu}_{nm} - \underline{\nu}_{nm}$, is called a *stoichiometric coefficient*. The matrix of stoichiometric coefficients

$$\mathrm{C} := (\nu_{nm})_{\substack{n=1,\ldots,N \\ m=1,\ldots,M}}$$

is called a *stoichiometric matrix*.

Equivalently, biochemical reactions network can be graphically represented by a directed bipartite graph known as the Petri net (w/o imposed semantics; see, e.g., Petri and Reisig, 2008); places correspond to species and transitions correspond to reaction channels.

The *rank of reaction* R_m is a sum of consumed species molecules, i.e.:

$$\mathrm{rank}\,(R_m) := \sum_{n=1}^{N} \underline{\nu}_{nm}.$$

We say that R_m is: *elementary* iff $\mathrm{rank}\,(R_m) \leq 2$; *monomolecular* iff

$\mathrm{rank}\,(R_m) = 1$; *bimolecular* iff $\mathrm{rank}\,(R_m) = 2$. Moreover, if R_m is bimolecular then we say it is: a *symmetric collision* if for some m we have $\underline{\nu}_{nm} = 2$; an *asymmetric collision* otherwise. The zero-ranked reactions represent creation of new molecules from components which are not explicit present in the model. Because it is very unlikely for three or more biomolecules to collide at the same time with appropriate energy and orientation for reaction to occur, it is a common belief that all biochemical reactions networks essentially consist of only elementary reactions, i.e. reactions of rank 3 or higher are hypothetically composed of some set of elementary reactions.

In the following Sections we will briefly present underlying mathematical models for so called well-stirred models, both deterministic and stochastic. Both types of these models, essentially as a biochemical reactions network, can be represented in the *Systems Biology Markup Language* (SBML; Hucka et al., 2003) — a data format, based on the *Extensible Markup Language* (XML; The World Wide Web Consortium, 2008).

2.1.1 Deterministic, well-stirred

In a context of the well-stirred deterministic modelling framework, the state of biochemical reactions network is represented by the time-dependent, non-negative, real-valued state vector of concentrations of reacting species $[\vec{S}]\,(t) \in \mathbb{R}^N_{\geq 0}$. The dynamics of the system is governed by the *reaction rate equations* (RRE) —a set of first-order ODE:

$$\frac{\mathrm{d}\,[\vec{S}]\,(t)}{\mathrm{d}\,t} = \vec{f}([\vec{S}]\,(t)) = \mathrm{C} \cdot \vec{v}([\vec{S}]\,(t)), \tag{2.1}$$

where $\vec{v}([\vec{S}]\,(t)) \in \mathbb{R}^M_{\geq 0}$ is a vector of *reaction rates* at a time point t. ODE, together with the initial state $[\vec{S}]\,(0)$, are known as the *initial value problem*.

The most basic form of reaction rates comes from the law of *mass action* (see, e.g., Lund, 1965):

$$v_m\left(\vec{s}\right) = \mathrm{k}_m \prod_{n=1}^{N} \left(s_n\right)^{\nu_{nm}}, \tag{2.2}$$

where $\vec{s} = \left[\vec{S}\right](t)$ and k_m denotes the m-th *reaction rate constant*.

2.1.2 Stochastic, well-stirred

In the well-stirred stochastic framework the state of biochemical reactions network is represented by the time-dependent probabilistic distribution over a non-negative, discrete state space of molecules of all reacting species $\#\vec{S}(t) \in \mathbb{N}^N$. One way to describe the time evolution of such distribution is to provide a set of linear, autonomous ODE, one for each possible state of the system. Such set of equations is called the *chemical master equation* (CME). The solution of the k-th equation at a time point t corresponds to the probability of the system being in that particular state at that time.

Occurrence of reaction R_m at a time t changes the molecule numbers $\#\vec{S}(t) = \vec{s}$ by $\vec{\nu}_m$, i.e. $\vec{s} \mapsto \vec{s} + \vec{\nu}_m$, where $\vec{\nu}_m$ is the m-th column of the stoichiometric matrix C. For each reaction R_m there exists a propensity function $a_m\left(\vec{s}\right)$ of a single occurrence of R_m in a time period Δt small enough that the probability of multiple occurrences of R_m is of the order $\mathrm{o}\left(\Delta t\right)$ (Gillespie, 1977). In other words, a probability of occurrence of at most one R_m in the infinitesimally small time interval $[t, t + \Delta t)$ is accurately approximated by $a_m\left(\vec{s}\right) \cdot \Delta t + \mathrm{o}\left(\Delta t\right)$.

The CME describing the time-dependent distribution over states $\vec{s}$, given an initial distribution $\vec{s}_0$,

$$\mathbb{P}\left(t; \vec{s}, \vec{s}_0\right) = \mathbb{P}\left(\#\vec{S}(t) = \vec{s} \;\middle|\; \#\vec{S}(0) = \vec{s}_0\right) \tag{2.3}$$

is then given by a set of first-order ODE:

$$\frac{\mathrm{d}\,\mathbb{P}\left(t;\vec{s},\vec{s}_0\right)}{\mathrm{d}\,t} = \sum_{m=1}^{M}\Big(a_m\left(\vec{s}-\vec{\nu}_m\right)\mathbb{P}\left(t;\vec{s}-\vec{\nu}_m,\vec{s}_0\right) - a_m\left(\vec{s}\right)\mathbb{P}\left(t;\vec{s},\vec{s}_0\right)\Big), \tag{2.4}$$

one for each reachable state $\vec{s}$. Because the propensity functions a_m are time-independent, the CME represents a *continuous-time Markov process* (CTMC). More precisely, a CME solution gives the transient probabilities for all states of CTMC.

Analogously to the mass action kinetics, propensity a_m is practically always expressed as a combinatorial number of possible *collisions* of molecules, according to R_m consumption stoichiometry (Gillespie, 1977), i.e., assuming that $\binom{n}{k} = 0$ for $n < k$,

$$a_m\left(\vec{s}\right) = \kappa_m \prod_{n=1}^{N}\binom{s_n}{\nu_{nm}}, \tag{2.5}$$

where, κ_m denotes the m-th *reaction propensity constant*.

2.1.3 Link between well-stirred models

Conceptually, deterministic concentrations represent the mean number of molecules of the stochastic process (cf. Eq. (1.1)), i.e.

$$\left[S_n\right](t) = \frac{\mathbb{E}\left(\#S_n\left(t\right)\right)}{N_\mathrm{A}\cdot|V|} \quad \mathrm{M} \tag{2.6}$$

where M denotes a molar concentration unit.

Moreover, under a simplifying assumptions of no observable fluctuations of numbers of molecules of species and of no correlations between them, there is a direct correspondence between reaction rate and propensity constants of the mass action kinetics (Eq. (2.2)) and the collision kinetics (Eq. (2.5)), respectively. Namely, we can transform Eq. (2.4) by multiplication and sum over all possible states $\vec{s}$ and compare it to

Eq. (2.1) to obtain the following equality

$$\frac{\mathrm{k}_m}{(N_\mathrm{A}\cdot|V|)^{\mathrm{rank}(R_m)-1}}\prod_{n=1}^{N}\left([S_n](t)\right)^{\underline{\nu}_{nm}}=\kappa_m\,\mathbb{E}\left(\prod_{n=1}^{N}\binom{\#S_n(t)}{\underline{\nu}_{nm}}\right)$$

For a sake of simplicity, from now on we consider biochemical reactions network of only elementary reactions. Assuming that at any time point variances and covariances of number of molecules of all species are equal to zero, i.e.

$$\mathbb{E}\left((\#S_n(t))^2\right)=\left(\mathbb{E}\left(\#S_n(t)\right)\right)^2 \text{ and}$$
$$\mathbb{E}\left(\#S_m(t)\cdot\#S_n(t)\right)=\mathbb{E}\left(\#S_m(t)\right)\cdot\mathbb{E}\left(\#S_n(t)\right),$$

and approximating $\binom{n}{k}\approx n^k/k!$, which is valid for $n\gg 0$, we get:

$$\kappa_m\approx\frac{\mathrm{k}_m}{(N_\mathrm{A}\cdot|V|)^{\mathrm{rank}(R_m)-1}}\prod_{n=1}^{N}\underline{\nu}_{nm}! \tag{2.7}$$

For details of the thermodynamical limit and its assumptions, which underlie the link between CME and RRE see works of Gillespie (1977, 2009).

2.2 Numerical methods

In principle, one's knowledge of a dynamical system becomes more complete with a possibility of being able to represent it and simulate on a computer. To that end, because both RRE and, especially CME are analytically intractable in almost every but the simplest cases (cf. Laurenzi, 2000; Jahnke and Huisinga, 2007), it is a necessity to employ numerical methods.

2.2.1 Simulations

Many numerical simulation methods of both high and low precision are available for both the deterministic and the stochastic mathematical

framework for biochemical reactions networks. These methods allow to obtain sample trajectories of reacting species, thus, constituting a numerical basis for further analysis of a model.

Numerical integration of differential equations

As a basis for analysis of biochemical reactions networks expressed in the form of ODE we use numerical integration. Among many well-established methods for this task, the most popular are families of the predictor-corrector methods (e.g. Runge-Kutta) or the linear multistep methods (e.g. Adams-Moulton for non-stiff or backward differentiation formula for stiff systems; Butcher, 2008).

Stochastic simulations

Because of the analytical intractability of the CME, analysis of the underlying CTMC is usually based on randomly generated trajectories. The most basic method is an direct stochastic simulation algorithm (SSA; Gillespie, 1977), which generates each step of CTMC. More precisely, if $\#\vec{S}(t) = \vec{s}$, then next step is randomly generated based on a M-point distribution of choice of the next step, with $\mathbb{P}(R_k \text{ will occur next}) = a_k(\vec{s}) \Big/ \sum_{m=1}^{M} a_m(\vec{s})$, and an exponential distribution of a time of a single step $\text{Exp}\left(\sum_{m=1}^{M} a_m(\vec{s})\right)$. The most noticeable improvements of SSA are: the exact, faster, heap-based next reaction algorithm (Gibson and Bruck, 2000) and the recently developed partial-propensity direct methods (Ramaswamy et al., 2009; Ramaswamy and Sbalzarini, 2010), as well as the approximate τ-leaping methods (Gillespie, 2001), based on an assumption that all $a_m(\vec{s}) \cdot \tau$ are approximately constant for some τ;

For a record, a different approach, based on a stronger version of the τ-leaping method assumption, is an approximation of CME, known as the chemical Langevin equations (Gillespie, 2000). These equations, in principle, is RRE with addition of an temporally uncorrelated Gaussian white noise process (Brownian motion increments; for methods of numerical solutions of stochastic differential equations see, e.g., Kloeden and Platen,

1992). Finally, the Langevin equation can be transformed to a single partial differential equation (for which a separate, rapidly developing branch of numerical analysis applies), known as the Fokker-Planck equation (cf. Sjöberg et al., 2009). It describes the temporal evolution of the probability distribution $\mathbb{P}(\vec{s}, t)$ (cf. Eq. (2.3)). For a review of stochastic simulation methods for biochemical reactions networks see, e.g., Gillespie (2007) and Pahle (2009).

2.2.2 Optimisation

Optimisation methods in mathematical modelling of biological systems is used to find values of model parameters so that the modelled observable variables Y_i fit to data $\mathcal{D}$. Values of observable variables are usually obtained by numerical simulations of the model $\mathcal{M}$, for a given parameters vector $\vec{p} = (p_1 \ldots p_I)$. We will denote observable variables by $Y_i^{\mathcal{M}}(\vec{p})$ and corresponding data samples by $Y_i^{\mathcal{D}}$, where $i = 1, \ldots, N$ represents different observable combinations of species amounts as well as different time points at which these amounts are observed. The most popular error function F for this task is the *sum of squared errors* (SSE):

$$F(\vec{p}) := \sum_{i=1}^{N} \left(f_i(\vec{p})\right)^2, \tag{2.8}$$

where the *residue* is:

$$f_i(\vec{p}) := \frac{Y_i^{\mathcal{M}}(\vec{p}) - Y_i^{\mathcal{D}}}{\sigma_i}. \tag{2.9}$$

The optimisation (minimisation) task boils down to finding a set of parameters $\vec{p}_*$, such that

$$\vec{p}_* = \operatorname{argmin}_{\vec{p} \in \mathcal{P}} \{F(\vec{p})\}.$$

In case of SSE fit error function (Equation (2.8)) minimisation task is known as the *non-linear least squares* problem (NLS). There are many deterministic, numerical algorithms to solve this problem at the basis of

which are the gradient descent and the Newton's methods. The most common algorithm are the Levenberg-Marquardt algorithm, combining both earlier-mentioned methods, and, for an even more improved rate of convergence, the family of trust region algorithms. For a comprehensive description of these methods see, e.g., Nocedal and Wright (1999).

Main pitfall of the deterministic methods of solving NLS is finding a local minima of error function. In case of moderate-sized and larger models of signalling pathways the error surface has usually a very complicated structure with multiple minima (Moles et al., 2003; Rodriguez-Fernandez et al., 2006). To address the issue of local minima it is recommended to use Monte Carlo global optimisation methods such as the *simulated annealing* (SA; Kirkpatrick et al., 1983; Černý, 1985). SA is a *Markov chain Monte Carlo* (MCMC) optimisation method, based on the Metropolis et al. (1953) algorithm which samples from the Boltzmann/Gibbs distribution with a density function:

$$g\left(\vec{p}\right) = \frac{\mathrm{e}^{-\beta F(\vec{p})}}{Z_\beta},$$

where $\beta > 0$ is a temperature inverse parameter, Z_β is a normalising constant, i.e.:

$$Z_\beta = \int_{\mathbb{R}^I} \mathrm{e}^{-\beta F(\vec{p})}\, \mathrm{d}\, \vec{p} < \infty,$$

and the energy function $F\left(\vec{p}\right)$ must be such that Z_β is well-defined. The SA algorithm is globally correct — it converges to the global minimum $F_{\min}$ when the temperature decreases, i.e. in the $\beta \to \infty$ limit (if minimum exists, Markov chain distribution converges to a distribution centred on the ϵ neighbourhood of that minimum). However, number of iterations required for the convergence is in practice very high meaning that, in principle, the SA is computationally expensive (the rate of convergence depends on the energy function, but also on the choice of the cooling schedule, i.e. $\beta \to \infty$ convergence).

2.3 Analysis methods

Here we overview model selection (Section 2.3.1) and sensitivity analysis (Section 2.3.2) methods, both of which are extensively used in the JAK-STAT model selection case study (Section 3.1). Also both of these methods are selectively used in, respectively, efficacy of the hyperthermia treatment (Section 3.3) and property-specific sensitivity analysis (Section 3.2) case studies. We also give a brief overview of profile likelihood-based identifiability analysis (Section 2.3.3), used for the analysis of the JAK-STAT pathway model, and probabilistic model checking techniques (Section 2.3.4), used in property-specific sensitivity analysis and in investigation of the hyperthermia treatment efficacy. Finally, we present the original Tav4SB project (Section 2.4.2), which constitutes a software base for our property-specific sensitivity analysis case study.

Model selection methods find how well a model describes the data by scanning the space of the model parameters values. For instance, in Bayesian model selection the fit is calculated on average according to given prior distributions of parameters values. Sensitivity analysis is a different approach to assessing the influence of parameters. It investigates, and assign values to the relations between uncertain parameters of a model, and a property of the observable output (Saltelli et al., 2008). In particular, this output property may simply be the fit error function. Low sensitivities of model parameters may indicate robust design, but also a non-identifiable parameters if the model is too complex. To that end, we complement our approach with identifiability analysis, specifically, with the semi-automated SSE profile likelihood-based identifiability analysis (Raue et al., 2009).

Sensitivity analysis methods such as the multi-parameter sensitivity analysis leave room for specification of the property of an observable output of the model, and are independent of assumptions about the model character (e.g. linear or deterministic). These methodological features allow to explore models by means such as temporal logics and model checking. The former allows to formally express time-based properties and the latter allows to verify such properties automatically. We are particularly

interested in PMC techniques as a rigorous means of analysis of systems that exhibit a stochastic behaviour.

2.3.1 Model selection

The common, straightforward technique of model comparison is a *goodness of fit* (GOF) criterion measure such as χ^2 — the maximum likelihood interpretation of SSE (Eq. (2.8)). Namely, if SSE residues for N data samples $Y_i^{\mathcal{D}}$ (see Eq. (2.9)) are assumed to be independent, standard normal variables, or, in other words, $Y_i^{\mathcal{M}} \sim \mathcal{N}\left(Y_i^{\mathcal{D}}, \sigma_i^2\right)$ independently to each other, then, up to a linear scaling, SSE is a maximum log-likelihood estimator of model $\mathcal{M}$ parameters $\vec{p}$, given data $\mathcal{D}$, i.e.

$$\chi^2\left(\mathcal{M}, \vec{p}\right) \propto \ln\left(\mathbb{P}\left(\mathcal{D}|\mathcal{M}, \vec{p}\right)\right). \tag{2.10}$$

Arguably, GOF criterion is not good for assessing biological models due to theirs inherent uncertainty and, more importantly, due to the noisy data (Myung and Pitt, 2004). A good fit can be achieved by fitting to the noise instead of the regularity of the underlying phenomenon (the problem of overfitting). For that reason, model selection methods implement the Occam's Razor principle by including terms that penalise model complexity, thus, favouring the generalizability.

The most common measures of generalizability of a model $\mathcal{M}$ which explicitly penalise for the number of model parameters $\vec{p} = (p_1 \ \ldots \ p_I)$ are the *Bayesian information criterion* (BIC; Schwarz, 1978):

$$\mathrm{BIC}\left(\mathcal{M}, \vec{p}\right) = -2\ln\left(\mathbb{P}\left(\mathcal{D}|\mathcal{M}, \vec{p}\right)\right) + I\ln\left(N\right), \tag{2.11}$$

where N is a number of data points, and the *Akaike information criterion* (AIC; Akaike, 1974):

$$\mathrm{AIC}\left(\mathcal{M}, \vec{p}\right) = -2\ln\left(\mathbb{P}\left(\mathcal{D}|\mathcal{M}, \vec{p}\right)\right) + 2I. \tag{2.12}$$

Note, that if data points fit errors (residues) are normally distributed then both BIC and AIC are proportional to χ^2 with additional, explicit penalty

for a number of parameters (and considered data points in case of BIC).

However, more general, state of the art method implementing the generalizability principle is the *Bayesian model selection* (BMS) method. In fact, under assumptions that for a large data sample size N a determinant of the Fisher information matrix of the parameters distribution is negligible with respect to the $I \ln(N)$ term in Eq. (2.11), BMS becomes approximation of a half of the BIC index value (cf. Kass and Raftery, 1995; Myung et al., 2009, see also the following Section 2.3.1 for formal description of BMS). Directly, BMS gives the *Bayes factor* (BF) — a general gold standard of model comparison in Bayesian statistics (Kass and Raftery, 1995; Myung et al., 2009). BMS can be used for data of all sizes and is sensitive not only to the size complexity but also to the functional complexity, i.e. it is sensitive to how complicated is the model output expression when related to model parameters (for biological case-studies see, e.g., Vyshemirsky and Girolami, 2008b; Toni and Stumpf, 2010). In contrast to the BIC and AIC indices, which are very easy to compute, BMS/BF approach is computationally expensive.

A worth noticing general limitation of the model selection measures of generalizability, is that they summarise relationship between model and data into a single number (Myung et al., 2009). This makes a nonsubstantial result of the models comparison practically useless. We face this issue in the JAK-STAT model selection case study (Section 3.1).

Bayesian model selection (BMS)

The goal in BMS is to compare the likelihood (posterior probability) $\mathbb{P}(\mathcal{M}|\mathcal{D})$ of one model $\mathcal{M}$, given data $\mathcal{D}$, to the likelihood of competing model, given the same data set. In other words, in a fully probabilistic Bayesian approach, one compares competing hypotheses $\mathcal{H}_1$ and $\mathcal{H}_2$ representing models $\mathcal{M}_1$ and $\mathcal{M}_2$ by calculating the ratio of their posterior probabilities, i.e.

$$\frac{\mathbb{P}(\mathcal{M}_1|\mathcal{D})}{\mathbb{P}(\mathcal{M}_2|\mathcal{D})} = \frac{\mathbb{P}(\mathcal{M}_1)}{\mathbb{P}(\mathcal{M}_2)} \times \mathrm{B}_{12},$$

where

$$\mathrm{B}_{12} = \frac{\mathbb{P}\left(\mathcal{D}|\mathcal{M}_1\right)}{\mathbb{P}\left(\mathcal{D}|\mathcal{M}_2\right)} \tag{2.13}$$

is called the Bayes factor for models $\mathcal{M}_1$ and $\mathcal{M}_2$. The models are assumed to be equally probable which means that the prior probabilities $\mathbb{P}\left(\mathcal{M}_i\right)$ are equal ($i = 1, 2$). Thus, to compare models we have to calculate only B_{12} ratio (Eq. (2.13)), where

$$\mathbb{P}\left(\mathcal{D}|\mathcal{M}_i\right) = \int \mathbb{P}\left(\mathcal{D}|\mathcal{M}_i, \vec{p}\right) \cdot \mathbb{P}\left(\vec{p}|\mathcal{M}_i\right) \mathrm{d}\,\vec{p}. \tag{2.14}$$

is the marginal likelihood of data $\mathcal{D}$ coming from a model $\mathcal{M}_i$, and $\mathbb{P}\left(\vec{p}|\mathcal{M}_i\right)$ is *probability density function* (PDF) of a prior distribution over the real-valued space of model parameters $\mathcal{P}$.

To evaluate $\mathbb{P}\left(\mathcal{D}|\mathcal{M}_i, \vec{p}\right)$ PDF (Eq. (2.14)), i.e. the likelihood of reproducing data given the particular parameters set, it is further assumed that data $\mathcal{D}$ consists of independent identically distributed samples of observable variables $Y_i^{\mathcal{D}}$ and that the uncertainty inherent in the observable data is normally distributed with the standard deviation σ. In such case, given the set of parameters $\vec{p}$, we have

$$\mathbb{P}\left(\mathcal{D}|\mathcal{M}, \vec{p}\right) = \prod_{i=1}^{N} \mathbb{P}_i^{\mathcal{M},\vec{p}}\left(Y_i^{\mathcal{D}}\right)$$

where $\mathbb{P}_i^{\mathcal{M},\vec{p}}$ is PDF of a normal distribution $\mathcal{N}\left(Y_i^{\mathcal{M}}\left(\vec{p}\right), {\sigma^2}_i\right)$. Please note here the Bayesian approach, in contrast to a descriptive χ^2 GOF criterion. Namely, mean of the assessed marginal distributions is a simulated value, not the data sample value. Dominating cost of BF computation is estimation of the marginal likelihood (Eq. (2.14)). There are several approaches to obtain unbiased estimates, for instance, the importance sampling estimators (Newton and Raftery, 1994).

2.3.2 Sensitivity analysis

Sensitivity analysis has been used for various parametrization tasks of models of biological systems. This includes finding essential parameters for research prioritisation (e.g., Yue et al., 2008), identifying insignificant parameters for model reduction (e.g., Shankaran et al., 2006) or parameters clustering (e.g., Mahdavi et al., 2007).

In principle, sensitivity analysis quantifies the relation between uncertain parameters $\vec{p}$ of a model, and a property of the observable outcome $\phi(\vec{p})$ (Saltelli et al., 2008), which represents some phenotypical features of the modelled system. The uncertainty in parameters values is defined by assuming their prior distribution.

Classically, sensitivity of the model is determined by the partial derivatives of the outcome with respect to its parameters. Sensitivity analysis methods based on such quantities are called local and belong to the class of *one-factor-at-a-time* (OAT) methods. However, because most of the kinetic models of biological systems are highly non-linear, the OAT methods may be misleading (Saltelli et al., 2005). One solution is to investigate the influence of simultaneous changes in parameters values by assessing higher order partial derivatives (see, e.g., Mahdavi et al., 2007), where the order depends on the nonlinearity level of the model. Nevertheless, this is still a local method, highly dependent on the nominal values of parameters. To that end, the *global sensitivity analysis* (GSA) examines a range of input parameters values, which are also varied simultaneously. Exemplary implementations of the GSA indices are the model-free, global sensitivity measures such as the variance decomposition (Saltelli et al., 2008), or the parameters space mapping method of *Monte Carlo filtering* (MCF) such as the *multi-parameter sensitivity analysis* (MPSA Hornberger and Spear, 1981). In between, there are screening techniques which approximate the GSA indices by calculating local indices for a multiple parameters values. These are global but OAT-type of methods.

For the record, there are sensitivity analysis methods tailored specifically to the stochastic models based on CME (see, e.g., Gunawan et al., 2005). These methods recognise that the response is in form of the distri-

bution rather than a single value corresponding, for instance, to the mean value. Consequently for systems where a parameter disruption does not significantly influence the mean but it significantly influences the distribution itself, the generic sensitivity analysis indices can incorrectly indicate the lack of sensitivity of the model (cf. Degasperi and Gilmore, 2008). In this work, stochastic sensitivity analysis is represented by the original approach combining MPSA with PMC (presented in Section 3.2).

Local sensitivity indices

For a parametric model such as RRE, the most straightforward, standard implementation of the sensitivity concept are *local sensitivity coefficients* S_i^ϕ (LSC), i.e. the partial derivatives of the observable output property of an model ϕ with respect to a single parameter p_i, i.e.

$$\mathsf{S}_i^\phi := \frac{\partial \phi(\vec{p})}{\partial p_i}, \tag{2.15}$$

where $p_i \in \vec{p}$. LSC can be log-normalised (nLSC), giving

$$\log \mathsf{S}_i^\phi := \frac{\partial \log(\phi(\vec{p}))}{\partial p_i} \Big/ \frac{\partial \log(p_i)}{\partial p_i} = \frac{p_i}{\phi(\vec{p})} \cdot \mathsf{S}_i^\phi. \tag{2.16}$$

Parameters sensitivities quantified with indices based on LSC are called local as the derivative is taken at a fixed $\vec{p}$ value in the whole space of model parameters values $\mathcal{P}$. Moreover, these methods belong to the class of OAT methods, because the net effect of parameter p_i on the output property ϕ is calculated for fixed values of remaining parameters.

Screening methods

Screening methods of sensitivity analysis approximate the GSA indices. Parameters values are scanned globally, but in OAT manner. The most popular methods are the *weighted average of local sensitivities* (WALS; Bentele et al., 2004) and, just to mention, the elementary effects of Morris (1991). In WALS method, the nLSC index is calculated at multiple

random points and weighted by a probabilistic distribution function to approximate the global sensitivity.

Variance-based global sensitivity analysis (GSA)

The *first order sensitivity* (FOS) index of a variance decomposition is the normalised variance of a model output ϕ that can be attributed to a parameter p_i, i.e.

$$V_i^{\phi} = \frac{\mathrm{Var}_{p_i}\left(\mathbb{E}_{\vec{p}_{-i}}\left(\phi|p_i\right)\right)}{\mathrm{Var}\left(\mathbb{E}\left(\phi\right)\right)} \tag{2.17}$$

is the variance of the conditional expected value of ϕ, for a distribution of $\vec{p}$ with a fixed values of the p_i (denoted as $\vec{p}_{-i}$). The *total effects* (TE) index of variance decomposition, is the variance of a model output ϕ that can be attributed to a parameter p_i in all combinations of relations with other parameters, i.e.

$$\mathrm{TE}_i^{\phi} := V_i^{\phi} + \sum_j V_{i,j}^{\phi} + \sum_{j,k} V_{i,j,k}^{\phi} + \ldots, \tag{2.18}$$

where higher order variance decomposition indices $V_{i,j,\ldots}^{\phi}$ are, analogously, the normalised variances of the conditional expected value of ϕ, for a distribution of values of parameters p_i, p_j, ….

The V_i^{ϕ} and TE_i^{ϕ} indices can be effectively estimated, for instance, with the Fourier amplitude sensitivity test (FAST; see, e.g., Cukier et al., 1978; Saltelli et al., 1999), or with the Sobol (1993, 2001) method, based on a Monte Carlo sampling.

The *total TE* (TTE) index is given by

$$\mathrm{TTE}^{\phi} := \sum_{i=1}^{M} \mathrm{TE}_i^{\phi} = \sum_{m=1}^{M} m \cdot \sum_{1 \le i_1 < \ldots < i_m \le M} V_{i_1,\ldots,i_m}^{\phi}, \tag{2.19}$$

where the right-hand side follows from Eq. (2.18). Moreover, for independent factors p_i, from HDMR-ANOVA decomposition (Rabitz et al., 1999):

$$\mathrm{Var}\left(\mathbb{E}\left(\phi\right)\right) = \sum_{m=1}^{M} \sum_{1 \leq i_1 < \ldots < i_m \leq M} V^{\phi}_{i_1,\ldots,i_m},$$

we have the following relations between the total indices:

$$0 \leq \mathrm{TFOS}^{\phi} \leq 1 \leq \mathrm{TTE}^{\phi},$$

where *total FOS* is simply $\mathrm{TFOS}^{\phi} = \sum_{m=1}^{M} V^{\phi}_{m}$.

Multi-parameter sensitivity analysis (MPSA)

Monte Carlo filtering is a GSA method, which by Monte Carlo sampling the space of parameters values $\vec{p} \in \mathcal{P}$ measures what fraction of the model outputs falls within established bounds or regions and maps those regions into the parameters space (Saltelli et al., 2008). Then, based on if output falls into behavioural or non-behavioural region, samples are classified as acceptable or unacceptable to approximate two marginal distributions of each parameter p_i. When the distributions are significantly different for a parameter p_i projection, then p_i is considered as an influential factor with respect to the investigated behaviour of the system. A known implementation of the Monte Carlo filtering concept is the MPSA method (also known as the regionalised sensitivity analysis; Young et al., 1978; Hornberger and Spear, 1981). MPSA outline is presented in the Algorithm 1 pseudocode listing.

Calculation of the model output is usually a step which determines the MPSA procedure running time; a costly model simulation is required for generated sample. Parameters are by default sampled from a uniform distribution over a given range, i.e. $\vec{p} \sim \mathcal{U}\left(\widetilde{\mathcal{P}}\right)$, using the Latin hypercube sampling (LHS; McKay et al., 1979). LHS, independently of the sampled space dimension, gives similar accuracy with less samples than the straightforward Monte Carlo sampling, and it generates samples with distinct values per each coordinate. An example of a generic model output function is SSE with respect to the output value for the reference set of

Algorithm 1: Multi-Parameter Sensitivity Analysis

Data: // model output function
ModelOutput : $\mathcal{P} \to E$
// range of parameters values
$\widetilde{\mathcal{P}} \subseteq \mathcal{P} \in \mathbb{R}^I$
// number of samples
n

Result: parameters sensitivities with respect to ModelOutput

begin
  $\mathcal{P}_n \leftarrow \text{GenerateSamples}\left(\widetilde{\mathcal{P}}, n\right)$
  for $\vec{p} \in \mathcal{P}_n$ **do**
    $o_{\vec{p}} \leftarrow \text{ModelOutput}\left(\vec{p}\right)$
  end
  $\{\mathcal{P}_k, \mathcal{P}_l\} \leftarrow \text{ClassifySamples}\left(\{(\vec{p}, o_{\vec{p}})\}_{\vec{p} \in \mathcal{P}_n}\right)$
  // where $k + l = n$ and $\mathcal{P}_k \cup \mathcal{P}_l = \mathcal{P}_n$
  for $i = 1, \ldots, I$ **do**
    $s_i \leftarrow \text{Compare}\left(\text{ecdf}_{\mathcal{P}_k{}^{(i)}}, \text{ecdf}_{\mathcal{P}_l{}^{(i)}}\right)$
    // where ecdf_X is an empirical cumulative distribution function
    // function of a set X
    // and, assuming distinct values per coordinate,
    // $\mathcal{P}_m{}^{(i)} = \{p_i \mid \vec{p} = (p_1, \ldots, p_i, \ldots, p_I) \in \mathcal{P}_m\}$
  end
  return $\{s_i\}$
end

parameters. Then, by splitting samples by the mean or median of model outputs we can get the acceptable and unacceptable samples sets. Finally, a default method of comparison of the resulting marginal distributions is the two-sample *Kolmogorov-Smirnov test* (K-S test); Cho et al. (2003) used the *Pearson product-moment correlation coefficient* (PMCC).

Robustness

The MCF method is suited to model robustness – a concept closely related to the sensitivity. *Robustness* is a property of a system to maintain one or more of its functions under the external and the internal perturbations (Kitano, 2007). For example, one could be interested in the robustness to the input noise, that could be a result of the intrinsic stochasticity of the intercellular signalling which is out of the scope of the model (see, e.g., Shudo et al., 2007). It is desired that in case of the low input amount of a species, the system is capable of dampening the signal, so that an unwanted response is not induced. On the other hand, investigating, for instance, RRE simulations for the set of all perturbed reaction rate constants corresponds to the robustness of the modelled biochemical network to the varying environmental conditions such as the volume of solution or its temperature. For an overview of the robustness concept in the context of modelling biological systems (and the control theory) see, e.g., a review of Stelling et al. (2004) or an editorial of Kitano (2007). MPSA itself was already used for the purpose of analysing the robustness of signalling pathways models (e.g., Cho et al., 2003; Zi et al., 2005).

2.3.3 Identifiability analysis (IA)

Conceptually, *identifiability analysis* (IA) verifies if it is possible to infer the true values a model parameters, given the data. In principle, like the notions of sensitivity analysis and robustness, IA doesn't have a unique problem statement, thus many approaches to this concept are taken. In context of biochemical reactions networks models these include analytical analysis of ODE for a specific model, or recently developed, general

methods, for instance, IA based on the Fisher information matrix for stochastic models (Komorowski et al., 2011), or many methods for deterministic models, in particular RRE (see, e.g., Srinath and Gunawan, 2010), or more general mathematical frameworks like ODE (see, e.g., Miao et al., 2011) and differential algebraic equations (see, e.g., Roper et al., 2010).

In this dissertation we only use the *profile likelihood*-based (PL) IA (Raue et al., 2009) as a complementary method in the JAK-STAT model selection case study (Section 3.1), therefore we will only give a brief overview of PL-based IA.

Profile likelihood-based IA

IA presented by Raue et al. (2009) is based on the maximum likelihood interpretation of the SSE measure of parameters $L(\vec{p})$. Recall, from Eq. (2.10), that when data fit errors are assumed to be normally distributed, then $\chi^2(\vec{p}) \propto -\log(L(\vec{p}))$.

The PL function (see, e.g., Murphy and Vaart, 2000) of a parameter p_i is then defined as

$$\chi^2_{\mathrm{PL}}(p_i) = \min_{\vec{p}_{-i}} \chi^2(\vec{p}), \tag{2.20}$$

i.e. the maximum likelihood with respect to all parameters except p_i. Hence, the PL keeps the log-likelihood as small as possible alongside values of a single parameter.

The PL-based identifiability of p_i boils down to re-optimising the χ^2 function for a set of p_i values. This is done within a given range of parameter p_i values and within its pointwise or simultaneous, *likelihood-based confidence interval*:

$$\left\{\vec{p} \mid \chi^2\left(\vec{p}\right) - \chi^2\left(\vec{p}_{\min}\right) < \Delta_\alpha\right\}, \quad \text{where } \vec{p}_{\min} = \operatorname{argmin}_{\vec{p}}\left\{\chi^2(\vec{p})\right\},$$

and the threshold Δ_α is a α quantile of a chi-squared distribution with 1 (pointwise) or number of parameters (simultaneous) degrees of freedom, giving a confidence level α.

Parameter p_i is said to be: *structural identifiable* if a unique minimum of likelihood $\chi^2(\vec{p})$ with respect to p_i exists; *practically non-identifiable*, if the likelihood-based confidence interval is infinitely extended in increasing or decreasing direction of p_i values, although the likelihood has a unique minimum (Raue et al., 2009).

2.3.4 Model checking

Model checking is a method of formal, automatic verification of a given model property. Typically, the property contains safety requirements for critical states of the finite-state transition system. In order to solve the problem automatically, system properties are expressed as formulas of some propositional logic. For the dynamic systems this is logic from a class of temporal logics, as properties of interest are usually qualified in terms of time. Among temporal logics, the most established are computation tree logic (CTL), which, intuitively, quantifies over possible system paths, and linear temporal logic (LTL), which, intuitively, quantifies over time (these are not equivalent however both are fragments of CTL* logic). Both CTL and LTL model checking has been proposed as methodologies of analysis of deterministic models of biological systems (see, e.g., respectively, Monteiro et al., 2008; Rizk et al., 2009).

In two of our case studies (Sections 3.2 and 3.3) we employ a formal model checking technique called *probabilistic model checking* (PMC), which is suitable for systems exhibiting stochastic behaviour, in particular CTMC. Recent research demonstrated a considerable success in adapting PMC to analysis of biological systems, including biochemical pathways. Among systems analysed recently with the use of the probabilistic model checker PRISM are: the MAPK cascade (Kwiatkowska et al., 2008), the RKIP inhibited ERK pathway (Calder et al., 2006), the FGF pathway (Heath et al., 2008) or the T cell signalling pathway (Owens et al., 2008); see Calder et al. (2010) article for an overview.

Probabilistic model checking (PMC)

PMC is an extension of model checking, a well-established formal method successfully applied in a range of analyses of computer systems. PMC requires two inputs: a description of the probabilistic system, usually given in some high-level modelling language; and a specification of desired properties of the system, typically in probabilistic temporal logics such as: *probabilistic computation tree logic* (PCTL Hansson and Jonsson, 1994) for probabilistic timed automata or PCTL* for discrete time Markov chain and Markov decision process, both extensions of CTL*; or *continuous stochastic logic* (CSL Aziz et al., 1996), an extension of PCTL for CTMC. Adopting a stochastic modelling paradigm allows us to take advantage of efficient probabilistic model checker PRISM, that implements all mentioned variants of PMC. The motivation for using PMC is the belief that when used in conjunction with other, well-established approaches, such as ODE simulations, may offer a greater insight into the complex interactions present in biological pathways.

Models are described using the compositional PRISM language. It is a simple, state-based language, supporting a wide range of probabilistic models and their extensions with costs and rewards. In our experiments we have used CTMC as our principal model. In short, to define CTMC one defines *modules* with state variables and *commands* as follows:

```
ctmc

module module 1
    variable 1 : [min..max] init init;
    …
    variable n : …

  [command 1] activation guard -> rate: variables updates;
    …
    [command m] …
endmodule
…
```

By default, same commands are synchronised among modules with a CTMC transition rate equal to a product of rates assigned to updates. Total rates for all commands which satisfy all activation guard conditions determine exponentially distributed CTMC transition rate and are selected randomly, proportional to the rates.

In PRISM, properties are expressed in temporal logic suitable for chosen type of the probabilistic model. PRISM incorporates extensions to these logics for quantitative specifications and rewards (see, e.g., Kwiatkowska et al., 2006). In our experiments we have used CSL for CTMC model checking, which has the following grammar:

$$\begin{aligned} \psi &::= \text{true} \mid a \mid \psi \wedge \psi \mid \neg\psi \mid \mathrm{S}_{\sim p}(\psi) \mid \mathrm{P}_{\sim p}(\phi) \\ \phi &::= \mathrm{X}\,\psi \mid \psi\,\mathrm{U}\,\psi \mid \psi\,\mathrm{U}^{I}\,\psi, \end{aligned}$$

where a is an atomic proposition, $\sim \in \{\leq, \geq\}$ and $I \subset \mathbb{R}_{\geq 0}$ is an interval. Interpretation of the non self explanatory operators is as follows: true denotes truth in all states; a is a expression on state variables, which is true in all states that satisfy this expression; $\mathrm{S}_{\sim p}(\psi)$ means that probability of satisfying formula ψ in steady state is $\sim p$; $\mathrm{P}_{\sim p}(\phi)$ means that probability of satisfying path (temporal state) formula ϕ is $\sim p$; $\mathrm{X}\,\psi$ says that formula ψ is satisfied in the next state on the path; $\psi\,\mathrm{U}\,\psi$ says that from some moment right hand side formula is satisfied and until then left hand side formula is satisfied; and $\psi\,\mathrm{U}^{I}\,\psi$ (bounded until) is analogous, with a constraint that moment at which right hand side formula becomes satisfied is in I interval. Formal semantics of CSL is defined on a probability distribution over paths of CTMC, that is obtained by a construction of the smallest σ-algebra over cylinders (sets of paths with limited times of transitions; see, e.g., Baier et al., 2000).

In fact, in PRISM you can directly ask for probability which is estimated anyway by putting $=?$ instead of $\sim p$ in S and P operators. Typical property:

$$\mathrm{P}_{=?}(\phi)\,, \tag{2.21}$$

asks about the probability that a path in the model state space satisfies ϕ.

In other words, PRISM computes the fraction of all paths over model states that satisfy ϕ.

The PRISM rewards extension for CSL introduces reward operator $\mathrm{R}_{X\sim k}(\varphi)$, where k expresses boundary value of reward X (random variable defined over model variables), and φ is a reward formula with grammar:

$$\psi \quad ::= \quad \Diamond\psi \mid \mathrm{C} \leq t \mid \mathrm{I} = t \mid \mathrm{S}\,.$$

Interpretation of these operators is: $\Diamond\psi$ (finally) is an accumulated reward until state satisfying ψ is reached or is equal to ∞ if such state is never reached; $\mathrm{C} \leq t$ (cumulatively) is an accumulated reward until time t; $\mathrm{I} = t$ (instantaneously) is a reward value at a time point t; S is a steady sate value of the reward. Analogously one can put $=?$ instead of $\sim k$ to ask for the reward value. Note that probabilistic $\Diamond$ operator can be defined as:

$$\mathrm{P}_{\sim p}(\Diamond\phi) := \mathrm{P}_{\sim p}(\mathrm{true}\,\mathrm{U}\,\phi)\,. \tag{2.22}$$

Rewards are defined in the model as:

```
rewards
    "reward 1" counting guard: reward expression;
    …
endrewards
```

counting guards are boolean expressions on a model variables which determine when the reward is counted (e.g. true if all the time) and reward expression is an actual definition of the random variable over CTMC states.

Approximate PMC (APMC)

The model analysed in our experiments is so large that standard model checking becomes unfeasible. We have thus decided to use more efficient techniques that trade accuracy for efficiency. PRISM includes a range of approximate analysis techniques, based on sampling: generating a number of random paths through the model state space (model trajectories) by stochastic simulation, and evaluating the property on each run (for an overview see Nimal, 2010). This information is used to compute an

approximate result. In our experiments we have used the simplest and the most flexible CI implementation of APMC (cf. Grosu and Smolka, 2005). CI computes a *confidence interval* for the value of a given property, such as the one in Eq. (2.21). CI method takes three parameters: interval half-width w, confidence level α and the number of sampled paths N. On the basis of evaluation of sampled paths, the method computes an approximate value y of a formula (2.21), determining the confidence interval $(y - w, y + w)$. The exact (unknown) value x of formula (2.21) falls into the confidence interval with probability $1 - \alpha$.

2.4 Science as a Service

"Science as a Service" (SaaS; Foster, 2005, 2011) is an idea where any researcher can comfortably carry out complex analysis which may rely on large data sets or heavy computations. Comfortably meaning that the analysis can be done using a moderate personal computer, at a preferred location, without putting a significant of technical effort in it.

Such problem formulation pose an requirement of a remote, public availability of data retrieval and analysis functions, for which a single standard are Web services (WS; The World Wide Web Consortium, 2002). The additional building brick imposing itself are computational grid environments, which enable a usage of a specialised, physically scattered hardware. The only non-standard requirement which is not compliant with most of currently deployed scientific grids (e.g., Kitowski and Dutka, 2010; Kitowski et al., 2011) is that they need to expose their functionality in a public domain in a standardised manner, such as WS.

Finally, there should be some standard way of putting together the analysis pipelines, such that they are interoperable across different client machines. There is no distinctive way to achieve that but an idea worth noticing, besides direct scripting in the modern WS-compliant programming languages, are the workflow management systems, such as the Taverna Workbench (Hull et al., 2006).

Of course, there is much more to SaaS concept. The least to mention the support for Semantic Web services and ontologies, which facilitate

the discovery and interoperatibility of scientific WS (Bhagat et al., 2010; Wilkinson et al., 2008; Courtot et al., 2011, see, e.g.,). These subjects however are essentially out of the scope of our work.

2.4.1 Workflows and the Taverna Workbench

The Taverna Workbench facilitates the design and execution of *in silico* experiments. The experiments, constructed as workflows, can be stored and executed when needed. The building blocks of a workflow are services, also known as processors. Technically, *workflow* is a set of processors, together with connections between their inputs and outputs. The remote processors are implemented as WS operations. Scattered physically throughout computational resources of numerous scientific facilities and combined together, the WSs operations and local, intermediate processors enable a highly complex analysis, surpassing limits of a common workstation.

Taverna services come from a diverse set of life science domains. In the field of computational biology, the Taverna Workbench provides an access to services which are mainly related to the sequence annotation and analysis. Here, we present the Tav4SB project, which contains remote processors that extend Taverna's functionality in the domain of systems biology, specifically, in the analysis of kinetic models of biological systems. Our hardware base offers computational resources sufficient for computationally demanding experiments, such as multiple invocations of the model-checking procedure. Essentially, the Taverna Workbench provides a convenient user interface for our WS operations. Without programming their own WS client, users can analyse the behaviour of cellular systems under various conditions.

2.4.2 Tav4SB project

The aim of the Tav4SB project is to support the orchestration of physically scattered tools for execution of repeatable scientific experiments. To understand a place of Tav4SB in a plethora of similar software, con-

sider the following, mundane technical problem. You have a set of scripts, command line tools or any other form of legacy code, installed on one or more computational servers, not necessarily in the same local area network. For instance, you might have a MATHEMATICA (Wolfram Research, Inc., 2008) script which can be only executed on a server which has MATHEMATICA installed on it; and simultaneously you might need to use PRISM (Kwiatkowska et al., 2011), installed on a remote server with a large amount of required memory. You want to connect these tools in an *in silico* experiment, say described by a workflow. Moreover, in case the experiment doesn't go as planned, you want to be able to easily modify and re-run your workflow.

TAV4SB project is a realisation of a minimalist approach to a platform-independent solution, based on the workflow management system and a service-oriented architecture built around the Web service standard and a straightforward queue of computational tasks.

TAV4SB project consists of two parts. The client part of the project (TAV4SB client) is a library of sample workflows and helper scripts for analysis of kinetic models of biological systems, using earlier described features. The server part of the project (TAV4SB server) is a simple grid environment which wraps aforementioned computational tools. Those tools are intended to be run in a multi-threaded manner, on one or more, possibly remote, computational servers.

As an utility for wrapping scientific software in Web services, the TAV4SB project enters premises of projects such as Soaplab2 (Senger et al., 2008) and Opal2 (Krishnan et al., 2009; Ren et al., 2010). The main difference is that the support for the physical scattering of computational tools is an integral part of the TAV4SB server. Moreover, TAV4SB server easily allows for a direct connection with legacy code. If necessary, the Java Native Interface (JNI; Oracle Corporation) can be used to connect with the platform-specific libraries written, for instance in C, C++, or Fortran. However, in the current state of the project, all that comes at a cost of moderate programming skills required from a user of the TAV4SB server, when compared to Soaplab2 and Opal2 strategy with the custom configuration file languages. Please note however that these languages need to be learned and they pose an easier approach for

the user only to a limited extend. Also note that, as a minimalist solution with the stateless Web service interface, the Tav4SB server doesn't comply with the standards of an open, stateful grid services architecture (cf. Web Services Resource Framework; OASIS WSRF Technical Committee, 2006), which the most prominent representative is Globus Toolkit (Foster, 2006, 2011), a full-fledged grid environment.

Features

Unlike the Tav4SB project, almost all of the Web-based applications reviewed by Lee et al. (2009) allow for the analysis of only deterministic representations of biological systems.

Operations provided by our Web server allow for:

1. numerical simulations for the deterministic formulation of a biochemical network model, using the *SBML ODE Solver* library (SOSLib; Machné et al., 2006),

2. probabilistic model checking of CSL formula over a CTMC, using PRISM,

3. visualisation of data series, such as RRE trajectories or values of parametric CSL properties, and probabilistic distribution sampling, using Mathematica, and

4. high-level analysis, such as MPSA of biological models, with error calculation via either numerical simulations or the probabilistic model checking technique.

SOSLib enables numerical analysis of models encoded in SBML. The library employs libSBML (Bornstein et al., 2008) to automatically derive RRE, plus their Jacobian and higher derivatives, as well as the CVODES package — the state of the art numerical integration library from SUNDIALS (Hindmarsh et al., 2005).

PRISM is one of the leading tools implementing probabilistic model checking. Some recent works, see, e.g., work of Heath et al. (2008) and

Kwiatkowska et al. (2008), demonstrate applicability of PRISM to analysis of models of biological systems. Case studies include models of cell cycle control, fibroblast growth factor signalling, and MAPK cascade (PRISM Web page). PRISM handles models defined in the PRISM input language. Currently, a prototype translator from SBML is not integrated into the application itself. Therefore, we also provided a separate operation to automatically translate from SBML to the PRISM language, using the prototype translator.

Finally, Wolfram's MATHEMATICA is a tool with one of the most advanced graphics engines among plotting software. TAV4SB provides MATHEMATICA's two- and three-dimensional list plots together with a versatile set of options for customising their display. Additionally, TAV4SB allows to sample from the extensive collection of parametric probability distributions available in MATHEMATICA.

ARCHITECTURE

We have chosen the popular SBML data format, to represent kinetic models of biological systems. Due to the wide range of dedicated software and due to the support by models repositories like BIOMODELS (Novère et al., 2006), SBML can be used without a detailed knowledge of the language specification.

Figure 2.4.1 depicts the architecture of our solution. The client side includes a workstation with the TAVERNA WORKBENCH installed. Besides remote processors, the TAVERNA WORKBENCH provides access to local processors. These might be locally-installed command-line programs, including environments for running scripts, which enable data manipulation on the client side. Moreover, scripts written in BeanShell — an interpreter for a simplified version of Java language, are natively supported by the TAVERNA WORKBENCH, constituting a highly portable workflow design. Thanks to local processors, lightweight computations can be executed on a user's machine. This makes workflows more effective by reducing network load, response time and the burden on the server side. To that end, we used a native Java SBML library (JSBML; Dräger et al., 2011).

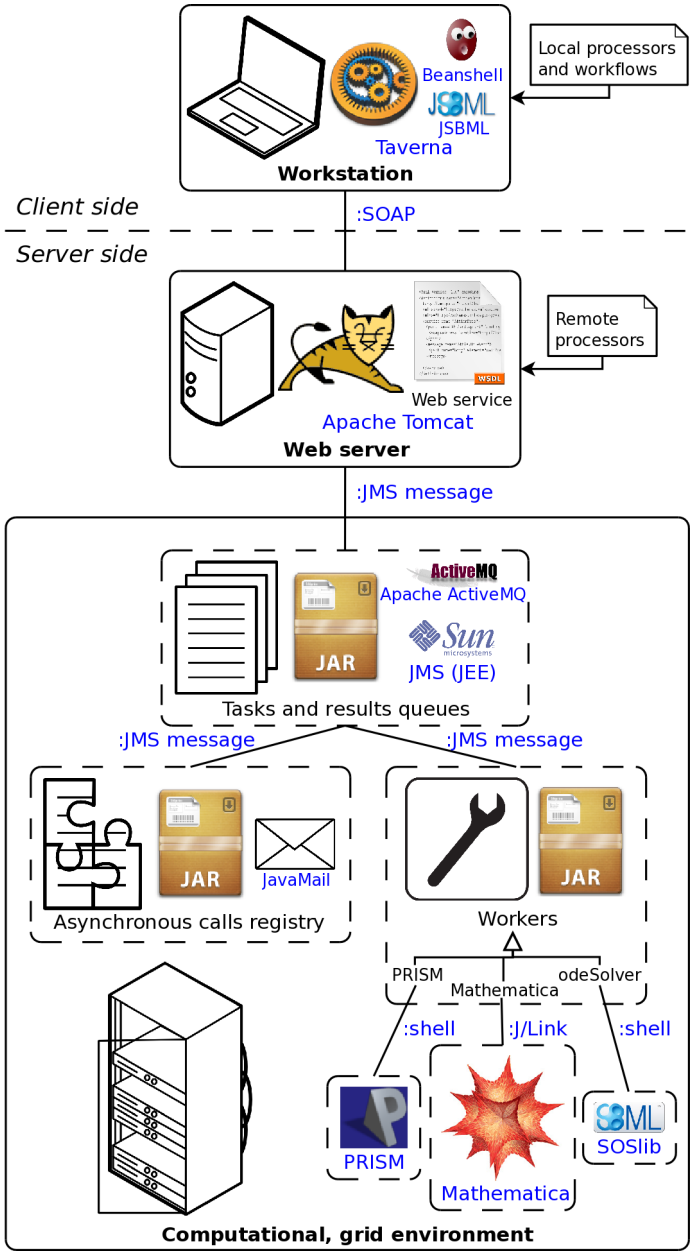

Figure 2.4.1: The implementation architecture. Names of a particular software, technology or standard are written in blue. The communication type is specified on edges which connect components of the system. See text for details.

JSBML enables client side manipulation of the SBML models, for instance to extract parameter names from a model and to set their values.

Client communicates with the server side via WS operations, using Simple Object Access Protocol (SOAP; The World Wide Web Consortium, 2007). These operations represent the workflow's remote proces-

sors. Their signatures are defined in a Web Service Definition Language (WSDL; Christensen et al., 2001) file. We employed a "WSDL first" approach: the WSDL file was manually written (in a `document/literal` style). Java Web service classes were automatically generated from the WSDL file.

The WSDL file is hosted by the Apache Tomcat servlet container. It acts as a proxy between the client and the computational part of the server. A Web service operation call is translated into a Java Message Service (JMS; Hapner et al., 2002) messages. JMS Application Programming Interface (API) allows Java applications to create, send, receive, and read messages. It is a part of the Java Platform, Enterprise Edition (JEE) standards. In our system, JMS messages represent computational tasks, and their results. One operation call can be translated into multiple tasks, enabling seamless, tool-specific parallelization of a submitted job.

Computational cluster management modules are written in Java using the Apache ActiveMQ implementation of the JMS standard. These modules are deployed as the Java Archive (JAR) files. The JMS messages are sent over TCP/IP, which basically makes modules independent of their physical location.

New tasks, created by the Web server module, are added to the tasks queue. At this point tasks are assigned to any available worker of a compatible type. Results are collected in a temporary queue, exclusive for a single WS operation call. Long-running tasks use an asynchronous call registry. In such case, direct (synchronous) response to the WS operation call is merely a message reporting the start of computations. The computed results are collected in a dedicated queue and, when completed, sent to a caller by email (using the JavaMail package).

Worker translates both a JMS task message into running computational processes and results of these processes back into a JMS result message. Each worker supports a specific type of computation and can communicate with an actual computational tool differently. Currently we implemented three types of workers: MATHEMATICA worker which communicates with MATHEMATICA via J/Link library, PRISM and ODESOLVER workers which communicate with, respectively, PRISM and SOSLIB via a command-line interpreter (shell).

Performance

To measure the network load and the overhead of the task management in Tav4SB server we ran a performance test. The test was set up with the MAPK cascade case study from the PRISM Web page (PRISM Web page) and with the asynchronous version of the PRISM WS operation. Recall, that this version of the PRISM operation sends computation time statistics, together with results (by email). Details of the test can be found in Lula (2009); Rybiński et al. (2012).

# of: machines / threads	**1**	**2**	**4**	**8**	**14**
1	271,25	137,84	71,22	38,06	23,85
2	149,09	71,12	38,00	21,51	14,55
4	124,53	54,37	26,06	13,68	9,75
8	70,44	37,53	23,78	17,39	16,44

Table 2.4.1: Results of the performance test of the Tav4SB server. Table cells contain the average longest computation time in minutes, in different configurations of a number of machines and a number of worker threads. Product of these two quantities determines the total number of worker threads. Highlighted are the best performances for each number of quad-core machines (columns) with respect to a number of worker threads.

Table 2.4.1 contains the average longest computation time with varying numbers of machines and numbers of threads for each worker on each of the quad-core machines. In short, with a separate core for each worker and with enough workers to cover 50 long running computations (4 threads on 14 machines) one can observe an effect of running a single time point simulation. Tav4SB server scales well in a local, homogeneous environment. There is only a small overhead which may be attributed to the worker initialisation, the task management and the network load. In a situation of a sufficient or almost sufficient number of workers, running more threads than the available number of cores (8 threads on 8 or 14 machines), the environment significantly slows down. It happens because on some of the machines workers compete for the processor time, causing the operating

system to frequently switch context of a current processor task. On the other hand, in a situation of high deficiency of workers (1 or 2 machines) it is better to have more threads than cores on each machine. This results mainly from an overhead of the tasks queuing, initialisation of workers the communication between grid components. To sum up, for the optimal production deployment, one must consider the amount and the time profile of tasks which are being executed with respect to the thread per core ratio which must be adjusted accordingly; basically, high ratio for many short tasks and inversely for long running tasks.

Some people see things that are and ask, Why? Some people dream of things that never were and ask, Why not? Some people have to go to work and don't have time for all that.

George Carlin

3

Case Studies

Whilst theoretical analysis is indispensable for scientific breakthroughs, many of the practical problems in computational biology are specific to the data or the model under consideration. These problems are usually complex, often NP-hard, as, for instance, in the bioinformatics methods of sequence analysis. Still, it is common for a computational biologist to tackle such hard problems. Especially in the modelling domain, not necessarily a heuristic or numerical solution itself, but the process that leads to them, may provide invaluable insight into the analysed biological phenomenon, and thus modify the problem statement, as well as give possible directions for establishing future theoretical foundations. In this fashion, we set our focus on practical applications of diverse model analysis methods to models of peculiarly interesting intracellular signalling.

3.1 JAK-STAT pathway model selection

In this Section we are selecting the most plausible variant of a JAK-STAT pathway activation mechanism; this an model selection analysis that is based solely on ODE model representation. In this case study we exert a concept of robustness based on sensitivity analysis.

3.1.1 Background

The *Janus Kinase* (JAK) and *Signal Transducer and Activator of Transcription* (STAT) pathways are a family of highly conserved intracellular signalling pathways of eukaryotic organisms (Kisseleva et al., 2002). These pathways have co-evolved with fundamental cellular signalling events, such as innate and adaptive immune responses (Aaronson and Horvath, 2002), cell growth and apoptosis processes regulation (Yu and Jove, 2004) or embryonic stem cell self-renewal control (Raz et al., 1999).

JAK-STAT pathways are relatively small. They provide a direct route from the membrane to the nucleus via STAT family members. When translocated, STAT dimers act as transcription factors. STATs themselves can be activated by JAKs — members of a family of tyrosine kinases which bind to the cytokine receptors. The latter are stimulated by numerous ligands such as various kinds of *Interferon* (IFN), *Interleukin* (IL) or *Erythropoietin* (Epo). In short, there are three main stages involved in signalling through any JAK-STAT pathway: activating the receptor, directly translocating the signal to the nucleus and expressing target genes. Each stage takes different time to execute — it ranges from seconds up to hours, depending on an organism and a tissue. The transduced signal is attenuated on all levels. The key players here are the *Protein Tyrosine Phosphatases* (PTP) which dephosphorylate receptors and activated STATs, *Protein Inhibitor of Activated STAT* (PIAS) which blocks STAT dimers in the nucleus and, expressed as a negative feedback, *Supressor of Cytokine Signalling* (SOCS) proteins, which block STAT docking sites on the receptor.

Related research

Details of a structure of a biochemical reactions network which represents a signalling pathway are investigated to understand role of its design parts. Examples include comprehension of a function of cascade layers (Huang and Ferrell, 1996) and negative feedback (Kholodenko, 2000) in the MAPK/ERK pathway or a role of negative regulators (Yamada et al., 2003), nuclear export (Swameye et al., 2003) and dimerization steps (Shudo et al., 2007) in the JAK-STAT pathway.

Our subject of interest is the model of the JAK1/2-STAT1 signalling pathway introduced by Yamada et al. (2003). The model itself is relatively complex. It captures all essential elements in the JAK1/2-STAT1 signalling, with exception of the PIAS inhibition, together with many short-lived, intermediate species. An important, practical advantage of the Yamada et al. (2003) model is that it is curated in DOQCS (Sivakumaran et al., 2003) and BioModels databases (Novère et al., 2006; Li et al., 2010). The model consists of over 30 variables representing species and of over 60 parameters of reaction rates. Originally, it was used to confirm importance of the pathway negative regulators, i.e. importance of phosphatases and negative feedback created by SOCS protein. The same model was analysed in Zi et al. (2005) and in Shudo et al. (2007), where it was subject to purely *in silico* experiments.

Motivation

The most valuable insight into mechanisms of signalling pathways can be obtained through a combination of theoretical and experimental analysis. Our work regards the JAK1/2-STAT1 pathway, which is stimulated by the Type II IFN-γ. We start with the model which is based on the experimental data (Yamada et al., 2003). There are noticeable differences against the data (cf. Brysha et al., 2001; Krause et al., 2002; Schuster et al., 2003) but the overall, qualitative behaviour of the JAK1/2-STAT1 pathway was validated.

A significant amount of new, experimental data for the JAK-STAT

pathways is available in the recent literature. However, vast majority of this data concerns JAK-STAT pathways activated by Epo (Bachmann et al., 2011), IL (Mahdavi et al., 2007) or Type I IFN (Smieja et al., 2008; Maiwald et al., 2010). Moreover, these pathways involve STATs heterodimerization ($A+B \to \ldots$) which, from the point of view of the kinetic modelling, differs substantially from the JAK1/2-STAT1 homodimerization process ($A + A \to \ldots$). See Vera et al. (2011) paper for a comprehensive review of data-driven approaches to the modelling of JAK-STAT pathways).

More importantly, it seems that the receptor activation mechanism, is not easily accessible for experimental measurements. Even if the data is relevant to the JAK1/2-STAT1 pathway, as in the work of Rateitschak et al. (2010), the measurements are done for the pathway keys species, such as already activated JAKs and receptors or the STAT proteins. Therefore, most often the activation mechanism of the JAK-STAT pathway receptor complex is greatly simplified (cf. Swameye et al., 2003; Vera et al., 2008; Rateitschak et al., 2010; Bachmann et al., 2011). Small but noticeable differences as these that can be observed between the model by Yamada et al. (2003) and its subsequent version by Shudo et al. (2007) escape the attention. The latter version lacks a reaction of dimerization of the receptor. This reduction is based on the assumption that the receptors are already assembled on the membrane. This difference is what we will focus on.

From a mathematical point of view, dimerization (symmetric collision) is the only elementary reaction that directly yields nonlinear (quadratic) dependency of a product change rate on its substrate. The question is if in a model of a considerable size, like the Yamada et al. (2003) JAK1/2-STAT1 model, the structure of a fast reacting peripheries, such as the receptor activation mechanism, is identifiable when related to the slowly produced output of the whole signal transducing process?

Receptor activation mechanism

Stimulation of signalling pathways via membrane receptors often involves formation of receptor dimers. Early experimental methods used to understand the process of activation of receptors, such as the immunoprecipitation, did not provide clear explanation of the underlying molecular mechanism. It was so, because such experiments are invasive — cell membrane has to be broken in order to conduct measurements (Krause et al., 2002). Classic hypothesis states that under a stimulation by ligand, such as cytokine, a reaction of almost simultaneous binding of three molecules occurs (Berg et al., 2006). This reaction contains a step of binding of the ligand to the extracellular domain of the receptor, which, in turn, induces a very fast creation of the dimer. This would mean that reaction $L + 2R \rightleftharpoons L(R)_2$ decomposes to two reversible reactions: $L + R \rightleftharpoons LR$ and $LR + R \rightleftharpoons L(R)_2$, where L and R represent, respectively, ligand and receptor species. Reactions denoted by longer arrows are relatively fast (highly probable); the reaction of dissociation of the whole assemblage is very slow (very unlikely to happen).

In the JAK1/2-STAT1 pathway, the active cytokine receptor consists of a IFN-γ ligand bound to a dimer of cytokine receptors, which itself are complexes of JAK2 and two receptor chains, each bonded by JAK1 (Krause et al., 2006). Taking into account molecular crowding on the membrane, it is very unlikely that such a complex biomolecule is created in a reaction that relies only on diffusional principles of a well randomised environment. Indeed, it has been verified experimentally that the cytokine receptors assemble on the membrane before the external stimuli is present (Krause et al., 2002, 2006; Schuster et al., 2003). These experimental results were used as an argument to remove the dimerization of a receptor from the model presented by Shudo et al. (2007).

Our contribution

We compare four variants of the Yamada et al. (2003) model. These variants correspond to the biochemical hypothesis, and to already studied

computational models. Specificity of the differences between model variants is the main difficulty to overcome: we compare peripheral component, which is relatively small and fast with respect to the whole network of biochemical reactions, within which the component is contained. Although the original model, in principle, is based on the experimental data (Yamada et al., 2003; Brysha et al., 2001; Krause et al., 2002; Schuster et al., 2003), our approach is purely theoretical.

The GOF criterion measure, such as the SSE, is not good for assessing biological models due to theirs inherent uncertainty and noisy data, which may cause overfitting (Myung and Pitt, 2004). On the other hand, generalizability favouring methods which penalise for model complexity, such as AIC, BIC or state of the art Bayesian model selection (BMS) and the directly related Bayes factor (BF), summarise relationship between model and data into a single number. Thus, if results of models comparison are nonsubstantial, as happens to be in our case study, then these results are of little use.

To address deficiencies of BMS, we use sensitivity analysis. It investigates the relation between uncertain parameters of a model, and a property of the observable output (Saltelli et al., 2008). More specificaly, based on the global sensitivity analysis (GSA), we use the robustness concept to tackle our model selection case study. Low sensitivities may indicate robustness, but also non-identifiability of reactions parameters in too complex models. To that end, we complement our analysis with the profile likelihood-based identifiability analysis (Raue et al., 2009), to penalise for the lack of generalizability.

Our main results are:

- proposing rigorous models for different variants of activation mechanism of the JAK1/2-STAT1 pathway,

- evaluating model selection methods in a case study of *de novo* analysis of a large-scale pathway model,

- identifying the most robust design of the JAK1/2-STAT1 pathway receptor activation mechanism.

3.1.2 Models

Following Yamada et al. (2003) and Shudo et al. (2007), all further analysis is based on numerical simulations of RRE (Eq. (2.1)). Here, all rates follow the mass action kinetics (Eq. (2.2)).

We distinguish three functional modules in the JAK1/2-STAT1 pathway models (cf. Figure 3.1.1):

- Receptor module: ligand IFN is the input of this module, the output corresponds to the active receptor complex $(\mathrm{IFNRJ_2})^*$.
- Transcription factor module (the STAT life-cycle): the active receptor complex is the input, while an active transcription factor in the nucleus $(\mathrm{STAT1n}^*)_2$ is the output of this module.
- Feedback (post-translation product) module: the active transcription factor is the input; a receptor inhibitor SOCS1 is the output.

Dynamics of modules outputs for the of Yamada et al. (2003) model are depicted in Figures 3.1.1(b–d). The respective modules emit output signal for ca. 25 minutes, 50 minutes and 1.5 hours, with its peak activity in ca. 25^{th} minute, 55^{th} minute and 2.5 hour. We are interested in differences in the receptor module, which is the first and the fastest to react to the external, input signal.

For our model selection problem, we have selected four variants of the receptor activation mechanism, depicted schematically in Figure 3.1.2:

1. *original* — model proposed by Yamada et al. (2003), schematically presented in Figure 3.1.1(a). The computational model was taken from the BioModels database.
2. *no JAK* — version of the *original* model which represents the fact that the JAK protein is constitutively bound to the receptor.
3. *IFN to dimer* — the version in which signalling ligand molecule binds directly to the already dimerized receptor. It represents hypothesis that IFN binds only to a pre-assembled receptor dimer (cf. Krause et al., 2002, 2006)).

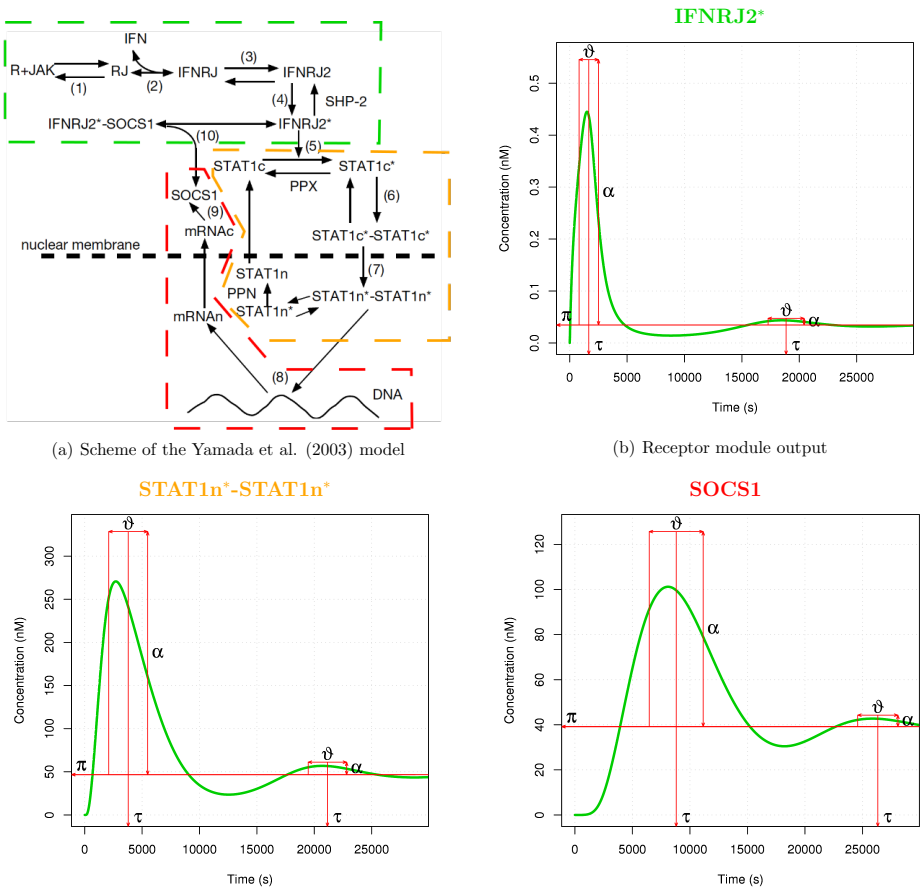

(a) Scheme of the Yamada et al. (2003) model

(b) Receptor module output

(c) Transcription factor module output

(d) Feedback module output

Figure 3.1.1: JAK1/2-STAT1 pathway modules denoted on the scheme from the Yamada et al. (2003) work (a) and their output species numerical simulations (b–d). Numerical simulations are decorated with the signalling properties defined by Heinrich et al. (2002), taken at the basal level $\pi = \lim_{t\to\infty}[S](t)$. These properties are: the n-th signal peak activity time $\tau_n = L_n/I_n$, where $L_n = \int_{t_n}^{\Delta t_n} t\cdot([S](t)-\pi)\,\mathrm{d}\,t$ and $I_n = \int_{t_n}^{\Delta t_n}([S](t)-\pi)\,\mathrm{d}\,t$; the duration $\vartheta = 2\sqrt{(Q_n/I_n)-\tau_n^2}$, where $Q_n = \int_{t_n}^{\Delta t_n} t^2\cdot([S](t)-\pi)\,\mathrm{d}\,t$; and the amplitude $\alpha_n = I_n/\vartheta_n$. The time period of the n-th signal, i.e. $[t_n, \Delta t_n)$, is defined as $\Delta t_0 = 0$, and for $n \geq 1$, $t_n = \min\{t > \Delta t_{n-1} \mid [S](t) > \pi\}$ and $\Delta t_n = \min\{t > t_n \mid [S](t) \leq \pi\}$. The input species IFN is constantly active, thus, the steady state values are relatively high. The signal shifts in time and elongates as it is propagated down the pathway. The temporal signal is completely attenuated after its second appearance.

4. *no dimerization* — model structure proposed by Shudo et al. (2007), where dimerization of receptor is omitted. It is based on the hypothesis that receptor dimer are pre-assembled on the cell membrane.

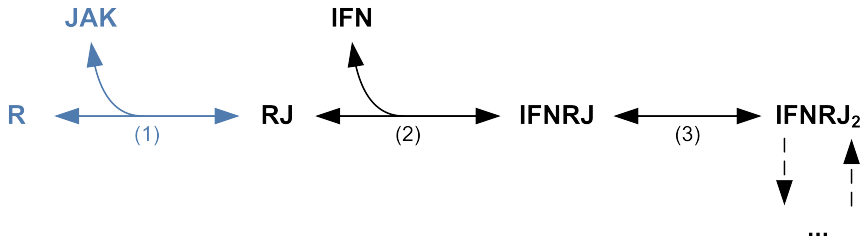

(a) Group I models, with IFN binding to a receptor monomer: the *original* model and the *no JAK* variant.

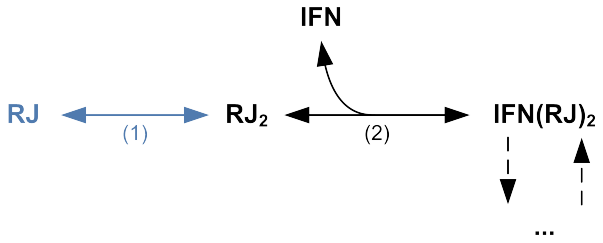

(b) Group II models, with IFN binding to a receptor dimer: the *IFN to dimer* binding case and its variant without receptor

Figure 3.1.2: Schemes of the variants of receptor complex formation mechanism in the JAK-STAT signalling pathway model. Each sub-figure represents two model variants: with or without the first reaction (highlighted).

These variants capture main and subtle differences in the mechanism of formation of the JAK-receptor complex in a context of the whole JAK1/2-STAT1 pathway. The *original* and *no JAK* variants are the group I models, and the *IFN to dimer* and *no dimerization* variants are the group II models, with IFN binding to a receptor monomer and a dimer, respectively.

For simplicity, there is a single variable R for both receptor chains as well as single variable JAK for both JAK1 and JAK2. Thus, JAK binding to the receptor represents a JAK1-mediated binding between the two chains of the receptor. On the other hand, receptor-bound JAK represents JAK2, which is responsible for the activation of the receptor and STAT1 proteins. Detailed activation of the dimerized receptor (cross-phosphorylation by JAK2) and detailed activation of the docked STAT1 (phosphorylation by JAK2) are simplified to a single reversible steps, respectively, $\mathrm{IFNRJ_2} \rightleftharpoons (\mathrm{IFNRJ_2})^*$ and $(\mathrm{IFNRJ_2})^*\text{-STAT1c} \rightleftharpoons (\mathrm{IFNRJ_2})^*\text{-STAT1c}^*$.

Steps of the activation of JAK1s and JAK2s (phosphorylation), which happen after IFN binds to the receptor, are omitted. Finally, in each model we assume that only after the IFN-bound receptor dimer is assembled, JAKs are active, i.e. the inactive receptor complex $IFNRJ_2$ is the first molecule on the signal downstream path where both JAK1 and JAK2 are active, and neither is active earlier.

Size of the models ranges from 34 to 30 species and from 72 to 64 reactions parameters. Conveniently, reactions leading to formation of the receptor complex, and their intermediate species, form a strongly connected component in a full bipartite graph of species and reactions. The inactive receptor complex $IFNRJ_2$ is a cut vertex in this graph, i.e. a node which removed splits graph into two unconnected sub-graphs. The component of formation of the receptor complex is sizing from 7 to 3 species and from 10 to 2 reactions parameters.

The SBML files with detailed biochemical reactions network for all variants of the JAK1/2-STAT1 model, including *original*, with re-estimated parameters values (explained in the following Section), can be found in the supplementary material to Rybiński and Gambin (2012) article.

3.1.3 Results and Discussion

For the purpose of a comparative analysis we have re-estimated parameters of all proposed model variants, so that they agree with the numerical simulations of the *original* variant. Because models differ only in one of two strongly connected components we took the cut vertex, i.e. the $IFNRJ_2$ variable, as a objective variable in a fit function — normalised SEE. It was sufficient to obtain good fit for all variables in the shared strongly connected component. Resulting fit is nearly perfect, meaning that errors are practically negligible as depicted in Figure 3.1.3. This result gives reconciled variants for a further comparison. It also undermines the significance of an error-based GOF criterion as the only criterion for the model selection task.

Knowing that the *original* variant agrees, to some extent, with the experimental data, and that we have a nearly perfect fit of numerical sim-

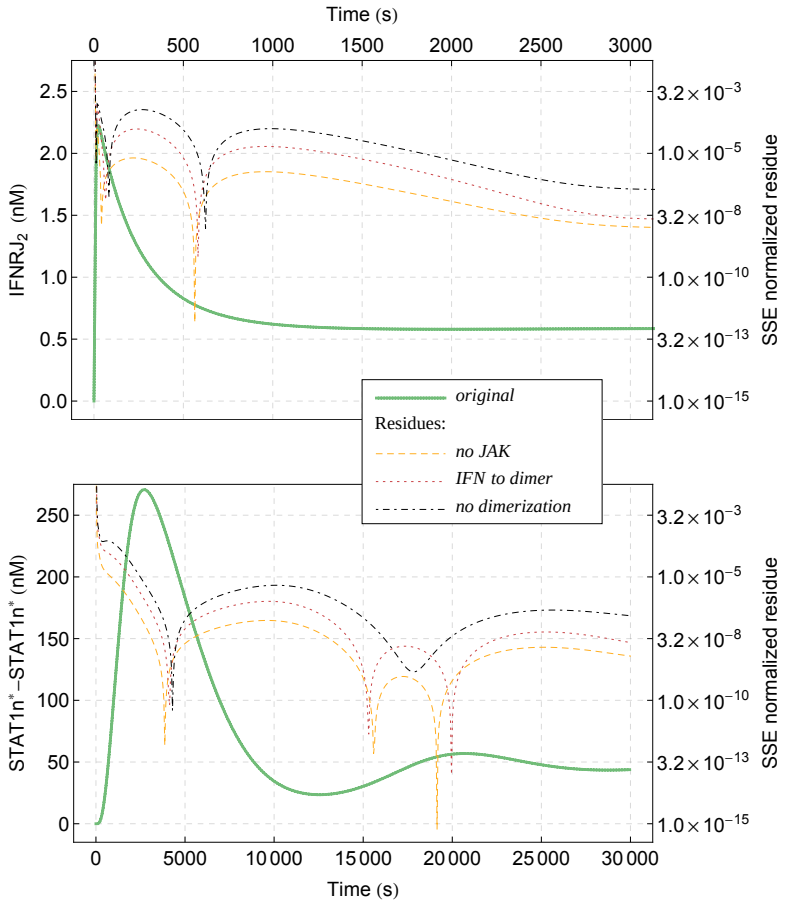

Figure 3.1.3: Numerical simulation of the cut vertex of the biochemical reactions network IFNRJ_2 (upper plot), and of the output species of the transcription module $(\mathrm{STAT1n}^*)_2$ (lower plot). The *original* model simulations are overlaid with values of the SSE residues for the remaining variants of the JAK1/2-STAT1 pathway ($\log_{10}$ scale on the right side). Residues values are normalised with the reference, simulation value. Both group II variants, with the pre-assembled receptors, have relatively high residues values in the beginning of the time course. Overall, the *no dimerization* variant has the worst fit. Nevertheless, the absolute residues values are very low throughout the whole time course. Optimisation was done for the IFNRJ_2 species variable. Low residues values for the $(\mathrm{STAT1n}^*)_2$ species variable illustrate the limited propagation of the fit error, which is practically negligible in the shared part of the biochemical model.

ulations for all of the proposed variants, we take the experimental data out of consideration. Our further comparison is done only among models which agree on the same, original behaviour. Conceptually, we base

the comparison on the ability of re-creating the original behaviour under perturbations of parameters, which corresponds to inherent stochasticity of biological systems observed at the level of biomolecules. To that end, we employed the parameter variation-based methods such as the Bayesian model selection (BMS) and the global sensitivity analysis (GSA). We complemented the latter with the identifiability analysis (IA) to account for feasibility of experimental measurements which may allow to precisely identify a correct reaction network.

BMS of the receptor activation mechanism

For the BMS comparison, we used a perturbed, simulated data series $\mathcal{D}$. It consists of two, arbitrarily selected, series of 10 time points of the transcription module output species $(\text{STAT1n}^*)_2$ (see Figure 3.1.4). For each of time point, we assumed a normally distributed noise with mean equal to the simulated value of $(\text{STAT1n}^*)_2$, and with a constant standard deviation. This type of noise corresponds to the maximum likelihood interpretation of the GOF criterion, with the SSE measure being a χ^2 log-likelihood (see, e.g., Raue et al., 2009).

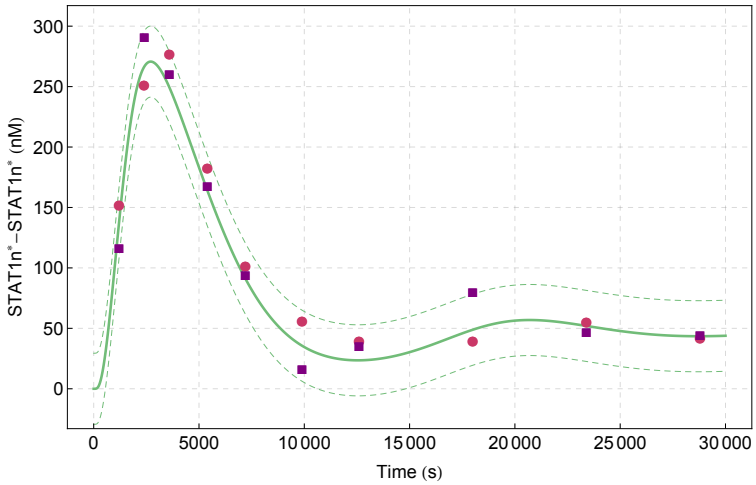

Figure 3.1.4: Two simulated data series of the transcription module output species $(\text{STAT1n}^*)_2$, with addition of a normally distributed noise ($\sigma = 0.05 \cdot 300$). Time points were selected arbitrarily. Dashed lines contain 95% of the noise distribution ($\approx +/- 1.96 \cdot \sigma$).

Because of the high time requirements for computing BF, we restricted ourselves to parameters of the receptor complex formation component. This component contains all differences between analysed variants (cf. Figure 3.1.2).

The theoretical basis for BF, together with our experiment setting is described in detail in Section 2.3.1. In short, we assume gamma distributed priors for all parameters, with shape equal to 1 and scales equal to the nominal values of parameters. Using a path sampling MCMC method we estimated the marginal likelihood of data $\mathcal{D}$, coming from a model $\mathcal{M}$ (cf. Eq. (2.14) in Section 2.3.1). Values of estimates of logarithm of the marginal likelihood are given in Table 3.1.1. In all cases estimators were efficient as highlighted by a low standard deviation. The BMS marginal log-likelihood is fully consistent with the common and easy to compute measures of generalizability (see Table 3.1.1): BIC and AIC. Also note, that for the simulated data $\mathcal{D}$, the maximum likelihood interpretation of SSE (χ^2), which doesn't account for the model complexity, comply with the statement of the slightly worse fit of the *no dimerization* variant, provided that all model variants are practically indistinguishable with the SSE GOF criterion (cf. Figure 3.1.3).

Model		**Generalizability**			**GOF**
Grp	Name	**BMS**	BIC	AIC	χ^2
I	*original*	25.26 +/- 0.050	84.95	75.00	18.24
	no JAK	25.77 +/- 0.019	66.95	62.97	18.213
II	*IFN to dimer*	25.73 +/- 0.005	66.96	62.98	18.219
	no dimerization	26.02 +/- 0.055	61.39	59.39	18.64

Table 3.1.1: Estimates of the BMS index (+/- standard deviation): logarithm of the marginal likelihood of data coming from a given JAK1/2-STAT1 model $\ln(\mathbb{P}(\mathcal{D}|\mathcal{M}))$, with unnormalised $\mathbb{P}(\mathcal{D}|\mathcal{M})$ values. Higher value means that the given model $\mathcal{M}$ better describes data $\mathcal{D}$. For comparison, other common measures of generalizability: BIC and AIC, as well as the GOF measure: χ^2 (in all cases lower value is better). These indices are calculated for the best fit of the model parameters to the simulated, noised data $\mathcal{D}$ — the same which was used in estimation of the BMS index. The noticeably best and worst scores are highlighted.

The logarithm of the BF values (ratio of the marginal likelihoods) are given in Table 3.1.2. The simplest *no dimerization* variant is preferred over all other variants, and all variants are preferred over the most complex *original* variant. The ranking agrees with the size complexity of models (with the *no JAK* variant being of the size of the *IFN to dimer* variant). However, such BF values give no substantial evidence support (Kass and Raftery, 1995; Jeffreys, 1998).

B_{ij} $(i,j=1,\ldots,4)$	1: *original*	2: *no JAK*	3: *IFN to dimer*
2: *no JAK*	0.22	—	0.02
3: *IFN to dimer*	0.20	—	—
4: *no dimerization*	0.33	0.11	0.13

Table 3.1.2: Estimates of the base 10 logarithm of BF, i.e. $\log_{10}(B_{ij})$. Only positive values are presented. The higher the value the more preferred is the model i in a row over the model j in a column. BF values are given as a base 10 logarithm for a direct interpretation in the $\log_{10}$ scale of BF evidence support. The most and the least discriminating values are highlighted.

BMS takes directly into account the variability in data but isn't sufficient to distinguish between models in our case study. Ability of fitting to the noisy data in the range of sampled parameters values is very similar for all model variants (cf. Table 3.1.2). With accordance to Occam's razor rule of thumb, which BMS implicitly implements, the most complex in size *original* variant turned out to be the least preferable and the simplest *no dimerization* variant the most preferable.

GSA & IA of the receptor activation mechanism

An exemplary GSA method implementation is MPSA (see Section 2.3.2). MPSA has been applied to models of signalling pathways (Cho et al., 2003), including the JAK-STAT pathway (Zi et al., 2005).We applied MPSA to the parameters of reactions of the receptor complex formation. We used the SBML-SAT (Zi et al., 2008) implementation of MPSA. Figure 3.1.5 depicts the influence of all investigated parameters on essential species. These species include the inactive receptor complex ($IFNRJ_2$; cut

vertex of the model graph), output species of pathway modules ($(\text{IFNRJ}_2)^*$, $(\text{STAT1n}^*)_2$ and SOCS1), as well as all species that were previously indicated as significant (Yamada et al., 2003; Zi et al., 2005; Shudo et al., 2007), i.e. unphosphorylated cytoplasmic and nuclear STAT (STAT1c and STAT1n), an active cytoplasmic STAT dimer ($(\text{STAT1c}^*)_2$), cytoplasmic, and nuclear phosphatases (SHP2, PPX and PPN) and nuclear mRNA (mRNAn).

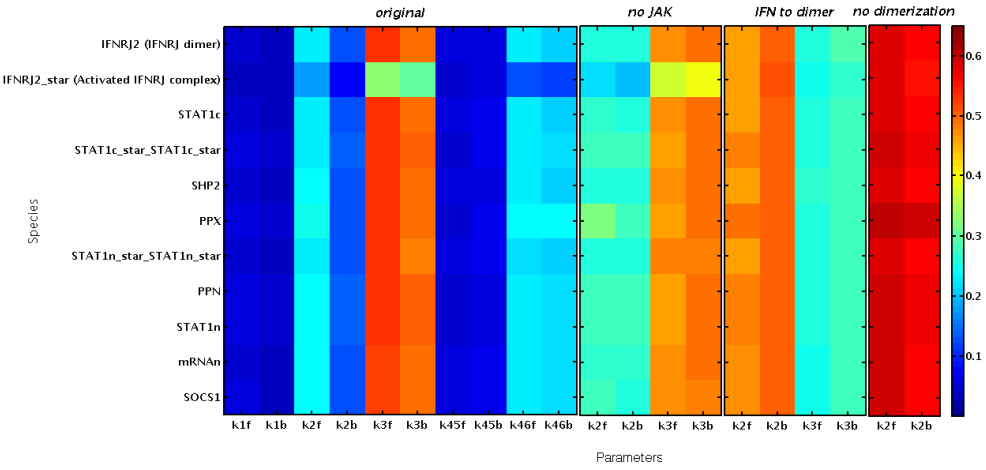

Figure 3.1.5: MPSA indices values for the parameters of the receptor complex formation component. The higher the value, represented by the colour, the more sensitive is the parameter (column) with respect to the target species (row). In each variant of the model, a distribution of the MPSA indices values among the parameters is highly consistent between the essential species. The kinetic parameters of association and dissociation of the receptor complex, respectively, k3f and k3b in the *original* and *no JAK* variants, and, respectively, k2f and k2b in the *IFN to dimer* and *no dimerization* variants, are the top 2 sensitive parameters in each combination.

The most sensitive parameters with respect to all essential species, for all JAK-STAT model variants under investigation, are the kinetic parameters of the reversible reaction connected to the cut-vertex species, i.e. the association and dissociation reactions of the inactive receptor complex IFNRJ_2.

For comparison, besides running MPSA, we also ran the Sobol (2001) method to estimate the well-established indices of the variance decomposition (Saltelli et al., 2008) — FOS and TE (cf., respectively, Eqs (2.17) and (2.18) in Section 2.3.2). The MPSA sensitivity, although in princi-

ple normalised to 1, implicitly includes the noise in an investigated output, whilst, the FOS and TE indices are normalised with the variance of the output. Values of the sensitivity indices for forward and backward reaction rates constants, with respect to the $IFNRJ_2$, are given in Table 3.1.3, together with the total indices, which explicitly penalise for the size complexity. Note that, additionally, the total TE index (TTE) linearly weights the high-order relations between parameters (cf. Eq. (2.19) in Section 2.3.2).

Model		**MPSA**			**FOS & TE**		
Grp	Name	Fwd	Bckwd	**Total**	Fwd	Bckwd	**Total**
I	*original*	0.33	0.30	**1.28**	0.40	0.30	**0.878**
					0.43	0.37	**1.106**
	no JAK	0.37	0.39	**1.17**	0.30	0.38	**0.877**
					0.37	0.41	**1.11**
II	*IFN to dimer*	0.46	0.51	**1.49**	0.26	0.37	**0.84**
					0.39	0.39	**1.102**
	no dimerization	0.58	0.55	**1.13**	0.46	0.48	**0.94**
					0.56	0.50	**1.06**

Table 3.1.3: Values of the total MPSA and variance decomposition sensitivities of the receptor component, together with sensitivity indices of kinetic parameters of the forward and backward reaction of formation of the inactive receptor complex $IFNRJ_2$. These are always the top 2 sensitive parameters. Presented parameters sensitivities were calculated with respect to the active receptor $(IFNRJ_2)^*$. The least and the most sensitive entries are highlighted, as well as models which have all parameters structural identifiable (see text for details).

The *no dimerization* variant is the most sensitive to changes in parameters of the reactions of association and dissociation of the inactive receptor complex $IFNRJ_2$. This is reflected in total FOS (TFOS), however, TTE and, more noticeably, total MPSA sensitivities of a receptor formation component for the *no dimerization* variant, are lower than the remaining variants (Table 3.1.3). In case of the latter total sensitivity measure the *no JAK* variant also performs well. In case of TFOS and TTE the differences between variants of the JAK1/2-STAT1 model are marginal.

On the other hand, it is now apparent how unimportant are many of 10 kinetic parameters of the biggest receptor module in the *original*

model, as indicated by very low increase in TTE with respect to TFOS (cf. Table 3.1.3) and, in general, very low sensitivity of these parameters (see Figure 3.1.5). Indeed, this model variant contains relatively short-lived protein complexes and fast reactions which could have been reduced without a loss of quantitative behaviour (cf. Bachmann et al., 2011). Unnecessary complexity of the receptor module in the *original* model can be easily explained with the analysis of the profile likelihood (PL) of the receptor module kinetic parameters.

PL-based identifiability analysis (Raue et al., 2009) is a method of analysis of the relation between parameter and the SSE (χ^2) output in terms of possibility of maintaining a low error value with respect to a systematical change of a value of one parameter and the best fit values for remaining parameters. In case of the *original* model almost all parameters are structurally non-identifiable within a reasonable range of values (see Figure 3.1.6). It means that increase in a quality or a quantity of available measurements will not allow to identify these parameters. Except for the dimerization parameters of the *IFN to dimer* variant, all parameters in the remaining model variants are structural identifiable (Section 2.3.3). In other words, only in case of the *no JAK* and *no dimerization* variants all kinetic parameters of the receptor module are identifiable. However, in contrast to the *no JAK* variant, the *no dimerization* variant requires less precise measurements to allow for identification of its parameters, which is a modelling advantage (cf. confidence interval proximity of PL in Figure 3.1.6).

An interpretive advantage of the Monte Carlo filtering method of GSA, such as MPSA, is that it can be viewed as an implementation of a concept of robustness of signalling pathways (cf. Morohashi et al., 2002; Kitano, 2007)). This is a property of a system to maintain one or more of its functions under the external and the internal perturbations. For example, one could be interested in the robustness to the input noise that could be a result of the extrinsic stochasticity of the extracellular signalling which is out of the scope of the model. In such setting, it is desired that in case of a low concentration of a input species, the system is capable of dampening the signal, so that an unwanted response is not induced (see, e.g., Shudo

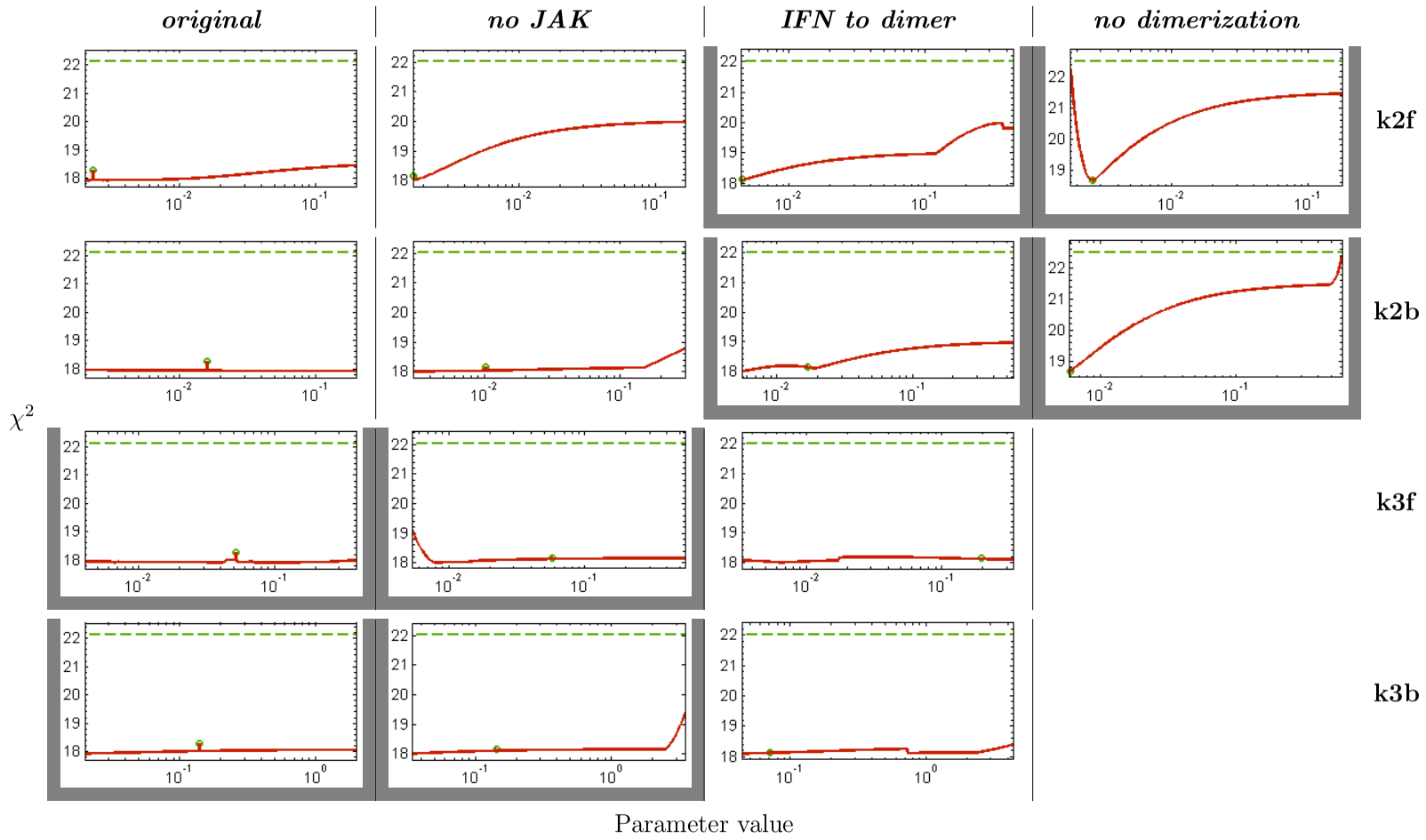

Figure 3.1.6: Estimated profile likelihood (PL) for kinetic parameters of the IFN binding (first two rows) and the receptor dimerization (last two rows). Estimation was done for the data set $\mathcal{D}$, used in BMS, in the range of $1/10$ of the nominal values of the parameters up to 10 times these values. Dots (green) represent the best fit to the data $\mathcal{D}$, in a constrained range. Dashed line (green) depicts the 95% pointwise confidence interval. Highlighted (in grey) are the PL plots of parameters of association and dissociation of the inactive receptor complex IFNRJ$_2$ (the cut-vertex). The estimated PL for remaining parameters of the *original* model are flat (not shown), similarly to PL of k2b (parameters structurally non-identifiable). All parameters of the *no JAK* variant and parameters of the IFN binding reversible reaction in the *IFN to dimer* and the *no dimerization* variants are structurally identifiable. Remaining parameters are structurally non-identifiable. PLs estimation was done using the PottersWheel toolbox (Maiwald and Timmer, 2008).

et al., 2007). Alternatively, investigating the simulations results of the mathematical model for the set of perturbed reaction rate constants can be interpreted as a robustness to the varying environmental conditions. Ability to preserve the functionality of the system under environmental changes may be an indicator of evolutionary preferable design (Morohashi et al., 2002).

With that in mind, note that the total parameters sensitivity to the integrated response of the receptor module output $(\mathrm{IFNRJ}_2)^*$, is visibly lower only in the *no dimerization* and *no JAK* variants (total MPSA in Table 3.1.3). This may indicate that these two variants, representing alternative IFN binding hypotheses, are more robust with respect to the behaviour of the active receptor.

Comparative histograms of the total MPSA, TFOS and TTE indices for all essential species are depicted in Figure 3.1.7. The assessment of the total MPSA and TE indices for all essential species clearly promotes the simplest *no dimerization* variant.

Note that, in general, the integrated response of the active receptor $(\mathrm{IFNRJ}_2)^*$ is the least sensitive to a simultaneous variations in values of parameters, whilst, quite the opposite for the single parameter variation (FOS index). The high robustness of the active receptor is somewhat expected due to the multiple negative regulators interacting with $(\mathrm{IFNRJ}_2)^*$, in particular, to the post-translational negative feedback loop provided by SOCS1 (cf., e.g., Fritsche-Guenther et al., 2011).

Altogether, for now, we conclude that the *no dimerization* variant is reasonable simplification of the Yamada et al. (2003) model in terms of the identifiability and the total robustness of kinetic parameters of the receptor activation mechanism. Binding of IFN to membrane pre-assembled dimers (the *no dimerization* variant) lowers robustness of the receptor activation mechanism. It has an improved overall environmental robustness but also, due to the simplicity, has more sensitive single elements (the reversible reaction of IFN binding to a dimer).

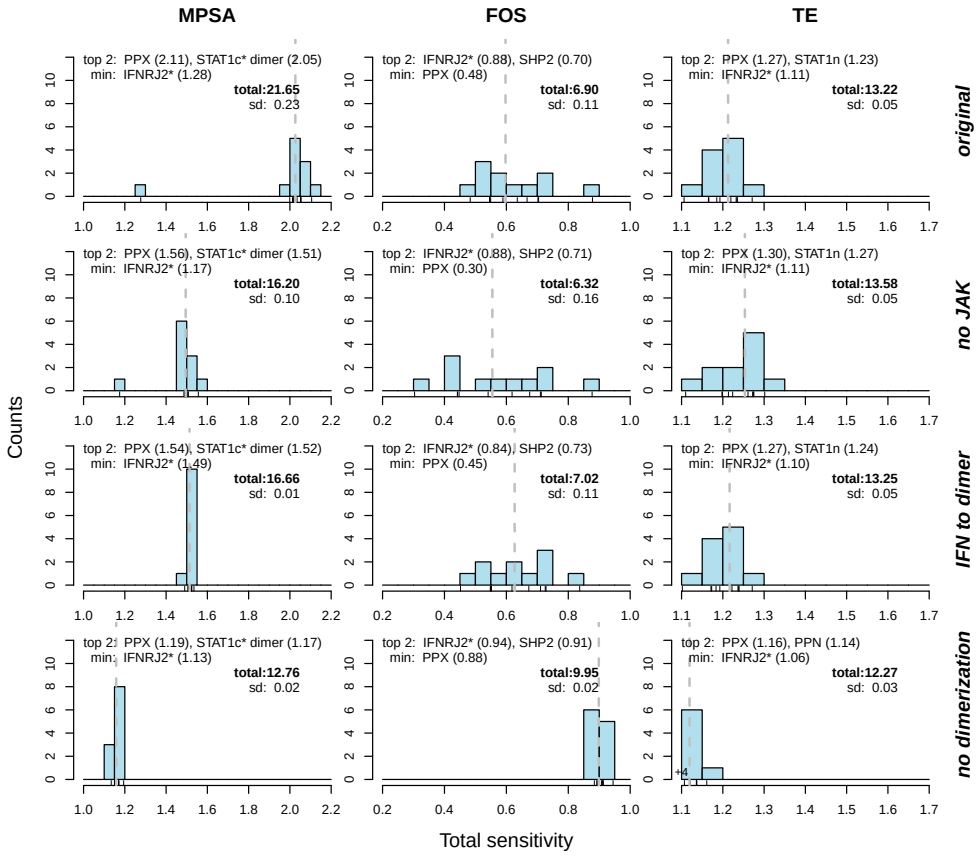

Figure 3.1.7: Histograms of total MPSA and variance decomposition indices for all essential species. Additional annotations include top 2 and the least sensitive species, a total sensitivity over all receptor component parameters and all essential species, a standard deviation of the total, per species indices, and their median (grey, dashed line).

Comprehensive GSA of kinetic parameters

The sensitivity analysis approach is much less computationally demanding as opposed to the Bayesian model selection method. We were able to easily extend our analysis to kinetic parameters of all reactions (over 60 parameters) and pursue the concept of a robustness-based model selection further. Nevertheless, to yield significant results, a specific GSA method should be executed for a limited number of input factors, in the setting this method is designed for. According to practical guidelines (Saltelli et al., 2008), Monte Carlo filtering should take no more than ca. 20 parameters to produce reliable results. To that end, we preprocessed the set

of kinetic parameters, by screening for the most sensitive parameters with WALS — a local approximation of global sensitivities. By aggregating ranks we selected the top 16 parameters common for all model variants under consideration. These parameters are listed in Table 3.1.4, together with the two parameters of the formation of the inactive receptor complex $IFNRJ_2$. Values of WALS indices for all parameters are depicted in Figure 3.1.8

Parameter	**Reaction description**	**Rank**
Receptor module		
k3f	IFN-Receptor complex dimerization	#10
k3b	IFN-Receptor dimer dissociation	#11
k4	IFN-Receptor dimer activation	#2
Transcription factor module		
k5f	$(IFNRJ_2)^*$-STAT1c binding	#6
k6	STAT1c phosphorylation	#1
k16	$(STAT1c^*)_2$ nuclear import	#16
k18f	PPN binding	#10
k18b	PPN unbinding	#17
k19	STAT1n* monomer dephosphorylation	#12
k20f	PPN-$(STAT1n^*)_2$ binding	#15
k20b	PPN-$(STAT1n^*)_2$ dimer unbinding	#13
k21	$(STAT1n^*)_2$ dephosphorylation	#9
Feedback module		
k24a	Transcription	#4
k24b	Transcription	#8
k26	SOCS1 synthesis	#5
k27	mRNAc degradation	#18
k28	SOCS1 degradation	#14
k36f	SHP2 binding	#3
k36b	SHP2 unbinding	#7

Table 3.1.4: The top 18 parameters selected with the WALS screening procedure, 16 of which are outside of the receptor formation component (the remaining parameters of the formation of the inactive receptor complex $IFNRJ_2$ are highlighted). WALS procedure was executed on the *original* model, with the integrated response of the three modules output species as an output properties. The rank is based on an aggregation of three rankings.

After selection of the local approximation of the globally most sensitive parameters, we carried out MPSA and TE-based robustness analysis in the

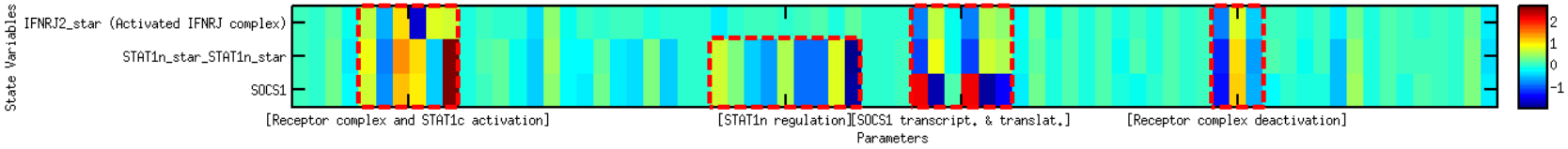

Figure 3.1.8: WALS sensitivity indices for different output species of JAK1/2-STAT1 pathway modules (in rows). Blue and red colours indicate high, weighted local sensitivity (positive and negative respectively). Sensitive groups of parameters, fairly consistent among different target species, are highlighted by red dashed lines. Functional meaning of these groups is written below the heat map. The parameters are listed from left to right in the document's order of the *original* model SBML file.

same setting as for the parameters of the receptor assembly component.

We summarised similarities in sensitivities among JAK-STAT pathway receptor activation variants with histograms and with pairwise *Spearman's rank correlation test*s (SRCC) of ranks obtained form the aforementioned GSA indices values (see Figures 3.1.9, 3.1.10 and 3.1.11).

The summary of total MPSA indices values (cf. Figures 3.1.11), as in the case of the receptor component, promotes the simplest variant. On the other hand, the TTE indices values allow only to disfavour the *original* variant. For further insight, we investigated the major differences in ranks induced by the TE index values (cf. Figure 3.1.9). In comparison to the *no JAK* and *IFN to dimer* variants, which yield almost identical results, the *no dimerization* variant has a less robust negative feedback species (mRNAn and SOCS1), but, more importantly, has more robust STAT1 forward signalling, in particular, the active, dimerized cytoplasmic STAT1 (also for the MPSA values; cf. Figure 3.1.11). The most sensitive reactions with respect to the latter species are STAT1c phosphorylation (k6) and $(\text{STAT1c}^*)_2$ nuclear import (k16), which is known to be one of the most sensitive design part of the STATs life-cycle (Swameye et al., 2003).

3.1.4 Tools and methods

For numerical integration we used the the Adams-Moulton backward differentiation method implemented in state of the art SUNDIALS' CVODES package. More precisely, we used CVODES through both PottersWheel (Maiwald and Timmer, 2008) and SBML ODE Solver Library (SOSlib; Machné et al., 2006). SOSlib automatically generates and numerically solves set of ODE for a model encoded SBML, which are read with the libSBML library (Bornstein et al., 2008). PottersWheel is a framework for a deterministic modelling of biochemical reactions network implemented as a MATLAB (The MathWorks Inc., 2011) toolbox; it also supports SBML (via SBMLToolbox; Keating et al., 2006).

For parameters re-estimation we used simulated annealing (SA) im-

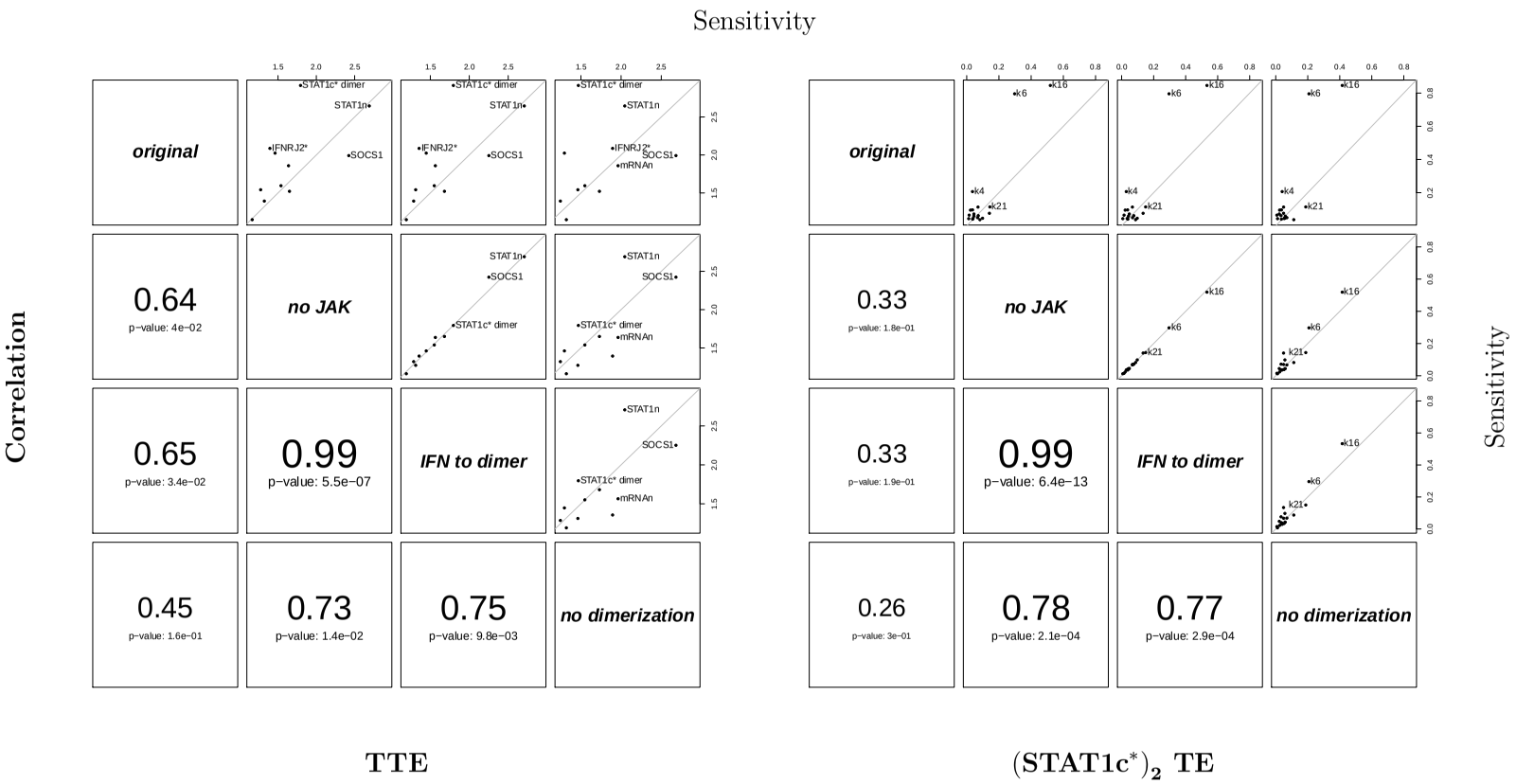

Figure 3.1.9: SRCC of TTE ranks for all essential species, and the $(\text{STAT1c}^*)_2$ TE for WALS top 16, common parameters. P-value was calculated with two-tailed null hypothesis, i.e. the rankings independence. Scatter plots of the rankings are depicted in the top right corner of the graph. Top 3 values of each of the two compared rankings are additionally labelled with corresponding species or parameter name. The deviation of data points above or below the diagonal promotes a variant in column over a variant in row or inversely in terms of TE-measured robustness.

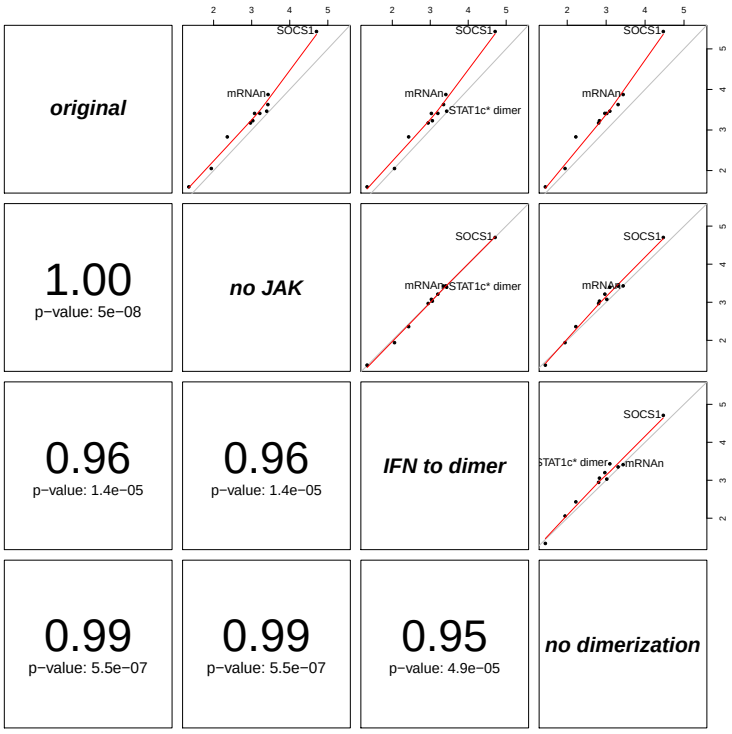

Figure 3.1.10: SRCC of the total MPSA rang for all essential species, common in all JAK1/2-STAT1 pathway model variants. P-value was calculated with two-tailed null hypothesis, i.e. the independence of rankings. Scatter plots of the rankings are depicted in the top right corner of the graph with LOWESS smoothing line in red. Top 2 values of each of the two compared rankings are additionally labelled with corresponding species name. In all cases the rankings are almost identical. The deviation of data points above the diagonal promotes a variant in column over a variant in row in terms of absolute values of total MPSA indices. In each combination of pairs the *no dimerization* variant is slightly preferred.

plementation from the OPTIM package of the Statistical computing language R (R Development Core Team, 2009).

In BMS, for all parameters p_i, we assumed gamma distributed priors $\Gamma(1, p_i^0)$, with shape 1 and scales equal to the nominal values of parameters p_i^0 (cf. Vyshemirsky and Girolami, 2008b). In such setting, mean and standard deviation of these priors are equal to the nominal value of the parameters (the range $[p_i^0/10, 10p_i^0]$ of values of a parameter p_i covers over 90% of the $\Gamma(1, p_i^0)$ distribution). $\mathbb{P}(\vec{p}|\mathcal{M})$ PDF is defined as a joint distribution of gamma priors. For estimation of the marginal

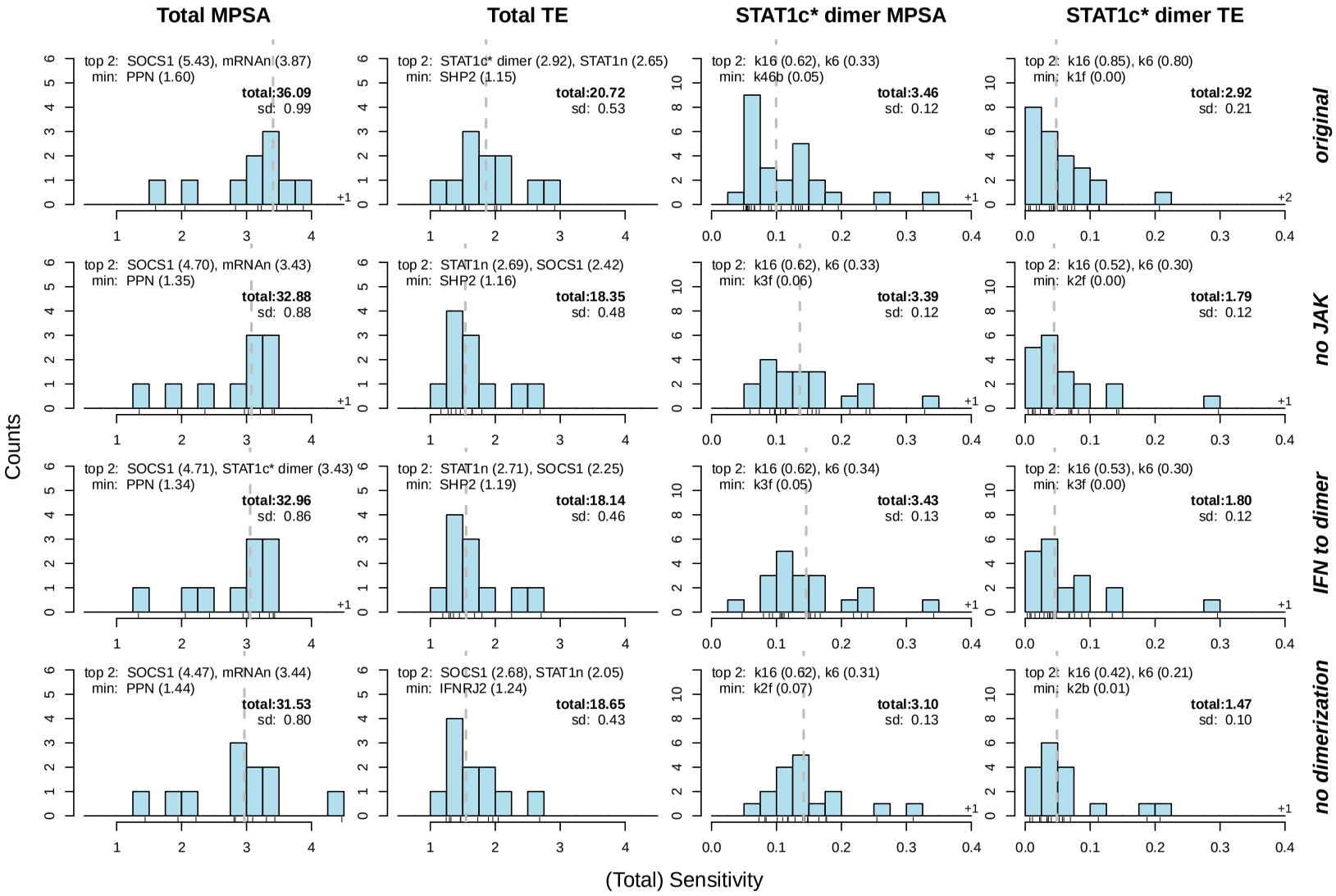

Figure 3.1.11: Histograms of total MPSA and TTE indices for all essential species, and the $(\text{STAT1c}^*)_2$ MPSA and TE indices for WALS top 16, common parameters. Additional annotations include top 2 and the least sensitive species, a total sensitivity over all receptor component parameters and all essential species, a standard deviation of the total, per species indices, and their median (grey, dashed line). The omitted instances are marked at the relevant end of an abscissa ($+n$).

likelihood (Eq. (2.14)) we've selected the path sampling MCMC method: the Annealed Importance Sampling (AIS; Neal, 2001) as implemented in BioBayes (Vyshemirsky and Girolami, 2008a). AIS is a high precision method with a reasonable time efficiency, as it is not necessary for obtaining useful estimate to wait until the underlying Markov chain converges to the stationary distributions. Nevertheless, AIS execution time limits its practical applicability of BMS to models which contain only several parameters.

For sensitivity analysis, we ran the MPSA, Sobol's and WALS methods implemented in SBML-SAT (Zi et al., 2008). For MPSA we took 2000 parameters samples, drawn uniformly form the range of 1/10 of the nominal values of the parameters up to 10 times the nominal values of the parameters. The error function is SSE between the output property of the model for the sampled parameter set and the reference parameter set (Zi et al., 2008). Here, the output properties were calculated as the integrated response for each of the essential species separately. Integrated response is the area under the time course of selected species, approximated in 50 equally distributed time points. The parameters samples were classified as acceptable or unacceptable by comparing with the mean error value. The final MPSA indices were calculated as the Kolmogorov-Smirnov test value for the empirical cumulative distribution functions of acceptable and unacceptable samples sets. To calculate the V_i^{ϕ} and TE_i^{ϕ} indices we used the Sobol's method with 2000 samples for the receptor component parameters and 5000 samples for the WALS top ranked parameters. In both cases, the distribution of parameters and the output properties were the same as in MPSA. For WALS we took 10^3 sample points, for which nLSCs were weighted by the Boltzmann distribution function. As the output property ϕ for nLSC, we took the integrated responses of the output species of the receptor, transcription factor and feedback modules.

For IA we used the PottersWheel implementation of the PL estimation. It was done for all receptor component parameters, for the data set used in BMS (see Figure 3.1.4). We took the range of 1/10 of the nominal values of the parameters up to 10 times these values, within a 95% pointwise confidence interval. The re-optimisation steps were done using the trust region optimisation algorithm.

Ranks aggregation

The Spearman's Footrule distance between two rankings σ^1 and σ^2 (permutations of the parameters vector $\vec{p}$), is defined as

$$F(\sigma^1, \sigma^2) = \sum_{i=1}^{M} |\sigma^1(i) - \sigma^2(i)|,$$

where $\sigma^j(i)$ is a position of the p_i in the σ^j ranking. The optimal, aggregated ranking σ^* of a given set of input rankings $\sigma^1, \ldots, \sigma^J$, minimises the weighted F distance between all (σ^*, σ^j) pairs.

We aggregated ranks of values of parameters WALS for output species of all modules ($(\text{IFNRJ}_2)^*$, $(\text{STAT1n}^*)_2$, SOCS1) in the *original* model (cf. Figure 3.1.8). To estimate the optimal ranking, we used the Cross-Entropy Monte Carlo algorithm (Pihur et al., 2007) implemented in the RangAggreg R package (Pihur et al., 2009). We used $10^3 \cdot M \cdot N$ samples, where $N = 18$ (size of the consensus ranking with the forward and backward parameters of the $(\text{IFNRJ}_2)^*$ assembly) and $M = 72$ (number of kinetic parameters in the *original* model).

3.2 Property-specific sensitivity analysis

We leave for a short while the biologically overloaded signalling pathways for the simple model of enzymatic reaction. We do that to illustrate an idea of a property-specific sensitivity analysis and, primarily, to present the Tav4SB project capabilities. Here, we apply MPSA with combination of both numerical ODE solving and the PMC technique for CTMC.

3.2.1 Model

Consider the simple, enzymatic reaction model of three reactions,

$$\begin{aligned} R_1: &\quad E + S \xrightarrow{k_1} ES \\ R_2: &\quad ES \xrightarrow{k_2} E + S \\ R_3: &\quad ES \xrightarrow{k_3} P + E \end{aligned} \tag{3.1}$$

where species names S, E, ES and P stand for substrate, enzyme, enzyme-substrate complex and product, respectively. Length of an arrow indicates the order of the reaction rate, i.e. both forward reactions: the complex formation reaction R_1 and the product conversion reaction R_3, are relatively fast when compared to the unproductive dissociation of the enzyme-substrate complex R_2. Initial amounts of species and kinetic parameters values, taken from (Cho et al., 2003) paper, are

$$\begin{aligned} &\mathrm{S}_0 = 12 \qquad \mathrm{E}_0 = 10 \qquad \mathrm{ES}_0 = 0 \qquad \mathrm{P}_0 = 0, \\ &k_1 = 0.184 \qquad k_2 = 0.016 \qquad k_3 = 0.211. \end{aligned} \tag{3.2}$$

Figure 3.2.1 depicts the RRE simulation workflow and a resulting plot for all variables in the initial value problem from Eqs (3.1) and (3.2). Corresponding ODE (cf. Eq. (2.1)) are derived automatically from a SBML model file, based on given rate laws of reactions. In the deterministic model of the enzymatic reaction, rates are described by the law of mass

action (cf. Eq. (2.2)), giving:

$$\begin{bmatrix} \frac{\mathrm{d}[S](t)}{\mathrm{d}\,t} \\ \frac{\mathrm{d}[E](t)}{\mathrm{d}\,t} \\ \frac{\mathrm{d}[ES](t)}{\mathrm{d}\,t} \\ \frac{\mathrm{d}[P](t)}{\mathrm{d}\,t} \end{bmatrix} = \begin{bmatrix} -1 & 1 & 0 \\ -1 & 1 & 1 \\ 1 & -1 & -1 \\ 0 & 0 & 1 \end{bmatrix} \begin{bmatrix} k_1 \cdot [S](t) \cdot [E](t) \\ k_2 [ES](t) \\ k_3 [ES](t) \end{bmatrix}$$

Numerical simulations for above ODE are calculated over a time period of 30 seconds.

The system stabilises in approximately 25 seconds with a peak activity at the 2-nd second. At that time point most of the enzymes are at work, i.e. they are bound to substrates, which, in turn, are converted into the product.

3.2.2 Results and Discussion

We run two variants of MPSA (cf. Section 2.3.2), differing in the way in which the error is calculated. In one variant we use RRE simulations and in the other one we exploit the PMC technique. We focus on kinetic parameters of two forward reactions of enzymatic reaction, i.e. k_1 and k_3. As an error function we take, respectively, mean SSE of an simulated trajectory of the product P and the absolute difference of the value of the CSL formula, in both cases between results for a parameters sample and for the reference values of parameters (Eq. (3.2)).

The formula being checked is expressed in the reward-based CSL extension (Kwiatkowska et al., 2006) as follows:

$$\mathrm{R}_{\{\#R_1=?\}} \left(\Diamond \left(P > 0.5 \cdot \lim_{t \to \infty} P(t) \right) \right). \tag{3.3}$$

Roughly speaking, formula (3.3) answers the following question: how many times, on average, the reaction R_1 of association of the enzyme-substrate complex has to occur, before the amount of the product P reaches 50% of its maximum? It is motivated by the half maximal effective concentration (cf. EC_{50} coefficient).

In turn, we obtain *empirical cumulative distribution function* (ECDF)

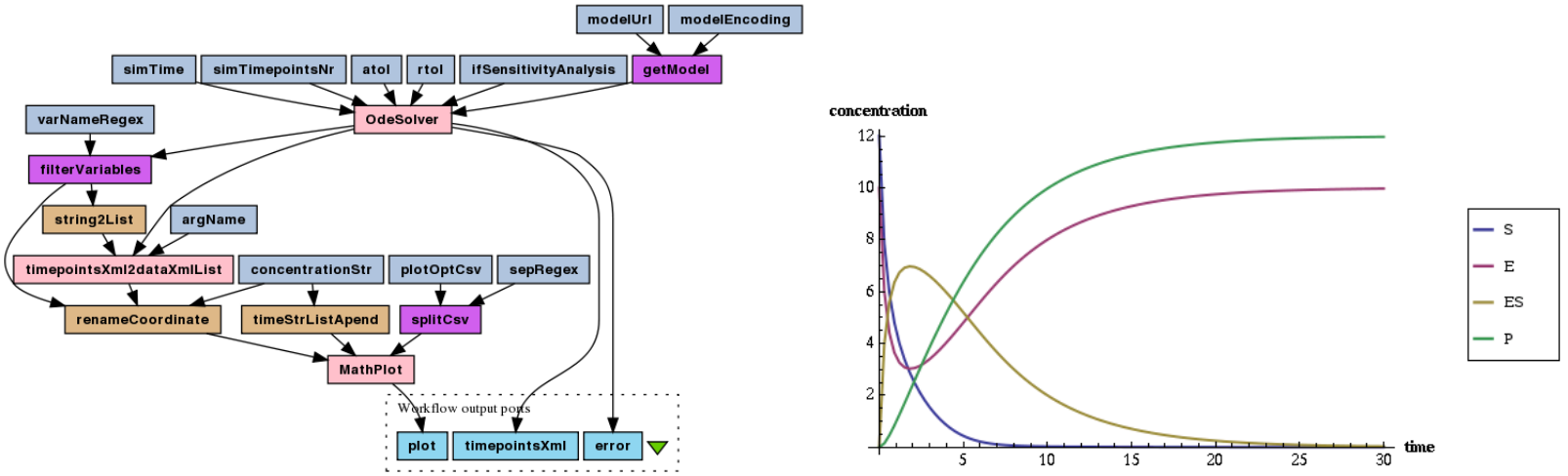

Figure 3.2.1: The "Simulate SBML-derived ODE" workflow (left) and resulting trajectories plot for the enzymatic reaction model (Eq. (3.1) and (3.2); right). Pink boxes represent nested workflows, corresponding to TAV4SB WS operations wrappers and a helper (see Section 2.4.2).

of acceptable and unacceptable samples, for each of the selected parameters. ECDFs are compared using K-S test and one minus PMCC. As a final output of the MPSA method, we get two rankings for each of the sensitivity indices: K-S test and PMCC.

Figure 3.2.2 depicts values of the error function and ECDFs of acceptable and unacceptable samples, for parameters k_1 and k_3, for both variants of the MPSA procedure. In the variant based on RRE simulations and the error function which measures changes in the product P trajectory, one clearly observes that parameter k_3 significantly dominates parameter k_1, as far as sensitivity of the system is concerned. This is an expected result. Firstly, k_3 is a rate parameter of a reaction which is directly responsible for a product creation. Secondly, from the Michaelis and Menten (1913) approximation:

$$\frac{\mathrm{d}\,[P]\,(t)}{\mathrm{d}\,t} \approx k_3\,[S]\,(0)\,\frac{[S]\,(t)}{[S]\,(t) + \frac{k_2+k_3}{k_1}} \quad , \tag{3.4}$$

one can expect that, for values from Eq. (3.2), variation of parameter k_3 will be more influential, with respect to the product rate, than variation of parameter k_1.

Interestingly, the results of the other variant of the MPSA procedure are significantly different; one observes that now k_1 dominates k_3. This may be ascribed to the particular choice of the formula (3.3) which calculates the average number of occurrences of R_1. Furthermore, an inspection of values of sensitivity indices given in Figure 3.2.2 brings to light that the domination is not as definite as in the first variant of MPSA. Results demonstrate that an application of the PMC technique may allow for revealing more subtle dependencies in the model, depending on the properties of interest.

MPSA combined with PMC may be applied as a pre-processing step which finds parameters that are insignificant for an analysis oriented on a very specific property of a model. This would provide a novel notion of a probabilistic abstraction (cf. Laplante et al., 2007), i.e. property-specific reduction of the probabilistic model. However, for a successful application, the pre-processing should have low running time, compared

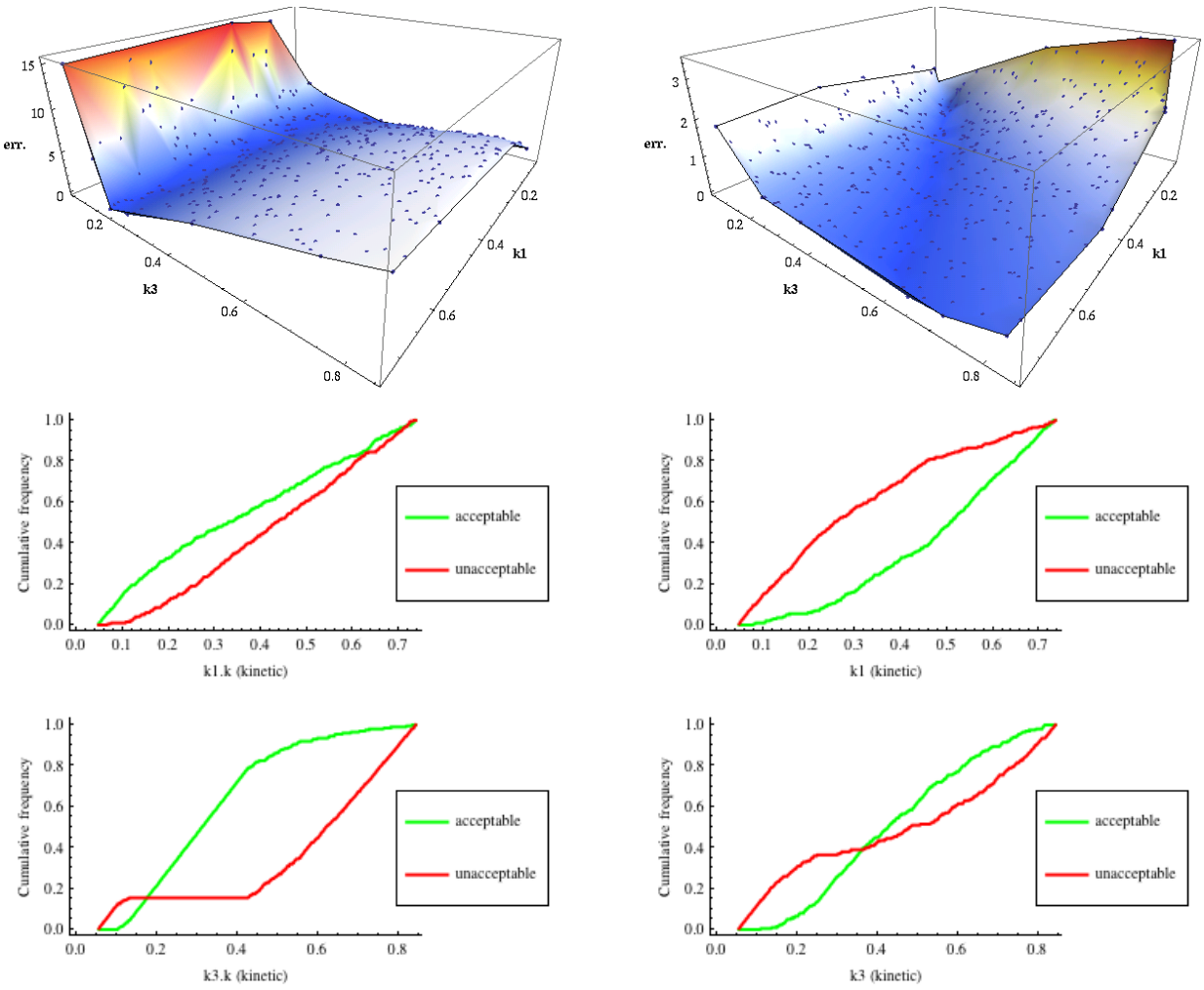

	KS-test	1−PMCC
$k1$	0.23	0.0158
$k3$	0.64	0.2709

	KS-test	1−PMCC
$k1$	0.42	0.0955
$k3$	0.25	0.0488

Figure 3.2.2: MPSA error surfaces, ECDFs and values of sensitivity indices for error calculated using deterministic model with the mean SSE of product trajectories (left column) and using stochastic model with the absolute difference of a value of the formula (3.3) (right column). Both procedures were run for 400 samples of parameters. Samples were generated using LHS, from a uniform distribution over a range from $\frac{1}{4}\times$ to $4\times$ the nominal value of each of investigated parameters (Eq. (3.2)). As a threshold for classifying samples as acceptable or unacceptable, we took median of error values. The larger the value of a statistics which compares ECDFs, the more significant is a parameter with respect to a property of interest.

to an analysis that follows. In our experiment this is not the case, as we run the exact PMC procedure, which is essentially the same one that would be ran during the further analysis. However, we conjecture that for the MPSA procedure the level of accuracy offered by PRISM is much too high. We suppose that satisfactory results may be obtained using an approximate approach, such as Monte Carlo model-checking (Grosu and Smolka, 2005).

3.2.3 Tools and methods

To define model we used the SBML-shorthand notation (Gillespie et al., 2006) — a convenient, compact format with converters to (and from) the over-verbose SBML standard. With a slight adjustment it is easy to obtain stochastic version of the deterministic model.

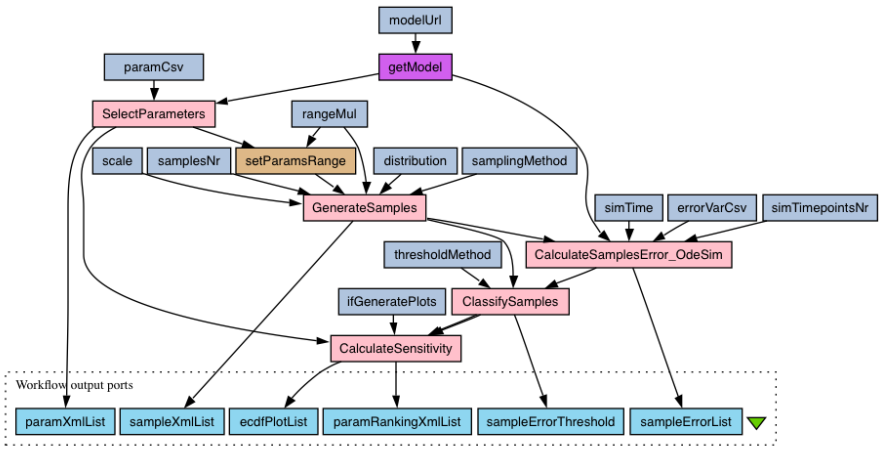

Figure 3.2.3: MPSA workflow with an ODE-based error function. Pink and brown boxes represent essential steps of the procedure. Remaining boxes represent workflow's parameters and outputs.

For all computations we constructed Taverna workflows, exploiting the Tav4SB WS operations (see Sec. 2.4.2). This includes RRE simulations (see Fig. 3.2.1) MPSA workflow (depicted in Fig. 3.2.3) as well as the error surface plotting workflow (not shown; cf. Fig. 3.2.2).

3.3 Efficacy of hyperthermia treatment

This case study is based on the *heat-shock response* (HSR) model. We exploit both deterministic and stochastic methods to investigate the thermotolerance phenomenon and the effect of a combined hyperthermia and a drug therapy of cancer. In terms of methodology this is the most model-specific case study; for instance, it contains a thorough investigation of a protein denaturation rate. On the other hand, this specificity is balanced by proposal of an approximate stochastic perturbation strategy generally for CTMC models.

3.3.1 Background

heat-shock proteins (HSP) are a group of highly conserved proteins involved in many physiological and pathological cellular processes. They are so called chaperones, as which they help with folding of new and distorted proteins into their proper shape. HSP synthesis increases under stress conditions. Induction of HSP increases cell survival and stress-tolerance. Elevated expression of different members of HSP family in tumour cells has been detected in several cases. Despite its importance, little is still known about how exactly HSP are involved in different processes related to cancer development.

HSP are classified into families according to their molecular mass. The family of heat shock protein 70 kDa (HSP70) is the best studied class of HSP. In mammals, at least two isoforms exists in the cytoplasm: the constitutively expressed HSP70 and the heat-shock inducible HSP70 protein (Wegele et al., 2004; Szymańska and Żylicz, 2009). This highlights the general principle that HSP70 plays important role under both physiological and inducible, stress conditions. We're interested in the latter. For readability, from now on we will denote HSP70 simply as HSP.

Motivation

Most of the non-surgical methods of cancer treatment (e.g. chemotherapy and radiotherapy) are based on the principle of putting some kind of stress on cancer cells. Unfortunately, in many cases the above methods fail. The fact that HSP prevent apoptosis induced by different modalities of cancer treatment explains how these proteins could limit the efficacy of these therapies. Therefore, in order to improve the efficacy of these treatments, recently much effort is focused on the multimodal oncological strategies, that is combined treatment of chemotherapy and hyperthermia (i.e. therapeutic procedure used to raise the temperature of a region of the body affected by cancer; Wust et al., 2002), or radiotherapy and hyperthermia. A synergistic interaction of radiotherapy and hyperthermia as well as some cytotoxic drugs and hyperthermia has already been confirmed in many experimental studies (Hildebrandt et al., 2002; Neznanov et al., 2011). Hyperthermia engages the HSR mechanism, whose main component are HSP, however, the precise mechanism of these interactions is still unclear. Moreover, cancer cells can have an already partially activated HSR, thereby hyperthermia may be more toxic to them relative to normal cells (Neznanov et al., 2011).

On the other hand, after a heat shock, all cell types show an impairment in their susceptivity to heat-induced cytotoxicity. This phenomenon, known as *thermotolerance*, is triggered by HSR (it is at least partially based on the induction of HSP; Hildebrandt et al., 2002). Thermotolerance is, in principle, reversible and persists for usually between 24 and 48 hours (Wust et al., 2002). Due to this phenomenon the applicability of the combined hyperthermia therapy may be, counter-intuitively, initially limited. This poses a question about the actual efficacy and about an optimal strategy of the hyperthermia treatment.

Related HSR models

There are basically two types of approaches to HSR modelling. They differ in how the heat-induced protein misfolding is captured in the model.

In one approach, the temperature is not a model variable and its increase is modelled by a direct change of the system state, that is an addition of an intermediate species like reactive oxygen species (ROS; see, e.g., Proctor and Lorimer, 2011), which causes native proteins to misfold. Peper et al. (1998) proposed an integral model of HSP regulation, where temperature-dependence is explicitly expressed in kinetic rate constant of native proteins misfolding reaction; the temperature change is modelled by a direct change of kinetic parameter of one reaction. This approach, with the same temperature-dependence function has been followed up in some of the recent papers which include HSR modelling (Szymańska and Żylicz, 2009; Petre et al., 2010; Mizera and Gambin, 2010). Similarly, Rieger et al. (2005) modelled temperature perturbation by a change of kinetic rate constants. However, in his approach misfolding is based on enzyme kinetics approximation of Michaelis and Menten (1913, see Eq. (3.4)) with arbitrarily selected kinetic values for four different temperatures. In fact, Rieger et al. (2005) approach boils down to model reduction by excluding the intermediate kinase of misfolding, such as ROS. Contrary to that, the Peper et al. (1998) approach follows purely mass action kinetics and the misfolding rate is based on experimental data on the level of protein denaturation for a range of 30–100°C (Lepock et al., 1993).

As far as the stochastic HSR models are considered, the counterpart of Petre et al. (2010) model was presented by Mizera and Gambin (2010). The authors thoroughly validated deterministic approximation. Another stochastic and deterministic pair of HSR models was recently presented in Proctor and Lorimer (2011) . It is worth noting, that although this biochemical model is, relatively, very complicated, its stochastic counterpart contains a unique feature of explicit probabilistic event of the cell death, which is not available for the deterministic version.

For our case study we have chosen the explicit temperature-dependent denaturation rate approach, in which the Szymańska and Żylicz (2009) model is the simplest. With many simplifications, such as direct trimerisation or no misfolding of HSR components, this model is able to capture the overall qualitative behaviour of the HSR mechanism. None of the abovementioned models have been used to investigate either thermotolerance or multimodal oncological strategies.

Our results

The main aim of this case study is to contribute to understanding of the involvement of the HSR mechanism in multimodal cancer therapies. We start with adapting the deterministic RRE model proposed by Szymańska and Żylicz (2009), which, despite of its simplicity, allows for a sound qualitative modelling of the HSR mechanism. We estimate a global function of a level of protein denaturation and derive a correct protein denaturation rate.

We also develop a stochastic extension of this model (a CTMC), which we then analyse using the PMC techniques. To ensure the feasibility of this approach we decided to use approximate techniques (APMC), implemented recently in the PRISM tool (see, e.g., Nimal, 2010).

Next, we formalise the notion of the thermotolerance, or the memory of the system of the previous temperature perturbation, or system desensitisation with respect to the second consecutive heat shock. We compute the size and the duration of the HSR-induced thermotolerance. Finally, we quantify the effect of a combined therapy of hyperthermia and an artificial, cytotoxic inhibition of proteins refolding. We are able to support the common belief that the combination of cancer treatment strategies increases therapy efficacy.

3.3.2 Model

In this case study we consider the dynamics of synthesis of HSP and its interactions with key intracellular components of HSR, i.e.: HSP; the *heat-shock factor* (HSF) and its trimer, which is a HSP transcription factor; HSP substrate — mainly denatured, misfolded native proteins; HSP gene — *heat-shock element* (HSE); and HSP mRNA. Figure 3.3.1 depicts the model scheme, Table 3.3.1 gives reaction list, whereas

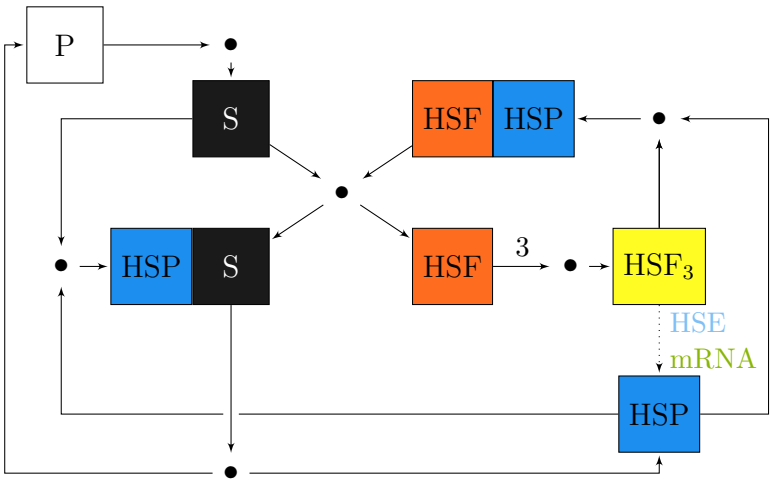

Figure 3.3.1: Scheme of the HSR model. On the left side of the scheme, the denaturation of native proteins P and denatured proteins S (substrate) refolding moderated by the HSP chaperones. On the right side, the adaptive HSP production loop, stimulated by HSFs, which trimerise and initiate HSE transcription and HSP mRNA translation (dotted arrow). As a negative feedback, HSP molecules promote HSF trimers dissociation and inhibit single HSF molecules by direct binding. To close the loop, inhibited HSFs are forced out of the complex with HSP by inflowing substrate.

Table 3.3.2 gives the implied mass conservation constraints. Structural changes with respect to the previous version of this model (i.e., model by Szymańska and Żylicz, 2009) include explicit native protein species (reactions (r9) and (r10)) and separate HSP mRNA degradation (reactions (r11) and (r12)). The addition of native protein species variable P is only a technical manipulation to increase model clarity; this variable can be removed from the model on basis of Eq. (c1).

Tables 3.3.3 and 3.3.4 summarise, respectively, the variables of the model with their initial values, as well as description and values of all kinetic parameters. Parameters k_i, and l_j denote the mass action reaction rates constants, respectively, for the forward and backward reactions. Value of the reaction rate constant k_{11}^{T} depends on the given temperature T.

Resulting RRE model consists of 10 ODE. Figure 3.3.2 depicts behaviour of this model, which starts in the state of homeostasis (i.e. in a steady state for $\mathrm{T} = 37°\mathrm{C}$), in response to the $\mathrm{T} = 42°\mathrm{C}$ heat shock.

$$
\begin{aligned}
\mathrm{HSP{:}HSF} + \mathrm{S} &\underset{l_6}{\overset{k_6}{\rightleftharpoons}} \mathrm{HSP{:}S} + \mathrm{HSF}, && \text{(r1)}\\
3 \cdot \mathrm{HSF} &\xrightarrow{k_3} \mathrm{HSF_3}, && \text{(r2)}\\
\mathrm{HSF_3} + \mathrm{HSE} &\underset{l_7}{\overset{k_7}{\rightleftharpoons}} \mathrm{HSE{:}HSF_3}, && \text{(r3)}\\
\mathrm{HSE{:}HSF_3} &\xrightarrow{k_8} \mathrm{HSE{:}HSF_3} + \mathrm{mRNA}, && \text{(r4)}\\
\mathrm{HSP} + \mathrm{HSF_3} &\xrightarrow{l_3} \mathrm{HSP{:}HSF} + 2 \cdot \mathrm{HSF}, && \text{(r5)}\\
\mathrm{HSP} + \mathrm{S} &\underset{l_1}{\overset{k_1}{\rightleftharpoons}} \mathrm{HSP{:}S}, && \text{(r6)}\\
\mathrm{HSP} + \mathrm{HSF} &\underset{l_2}{\overset{k_2}{\rightleftharpoons}} \mathrm{HSP{:}HSF}, && \text{(r7)}\\
\mathrm{HSP} &\xrightarrow{k_9} \emptyset, && \text{(r8)}\\
\mathrm{HSP{:}S} &\xrightarrow{k_{10}} \mathrm{HSP} + \mathrm{P}, && \text{(r9)}\\
\mathrm{P} &\xrightarrow{k_{11}^{\mathrm{T}}} \mathrm{S}, && \text{(r10)}\\
\mathrm{mRNA} &\xrightarrow{k_4} \mathrm{mRNA} + \mathrm{HSP}, && \text{(r11)}\\
\mathrm{mRNA} &\xrightarrow{k_5} \emptyset. && \text{(r12)}
\end{aligned}
$$

Table 3.3.1: The HSR biochemical reactions network. There are 16 reactions in total, as reactions (r1)–(r12) are reversible; l_i $(i = 1, 2, 6, 7)$ denotes reverse reaction rate constant. The T superscript denotes a temperature dependence.

$$
\begin{aligned}
\mathrm{P_{tot}} &= \mathrm{P}(t) + \mathrm{S_{tot}}(t),\\
&\quad \text{where } \mathrm{S_{tot}}(t) = \mathrm{S}(t) + \mathrm{HSP{:}S}(t), && \text{(c1)}\\
\mathrm{HSF_{tot}} &= \mathrm{HSF}(t) + \mathrm{HSP{:}HSF}(t) + 3 \cdot \mathrm{HSF_3}(t) +\\
&\quad + 3 \cdot \mathrm{HSE{:}HSF_3}(t), && \text{(c2)}\\
\mathrm{HSE_{tot}} &= \mathrm{HSE{:}HSF_3}(t) + \mathrm{HSE}(t). && \text{(c3)}
\end{aligned}
$$

Table 3.3.2: Mass conservation laws in the HSR biochemical reactions network. Neither concentrations nor molecules numbers are annotated because Eqs (c1)–(c3) hold for all $t \geq 0$ in both deterministic and stochastic models.

	Description	Value
HSP	free HSP	0.309
HSF	HSF monomers	0.151
S	substrate (denatured/misfolded protein)	0.113
HSP:HSF	HSP:HSF interacting complexes	2.588
HSP:S	HSP:substrate complexes	1.126
HSF_3	active HSF (trimer form)	0.044
HSE	free HSE	0.957
$HSE:HSF_3$	bound HSE	0.043
mRNA	HSP mRNA	0.115
P	native proteins (denaturation susceptible)	8.761

Table 3.3.3: Description of variables used in the HSR model, together with initial conditions for the deterministic version. These are a steady state concentrations in a non stressed cells ($T = 37°C$; see text for detail). Values are given in *arbitrary scale* molar concentration (a.s.M), as they are arbitrarily scaled with respect to each other to match numerical simulations presented by Szymańska and Żylicz (2009).

	Rate constant of...	Value
k_1	HSP:substrate association	0.42
l_1	HSP:substrate dissociation	0.005
k_2	HSP:HSF association	0.42
l_2	HSP:HSF dissociation	0.005
k_3	HSF trimers association (activation)	0.023
l_3	HSF trimers dissociation (inactivation)	0.00575
k_4	HSP translation	0.035
k_5	HSP mRNA degradation	0.013
k_6	HSP:HSF dissociation and HSP:substrate association	0.023
l_6	HSP:substrate dissociation and HSP:HSF association	0.00036
k_7	$HSE:HSF_3$ association	0.035
l_7	$HSE:HSF_3$ dissociation	0.035
k_8	HSP mRNA transcription	0.035
k_9	HSP degradation	0.013
k_{10}	misfolded protein refolding (substrate degradation)	0.014
k_{11}^{T}	protein misfolding (substrate production)	Eq. (3.6)

Table 3.3.4: HSR model parameters. All values, except for k_5 are taken directly from the Szymańska and Żylicz (2009) model. Note that all mass action rate constants (i.e. k_i and l_j) have units $\mathrm{min}^{-1}\,(\mathrm{a.s.M})^{-\mathrm{rank}(R_m)+1}$ (cf. Eq. (2.2); concentrations are given in arbitrary scale).

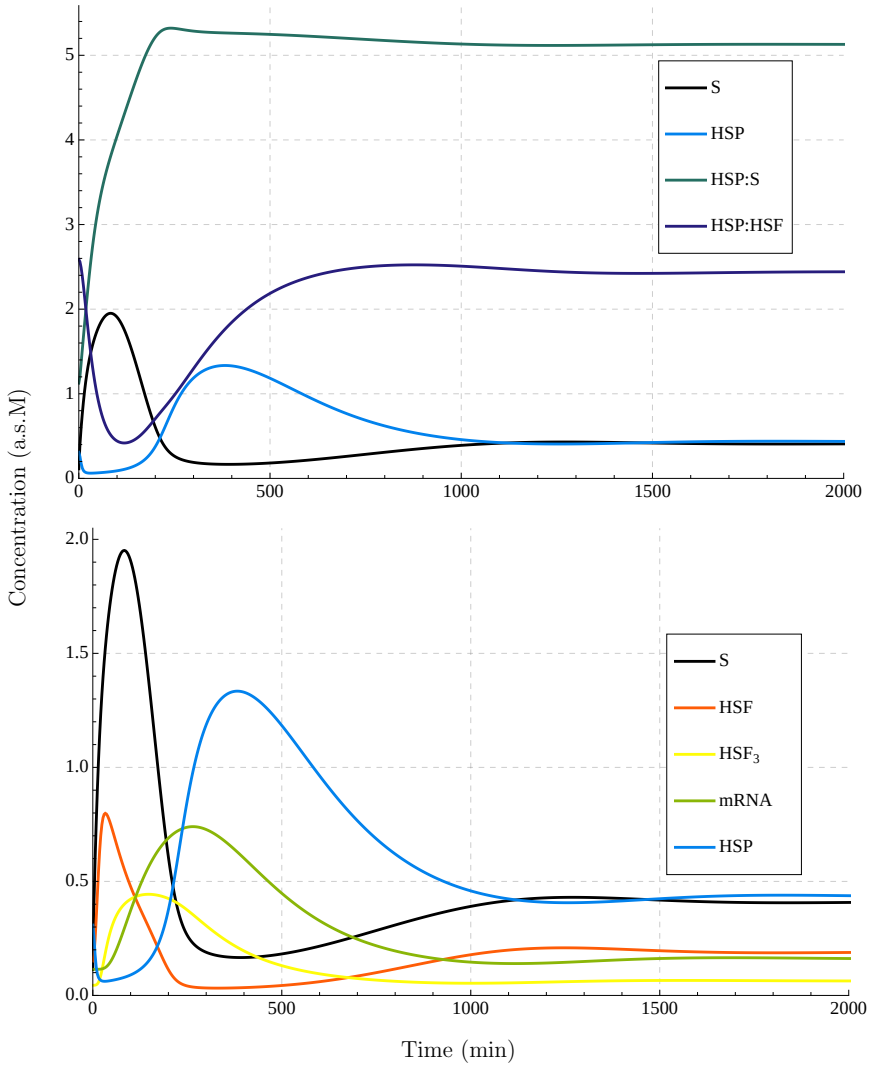

Figure 3.3.2: Numerical simulations of the HSR RRE model for a constant 42°C heating strategy. Simulation starts at a 37°C steady state.The upper plot depicts HSP response to the temperature-stimulated inflow of denatured proteins S (substrate). Free substrate is instantaneously bound into a HSP:S complex. Insufficient amount of free HSP causes its extraction from the HSP:HSF complex, forming an initiative response of the cell. Released in exchange HSF induces adaptive production of HSP molecules to complement its deficiency as indicated by accumulation of S, with peak at ca. 100 min. The excess of new HSP is used to inhibit HSF activity. System stabilises after ca. 30 h with most of constantly inflowing S secured in the HSP:substrate complexes.The lower plot depicts the adaptive HSP production, stimulated by HSF. It trimerises and initiate HSE transcription to mRNA, and its translation to HSP, as visible by the shifted activity of subsequent components.

3.3.3 Results and Discussion

We start with analysis of the rate constant of the substrate production k_{11}^{T}. To that end, we estimate a global function of a level of protein denaturation $V_{\mathrm{den}}(\mathrm{T})$ and we derive a correct dependence of k_{11}^{T} on the $V_{\mathrm{den}}(\mathrm{T})$ (cf. reaction (r10) in Table 3.3.1). Next, we give a stochastic extension of the model, compare it with the deterministic version, and we propose an approximate strategy for the stochastic perturbation of temperature. Equipped we these tools, we comparatively quantify the thermotolerance phenomenon in both types of models. Finally, we give a proof of concept quantification of an effect of combining hyperthermia with cytotoxic inhibition of denatured proteins refolding.

Rate constant of the protein denaturation

The level of protein denaturation as a function of temperature of heat shock and the localisation of denaturation within a cell have been studied by Lepock et al. (1993). The obtained, unit less dependence on the temperature, in 30–100°C range, is well approximated by the switch-like Hill function:

$$V_{\mathrm{den}}(\mathrm{T}) := 1 - \frac{1}{1 + \left(\frac{\mathrm{T}-\mathrm{T}_0}{\mathrm{T}_{0.5}-\mathrm{T}_0}\right)^{n_{\mathrm{T}}}}, \tag{3.5}$$

where T_0 and $\mathrm{T}_{0.5}$ are temperatures for which $V_{\mathrm{den}}(\mathrm{T})$ is equal to 0 and 0.5 respectively, and n_{T} is the steepness parameter. This is a different function than the function originally proposed by Peper et al. (1998), and recently reused in several works (Szymańska and Żylicz, 2009; Petre et al., 2010; Mizera and Gambin, 2010). We have chosen this form of the $V_{\mathrm{den}}(\mathrm{T})$ function over the previously proposed one because this model not only better describes experimental data of Lepock et al. (1993) for a local temperature range 37–45°C, as considered by Peper et al. (1998), but it also explains the global sigmoidal form of the level of protein denaturation for 30–100°C(see below for details).

For a given T we have:

$$k_{11}^{\mathrm{T}} = m_{11} \times \frac{V_{\mathrm{den}}(\mathrm{T})}{1 - V_{\mathrm{den}}(\mathrm{T})}, \tag{3.6}$$

where $m_{11} \approx k_{10}$, i.e. m_{11} is well approximated by k_{10} — the kinetic constant of a denatured protein refolding (reaction (r9)). Again, this is a different form of the denaturation rate $Q_{\mathrm{den}}^{\mathrm{T}}(t) = k_{11}^{\mathrm{T}} \cdot \mathrm{P}(t)$ than in previous models. In these models k_{11}^{T} depends linearly on $V_{\mathrm{den}}(\mathrm{T})$, which results in inconsistency in the physical units. We think that Eq. (3.6) expresses a correct dependence of the misfolding rate on the denaturation level (Eq. (3.6) is justified in details in the following paragraphs). Finally, from Eqs (3.5) and (3.6), we get the following formula for the denaturation rate constant:

$$k_{11}^{\mathrm{T}} \approx k_{10} \times \left(\frac{\mathrm{T} - \mathrm{T}_0}{\mathrm{T}_{0.5} - \mathrm{T}_0} \right)^{n_{\mathrm{T}}} \quad \mathrm{min}^{-1}. \tag{3.7}$$

Function of the level of protein denaturation

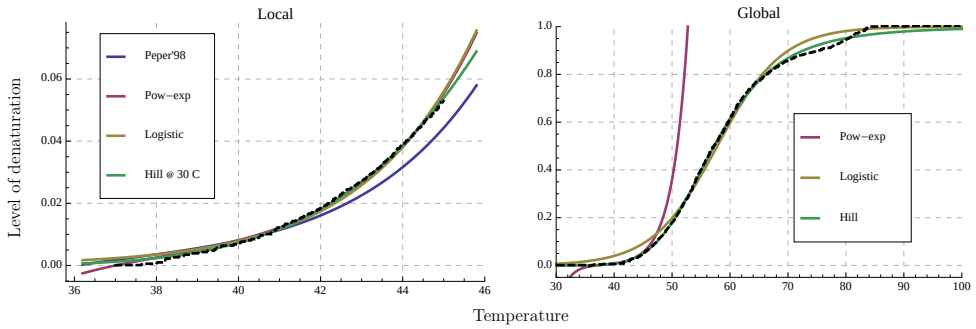

Figure 3.3.3: Model selection of a level of protein denaturation. Local and global data points were read from Lepock et al. (1993, Figure 8B and Figure 8A respectively; here, black dashed lines). Visually, the locally fitted functions are indistinguishable, but for the global fit only the Hill function model is able to reproduce both the sigmoidal shape and its steepness. For comparison we also present an instance of the local power-exponential model used by Peper et al. (1998, $a = 0.003$, $b = 0.4$, $c = 1.4$; cf. Table 3.3.5).

Peper et al. (1998) mistake was expressing k_{11}^{T} directly as $V_{\mathrm{den}}(\mathrm{T})$, and eventually obtaining the time-independent rate of protein misfold-

ing $V_{\mathrm{den}}(\mathrm{T}) \cdot \mathrm{P}$, which is incorrect (cf. Eq. (2.1)). Moreover, the power-exponential model proposed for $V_{\mathrm{den}}(\mathrm{T})$ by Peper et al. (1998) does not explain the global form of the temperature-dependent level of protein denaturation (cf. Figure 3.3.3). Therefore, we performed both local and global model selection for the original Lepock et al. (1993) experimental data, comparing the aforementioned power-exponential model with sigmoidal shaped logistic and Hill functions. Model selection results are presented in Table 3.3.5 and depicted in Figure 3.3.5. For our HSR model adaptation we have chosen the Hill function (Eq. (3.5)) with $\mathrm{T}_0 = 30°\mathrm{C}$, $\mathrm{T}_{0.5} = 56.5°\mathrm{C}$ and $n_{\mathrm{T}} = 5$. Nota bene, the Hill is well known in pharmacology, from the analysis of drug–response relationships (see, e.g., Goutelle et al., 2008), as well as in mechanistic modelling of biochemical reactions (cf., e.g., Eq. (3.4) or Huang and Ferrell, 1996).

Derivation of the protein denaturation rate constant

Consider the following, minimal model of protein misfolding with assumptions that the total amount of proteins susceptible to misfolding is constant and that only rate of misfolding depends on the temperature T:

$$\mathrm{P} \underset{b_1}{\overset{a_1^{\mathrm{T}}}{\rightleftharpoons}} \mathrm{S}_{\mathrm{tot}}. \tag{3.8}$$

Here, both non-negative rate constants a_1^{T} and b_1 have frequency units (min^{-1}). We consider RRE mathematical model and for sake of clarity we omit concentration notation $[\cdot]$. According to our first assumption we have:

$$\mathrm{P}\,(t) + \mathrm{S}_{\mathrm{tot}}\,(t) = \mathrm{P}_{\mathrm{tot}} \quad \mu\mathrm{M}, \text{ for all } t \geq 0. \tag{3.9}$$

After eliminating variable P using Eq. (3.9), the resulting ODE is:

$$\frac{\mathrm{d}\,\mathrm{S}_{\mathrm{tot}}(t)}{\mathrm{d}\,t} = a_1^{\mathrm{T}} \cdot (\mathrm{P}_{\mathrm{tot}} - \mathrm{S}_{\mathrm{tot}}\,(t)) - b_1 \cdot \mathrm{S}_{\mathrm{tot}}\,(t) \qquad \frac{\mu\mathrm{M}}{\mathrm{min}}. \tag{3.10}$$

By putting in Eq. (3.10) the steady state assumption $\mathrm{d}\,\mathrm{S}_{\mathrm{tot}}/\mathrm{d}\,t = 0$ and by additionally assuming that at least one of the rate constants is positive,

Model: $V_{\mathrm{den}}(\mathrm{T})$	**Local**: $\mathrm{T} \in [37, 45]$ Parameters	**BIC**	**Global**: $\mathrm{T} \in [30, 100]$ Parameters	**BIC**
Power-exp @ 37°C: $\mathbf{a}\left(\mathbf{1} - \mathbf{b}/\mathrm{e}^{(\mathrm{T}-\mathbf{37})}\right)\mathbf{c}^{(\mathrm{T}-\mathbf{37})}$ ↗ in $[a\,(1-b)\,, \infty)$ for $\mathrm{T} \in [37, \infty)$	$a = 0.00278$ $b = 1$ (max) $c = 1.454$	-4618	n/a	
Logistic: $\mathbf{1}/\left(\mathbf{1} + \mathrm{e}^{-(\mathrm{T}-\mathbf{h})/\mathbf{n}}\right)$ ↗ in $(0, 1)$ for $\mathrm{T} \in (-\infty, \infty)$	$h = 52.025$ $n = 2.486$	-4290	$h = 57.803$ $n = 5.588$	-4225
Hill: $\mathbf{1} - \mathbf{1}\Big/\left(\mathbf{1} + \left(\frac{\mathrm{T}-\mathbf{d}}{\mathbf{h}-\mathbf{d}}\right)^{\mathbf{n}}\right)$ ↗ in $[0, 1)$ for $\mathrm{T} \in [d, \infty)$	$d = 34.563$ $h = 60.448$ $n = 3.180$	-5336	$d = 30$ (min) $h = 57.253$ $n = 4.914$	-5665
Hill @ 30°C (global): as above for $\mathbf{d = 30}$	$h = 56.484$ $n = 5.042$	-4935	—	

Table 3.3.5: Model selection of a level of protein denaturation. The power-exponential model is not applicable in the global case, because its values quickly escape to the infinity with increasing temperature values. The globally well-defined logistic function model has the worst score both globally and locally (highlighted). Hill function is our function of choice for denaturation level of proteins. Even the globally constrained version (with $d = 30$), has better score than the power-exponential model (highlighted). However, in all cases a fit is so good, that a reduction of a number of parameters for extreme values (i.e. $b = 1$ in power-exponential model and $d = 30$ in Hill model global fit) has a marginal influence on the BIC score (not shown; cf. Eq. (2.11)). Local and global fit BIC scores were calculated for 422 and 966 data points respectively.

we get the amount of denatured proteins in a steady state $\mathrm{S}^{\mathrm{T}}_{\mathrm{tot}*}$, i.e.:

$$\mathrm{S}^{\mathrm{T}}_{\mathrm{tot}*} = \frac{a_1^{\mathrm{T}}}{a_1^{\mathrm{T}} + b_1} \cdot \mathrm{P}_{\mathrm{tot}} \quad \mu\mathrm{M}. \tag{3.11}$$

On the other hand, we have a function of a fraction of denatured proteins $V_{\mathrm{den}}(\mathrm{T}) \in [0, 1]$, taken of all denaturation-susceptible proteins at the steady state , i.e.:

$$\mathrm{S}^{\mathrm{T}}_{\mathrm{tot}*} = V_{\mathrm{den}}(\mathrm{T}) \cdot \mathrm{P}_{\mathrm{tot}} \quad \mu\mathrm{M}. \tag{3.12}$$

From both Eqs (3.11) and (3.12), it follows that, for $V_{\mathrm{den}}(\mathrm{T}) \in [0, 1)$, the temperature-dependent misfolding rate constant a_1^{T} in the minimal model of protein misfolding (Eq. (3.8)), satisfies:

$$a_1^{\mathrm{T}} = \frac{V_{\mathrm{den}}(\mathrm{T})}{1 - V_{\mathrm{den}}(\mathrm{T})} \cdot b_1 \quad \mathrm{min}^{-1}. \tag{3.13}$$

For $V_{\mathrm{den}}(\mathrm{T}) = 1$, i.e. for $\mathrm{S}^{\mathrm{T}}_{\mathrm{tot}*} = \mathrm{P}_{\mathrm{tot}}$, we have $b_1 = 0$ and a_1 can have any positive value (note that for $V_{\mathrm{den}}(\mathrm{T}) = 0$ the situation is inverse).

Relating above derivation to our HSR model (cf. reactions (r9) and (r10)), we have $a_1^{\mathrm{T}} = k_{11}^{\mathrm{T}}$. Intuitively, assuming that $\mathrm{S}^{\mathrm{T}}_{\mathrm{tot}*}/\mathrm{HSP{:}S}^{\mathrm{T}}_{*} < \epsilon$, we can roughly identify the refolding reaction in the minimal model with the reaction (r9) and say that $b_1 \approx k_{10}$. To formalise this intuition consider the following, extended model of protein refolding, under the same assumptions as for the minimal model (see Eq. (3.8)):

$$\mathrm{P} \xrightarrow{a_1^{\mathrm{T}}} \mathrm{S1} \underset{b_2^{\mathrm{T}}}{\overset{a_2^{\mathrm{T}}}{\rightleftharpoons}} \mathrm{S2} \xrightarrow{b_1} \mathrm{P}, \tag{3.14}$$

The interpretation for our HSR model (see Table 3.3.1) is the following: $\mathrm{S1} = \mathrm{S}$, $a_1^{\mathrm{T}} = k_{11}^{\mathrm{T}}$ (reaction (r10)), $b_1 = k_{10}$ (reaction (r9)), and $\mathrm{S2} = \mathrm{HSP{:}S}$, $a_2^{\mathrm{T}} = k_6 \cdot \mathrm{HSP{:}HSF}^{\mathrm{T}}_{*}$, $b_2^{\mathrm{T}} = l_6 \cdot \mathrm{HSF}^{\mathrm{T}}_{*}$ (reaction (r1)). Note that although we explicitly assumed that only a_1^{T} constant is temperature-dependent, a correct steady-state interpretation for HSR model requires to put temperature dependence on all reaction rate constants, which depend on the HSR species steady state values.

With $\mathrm{S}_{\mathrm{tot}} = \mathrm{S1} + \mathrm{S2}$, and the Eq. (3.9)-based elimination, we now have

two ODE:

$$\frac{\mathrm{d}\,\mathrm{S1}(t)}{\mathrm{d}\,t} = a_1^{\mathrm{T}} \cdot (\mathrm{P_{tot}} - \mathrm{S_{tot}}\,(t)) - a_2^{\mathrm{T}} \cdot \mathrm{S1}\,(t) + b_2^{\mathrm{T}} \cdot \mathrm{S2}\,(t)\,, \tag{3.15}$$

$$\frac{\mathrm{d}\,\mathrm{S1}(t)}{\mathrm{d}\,t} = a_2^{\mathrm{T}} \cdot \mathrm{S1}\,(t) - b^{\mathrm{T}} \cdot \mathrm{S2}\,(t)\,. \tag{3.16}$$

where $b^{\mathrm{T}} = b_1 + b_2^{\mathrm{T}}$. Analogously to previous derivation, we consider now a steady state, in which, from sum of Eqs (3.15) and (3.16), and directly from Eq. (3.16) we get, respectively:

$$0 = a_1^{\mathrm{T}} \cdot (\mathrm{P_{tot}} - \mathrm{S_{tot}}_*) - b_1 \cdot \mathrm{S2}_*, \tag{3.17}$$

$$\mathrm{S_{tot}}_* = \left(1 + \frac{b^{\mathrm{T}}}{a_2^{\mathrm{T}}}\right) \cdot \mathrm{S2}_*. \tag{3.18}$$

Eliminating $\mathrm{S2}_*$ from Eq. (3.17), using Eq. (3.18) and combining with Eq. (3.12), we get:

$$a_1^{\mathrm{T}} = \frac{V_{\mathrm{den}}(\mathrm{T})}{1 - V_{\mathrm{den}}(\mathrm{T})} \cdot b_1 \left(\frac{a_2^{\mathrm{T}}}{b^{\mathrm{T}} + a_2^{\mathrm{T}}}\right) \quad \mathrm{min}^{-1}. \tag{3.19}$$

In HSR model terms Eq. (3.19) is equivalent to Eq. (3.6), where

$$m_{11} = k_{10} \left(\frac{a_2^{\mathrm{T}}}{b^{\mathrm{T}} + a_2^{\mathrm{T}}}\right) \quad \mathrm{min}^{-1}.$$

Finally, assuming $\mathrm{S1}_*^{\mathrm{T}}/\mathrm{S2}_*^{\mathrm{T}} < \epsilon$, from Eq. (3.18) we get:

$$\frac{1}{\epsilon + 1} < \frac{a_2^{\mathrm{T}}}{b^{\mathrm{T}} + a_2^{\mathrm{T}}} \leq 1,$$

and, in fact, the multiplicative constant m_{11} in Eq. (3.19) approximates k_{10} (from below), if, for all T, $\mathrm{S}_*^{\mathrm{T}}/\mathrm{HSP{:}S}_*^{\mathrm{T}} < \epsilon$ (cf. Eq. (3.13) and the $b_1 \approx k_{10}$ intuition which we started this derivation with). In other words, if in any temperature in a steady state vast majority of the substrate is bound by HSP, then $m_{11} \approx k_{10}$. We found this assumption valid in our HSR model for investigated temperature range of 37–43°C(data not shown).

For a stochastic model we used the scaling coefficient δ which relates concentrations in the deterministic model to number of molecules in the stochastic model. Value of δ corresponds to a number of molecules per one unit of concentration, i.e. $\delta\,[S] = \#S$. It is equivalent to considering approximate stochastic model of packs of $N_\mathrm{A} \cdot |V|/\delta$ molecules as a single molecule (cf. Eq. (1.1)). Given HeLa cell volume of circa 2500 $\mu\mathrm{m}^3 = 2.5 \cdot 10^{-18}$ dm^3 (Milo et al., 2010), we have that for $\delta \approx 1.5 \cdot 10^6$ the stochastic model is accurate. We adjust reactions propensity constants according to Eq. (2.7), where $N_\mathrm{A} \cdot |V| = \delta$.

We find that for $\delta = 100$ the RRE model is in a good agreement with the stochastic variant for both 37°C and 42°C. Visual comparison of ODE and stochastic simulations is presented in Figure 3.3.4. Table 3.3.6 presents comparison of stochastic mean value with RRE values (cf. Eq. (2.6)) for $\delta = 100, 1000$. Sources of stochastic model error are two-fold: the rounding errors due to the molecules packaging and the propensity constants approximations, especially for the only reaction with $\mathrm{rank}\,(R_m) > 1$, i.e. the HSF trimerisation. Although, for $\delta = 1000$ the relative error in steady state is ca. 10 times lower, the stochastic simulation paths, and thus their running time, are over 10 times longer (data not shown). We find $\delta = 100$ to be a good compromise between accuracy and efficiency for our proof-of-concept case study.

Mean value of amount of each species was estimated using the confidence interval APMC method to verify the reward-based property:

$$\mathrm{R}_{\{\#S=?\}}\,(\mathrm{I} = \text{burn-in time})\,,$$

where $\#S$ reward for each species S is defined as:

`rewards "`$\#S$`" true :` S`; endrewards`

We start the stochastic process with a single point distribution, according to RRE values (cf. Figure 3.3.4), thus the burn-in time, which we assumed 1000 min for T = 37°C and 2000 min for T = 42°C.

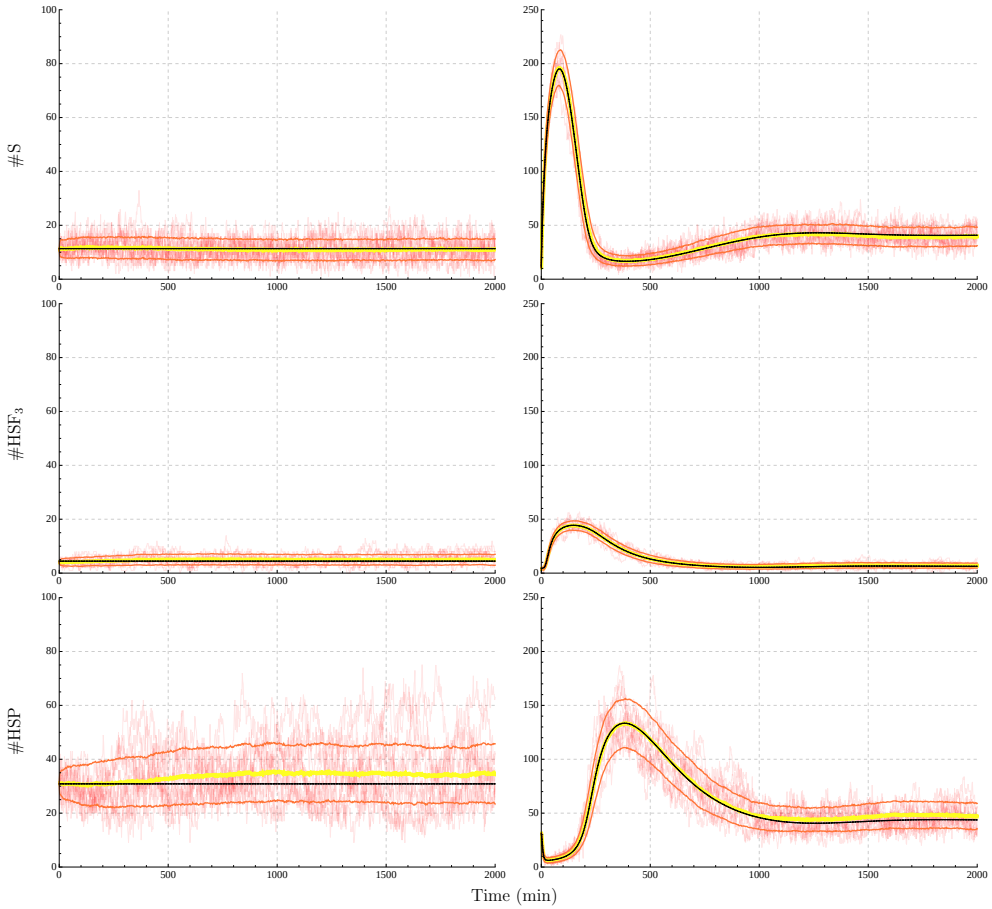

Figure 3.3.4: Comparison of the stochastic simulations with respect to ODE' numerical solutions for the HSR model. Both homeostasis (left column) and heat shock (right column) conditions are compared. Each plots shows 10 sample stochastic trajectories, estimated mean $+/-$ standard deviation of a sample of 10^3 stochastic simulations, and an ODE numerical solution (black). Here, we assumed 100 molecules per unit of concentration, i.e. $\delta = 100$.

The *variance-to-mean ratio*:

$$\mathrm{VMR}\,(X) = \frac{\mathrm{Var}\,(X)}{\mathbb{E}\,(X)}$$

quantifies noise of a species amount variable $X = \#S$ at a fixed time point in the stochastic model, with respect to the Poisson birth-death process (see, e.g., Wilkinson, 2011). The estimated steady state values of VMR are significant for some of the crucial species, both for the state of

Relative error +/− 95% confidence interval in %

Species	Homeostasis		Heat shock	
	δ=100	δ=1000	δ=100	δ=1000
HSP	12.5 +/− .68	1.31 +/− .19	8.4 +/− .55	0.83 +/− .16
HSF_3	12.1 +/− .86	1.45 +/− .26	9.4 +/− .75	0.71 +/− .23
HSP mRNA	12.1 +/− .79	1.23 +/− .24	8.8 +/− .67	0.79 +/− .21
HSE:HSF_3	11.4 +/− .87	1.37 +/− .26	8.5 +/− .74	0.86 +/− .23
HSF	6.9 +/− .72	0.88 +/− .24	5.1 +/− .68	0.76 +/− .23
substrate	2.5 +/− .69	0.34 +/− .22	2.9 +/− .44	0.33 +/− .14
HSP:HSF	1.6 +/− .06	0.21 +/− .02	1.8 +/− .09	0.21 +/− .03
HSE	0.6 +/− .04	0.06 +/− .01	0.5 +/− .05	0.05 +/− .01
HSP:substrate	0.1 +/− .17	0.04 +/− .05	0.1 +/− .05	0.01 +/− .02

Table 3.3.6: Estimates of a relative error of each species mean value with respect to its RRE value, i.e. $|\mathbb{E}(\#S) - [S]|/[S]$; values are given in percent. Relative errors were calculated in homeostasis ($\mathsf{T} = 37°\mathrm{C}$) and the heat shock steady state ($\mathsf{T} = 42°\mathrm{C}$), for two scaling coefficient δ values. Species are sorted according to error values in homeostasis; from the least to the most consistent with the RRE solutions. Steady state mean values were estimated using APMC with 10^4 independent simulation samples for each species.

VMR +/− 95% confidence interval

Species	Homeostasis	Heat shock
HSP	3.05 +/− 0.65	3.14 +/− 0.74
HSF	2.41 +/− 0.35	2.21 +/− 0.40
HSP mRNA	1.68 +/− 0.29	1.60 +/− 0.34
substrate	1.19 +/− 0.24	2.32 +/− 0.53
HSE:HSF_3	0.81 +/− 0.12	0.85 +/− 0.14
HSP:substrate	0.78 +/− 0.55	0.57 +/− 0.77
HSF_3	0.78 +/− 0.12	0.79 +/− 0.15
HSP:HSF	0.27 +/− 0.46	0.38 +/− 0.60
HSE	0.10 +/− 0.11	0.03 +/− 0.13

Table 3.3.7: Estimates of VMR for each species in homeostasis ($\mathsf{T} = 37°\mathrm{C}$) and the heat shock steady state ($\mathsf{T} = 42°\mathrm{C}$). VMR estimates were calculated for δ=100. Species are sorted according to the VMR values in homeostasis; from the most to the least disperse. Dashed, vertical line separates the over-dispersed and under-dispersed variables, with respect to the Poisson distribution. The dispersion doesn't change much with temperature, except for the substrate (highlighted). Mean and variance values were estimated using APMC with, respectively, 10^4 and $5 \cdot 10^4$ independent simulation samples for each species.

homeostasis and the steady state during the heat shock (see Table 3.3.7).

The steady state amount of substrate, HSP, HSF and HSP mRNA is over-dispersed with respect to the Poisson distribution, indicating their high stochasticity in our model. In general noise of the species amounts increases for the higher temperature parameter value: mean VMR in homeostasis is 1.23, whilst in the 42°C heat shock 1.32 (ca. 7.5% higher; see Table 3.3.7). This is only due to the almost two-fold increase in the substrate noise (highlighted). Note however, that although the number of HSP:substrate complexes, similarily to substrate amount, significantly increased during the heat shock steady state (cf. Figure 3.3.2), its noise has decreased by ca. 27%.

On a technical note, it is impossible to query for central moments in PRISM in a single run. Therefore, the variance value of amount of each species was estimated from the unbiased mean value and second moment estimators, i.e.

$$\widehat{\mathrm{Var}\,(X)} = \widehat{\mathbb{E}\,(X^2)} - \widehat{\mathbb{E}\,(X)}^2.$$

Second moment $\widehat{\mathbb{E}\,(\#S^2)}$ of species amount was estimated analogously to the mean value, using the confidence interval APMC method (see above). Having symmetric confidence intervals:

$$\mathbb{E}\,(X) \in \left(\widehat{\mathbb{E}\,(X)} - a_1, \widehat{\mathbb{E}\,(X)} + a_1\right) \quad \text{and}$$
$$\mathbb{E}\,(X) \in \left(\widehat{\mathbb{E}\,(X^2)} - a_2, \widehat{\mathbb{E}\,(X^2)} + a_2\right),$$

with α confidence level, the unbiased moments-based variance estimator $\widehat{\mathrm{Var}\,(X)}$ has an asymmetric confidence interval:

$$\begin{aligned}\underline{\mathrm{Var}\,(X)} := \left(\widehat{\mathbb{E}\,(X^2)} - a_2\right) - \left(\widehat{\mathbb{E}\,(X)} + a_1\right)^2 \\ \leq \widehat{\mathrm{Var}\,(X)} \leq \\ \left(\widehat{\mathbb{E}\,(X^2)} + a_2\right) - \left(\widehat{\mathbb{E}\,(X)} - a_1\right)^2 =: \overline{\mathrm{Var}\,(X)}.\end{aligned} \tag{3.20}$$

Analogously, for an unbiased VMR estimator $\widehat{\mathrm{VMR}\,(X)} = \widehat{\mathrm{Var}\,(X)} \Big/ \widehat{\mathbb{E}\,(X)}$,

we get asymmetric confidence interval, with α confidence level, from the following inequalities:

$$\underline{\mathrm{VMR}\,(X)} := \frac{\underline{\mathrm{Var}\,(X)}}{\widehat{\mathbb{E}\,(X)} + a_1} \leq \widehat{\mathrm{VMR}\,(X)} \leq \frac{\overline{\mathrm{Var}\,(X)}}{\widehat{\mathbb{E}\,(X)} - a_1} =: \overline{\mathrm{VMR}\,(X)}.$$

For a symmetric confidence interval with α confidence level (cf. Table 3.3.7), we simply take:

$$\widehat{\mathrm{VMR}\,(X)} \stackrel{+}{-} \max\left(\widehat{\mathrm{VMR}\,(X)} - \underline{\mathrm{VMR}\,(X)}, \overline{\mathrm{VMR}\,(X)} - \widehat{\mathrm{VMR}\,(X)}\right).$$

Approximate stochastic perturbation strategy

In our experiments we model scenarios of consecutive heat shocks imposed on the model, separated with gaps. In principle, we control time points when the heat shocks are activated or inactivated. However, to do that in a probabilistic model one have to either save the whole distribution over a possibly infinite state space or, if analysis is based solely on stochastic simulations, modify the simulation algorithm to test again a current time point and queued deterministic events. Essentially, these are solutions based on moving to a more general type of models, like the Markov decision processes, but the price to pay would be complication and impracticability of analysis (e.g., the APMC does not handle Markov decision processes).

We have thus chosen to consider heat shock as an approximate random perturbation event and, thereby to stay within the same mathematical model and seamlessly perform stochastic simulations or model checking of CTMC.

Our approach relies on introduction of the sequence of n_i-counting Poisson processes (a special case of one-dimensional CTMC), independent of other state variables. Each time i-th process reaches value n_i, it is replaced by another n_{i+1}-counting Poisson processes with rate $n_{i+1}\tau_{i+1}$, where $\tau_{i+1} = 1/(t_{i+1} - (t_i + \Delta t_i))$ is an inverse of a time gap between perturbations i and $i+1$. Because time between consecutive Poisson process events is exponentially distributed, i.e. $T_{ij} \sim \mathrm{Exp}\,(n_i\tau_i)$, the expected time for an approximate perturbation event equals to the time gap between de-

terministic perturbations time, i.e. $\mathbb{E}\left(\sum_{j=1}^{n} T_{ij}\right) = 1/\tau_i$. Moreover, due to independence of a time of occurrence of each count of the Poisson process T_{ij}, variance of the i-th perturbation event, calculated independently of prior $i-1$ perturbations, is $\mathrm{Var}\left(\sum_{j=1}^{n} T_{ij}\right) = \sum_{j=1}^{n} \mathrm{Var}\left(T_{ij}\right) = 1/n\tau_i^2$. In other words the precision of single perturbation event is linearly proportional to the number of counting levels and inverse linearly proportional to the time of its occurrence.

In PRISM modelling language we introduce two heat shock events, i.e. four temperature parameter T perturbation events, using Poisson processes with a common n levels for each parameter and an additional perturbation number counter i. Using the compositional description of variables, which represent CTMC state, and *commands*, which change CTMC state, the independent perturbation events module (i.e. not synchronised with any other commands) is defined as:

```
ctmc

// Model parameters
const double t1; // time offset for 1st heat shock
const double td1; // duration of 1st heat shock
const double t2; // time offset for second heat shock
const double td2; // duration of 2nd heat shock
const int Td; // heat shock temperature delta
const int n; // event switcher levels

module events
    i : [0..4] init 0; // number of perturbation
    ps: [0..1] init 0; // perturbation switcher
   cnt: [1..n] init 1; // actual poisson process variable

    //pre 1st heat shock
    [] i = 0 & cnt < n -> n/t1: (cnt'=cnt+1);
    [] i = 0 & cnt = n -> n/t1: (i'=1)&(ps'=1)&(cnt'=1);
    //1st heat shock
    [] i = 1 & cnt < n -> n/td1: (cnt'=cnt+1);
```

```
    [] i = 1 & cnt = n -> n/td1: (i'=2)&(ps'=0)&(cnt'=1);
    //pre 2nd heat shock
    [] i = 2 & cnt < n -> n/t2: (cnt'=cnt+1);
    [] i = 2 & cnt = n -> n/t2: (i'=3)&(ps'=1)&(cnt'=1);
    //2nd heat shock
    [] i = 3 & cnt < n -> n/td2: (cnt'=cnt+1);
    [] i = 3 & cnt = n -> n/td2: (i'=4)&(ps'=0)&(cnt'=1);
endmodule

formula T = (37+Td*ps); // temperature for misfolding rate
```

Clearly, increasing n increases the number of states of the model, and thus makes the experiments less efficient. A suitable value of the parameter n has been chosen experimentally by visual assessment of the substrate stochastic trajectories precision, taking under consideration simulations efficiency; see Figure 3.3.5 caption for details on choice of n in the HSR model.

Figure 3.3.5: Comparison of simulations of approximate perturbations in the stochastic model with respect to ODE simulations. The comparison is shown for different levels n of the independent Poisson process, which approximates the deterministic scheme of perturbations of the temperature (left column). Plots show examples of 50 stochastic simulations, and mean $+/-$ standard deviation, estimated from 1000 samples, for the temperature perturbation scheme (left column) and the substrate amount (right column). Variance of time of a temperature perturbation event T is a function of an perturbations time gap t and the precision levels n, i.e. $\mathrm{Var}\,(T) = t^2/n$. Therefore, the main time approximation error for our perturbation scheme lies within an event of the second heat shock with $t = 1200$ min (cf. left column). Note though, that errors for subsequent perturbation times accumulate, so the biggest error can be observed for the end of the second heat shock. Nevertheless, because start of the second heat shock creates high amounts of molecules in the system, it is the most error influencing event with respect to species amounts expected from the RRE numerical solutions (cf. right column). We found that for $n = 2^{13}$ the approximation of mean and standard deviation of the substrate amount in the second heat shock is in a good agreement with much more precise values in the first heat shock and with RRE solutions.

Figure on the next page.

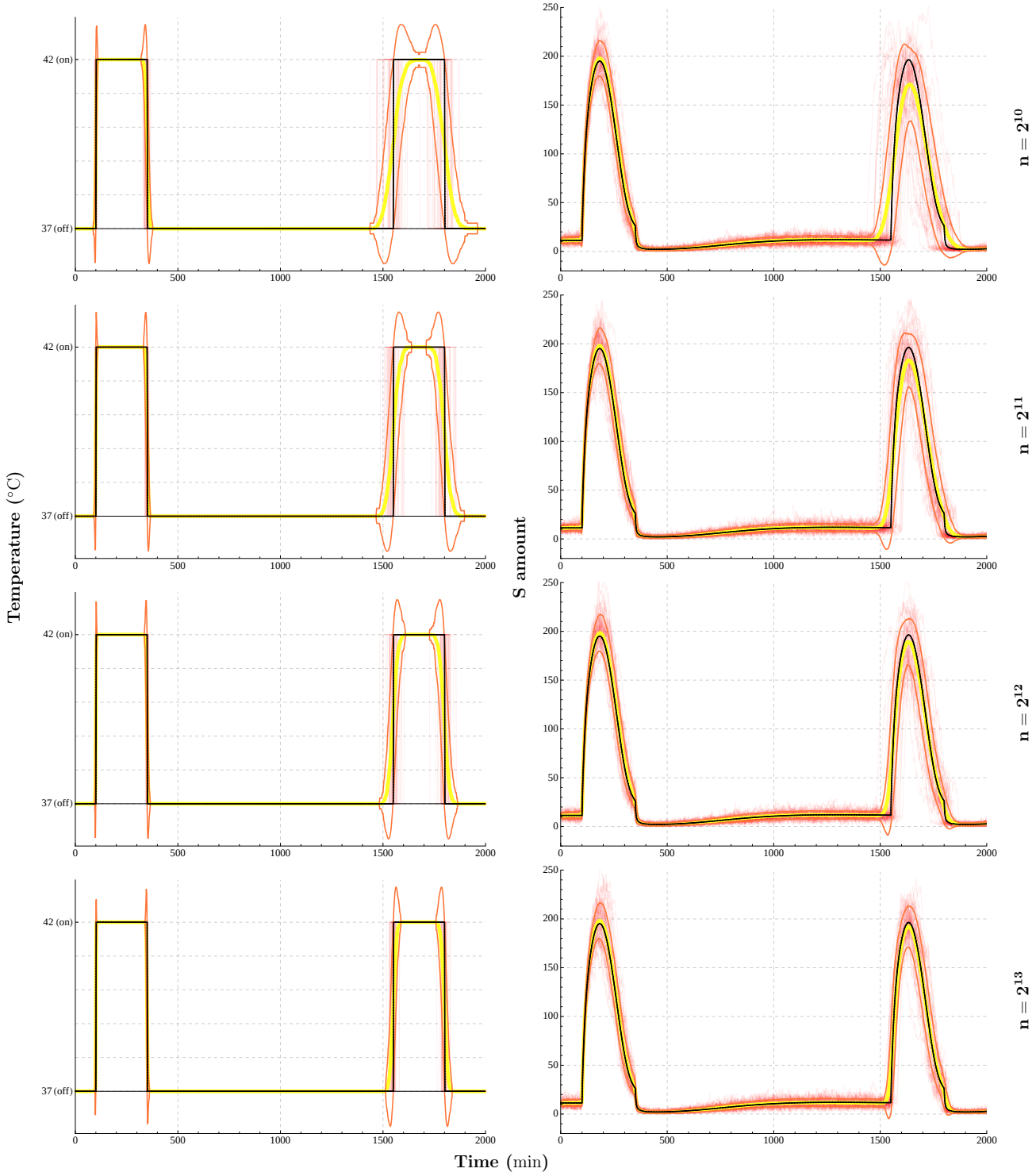
Temperature (°C)
42 (on)
37 (off)
S amount
$n = 2^{10}$
$n = 2^{11}$
$n = 2^{12}$
$n = 2^{13}$
Time (min)

Thermotolerance can be described as a desensitisation with respect to a consecutive heat shock, compared to the response to the first heat shock. In other words, thermotolerance represents a memory of the system about the first two, on and off, temperature perturbations, leading to a decreased response to the subsequent perturbation. Such system's memory is created by a propagating shift in species activity and the feedback loop of the HSR network (cf. Figure 3.3.2).

Figure 3.3.6 depicts the thermotolerance phenomena in the deterministic HSR model. Duration of the memory of the first temperature perturbation can be tracked by the activity of the HSP, as depicted in Figure 3.3.7.

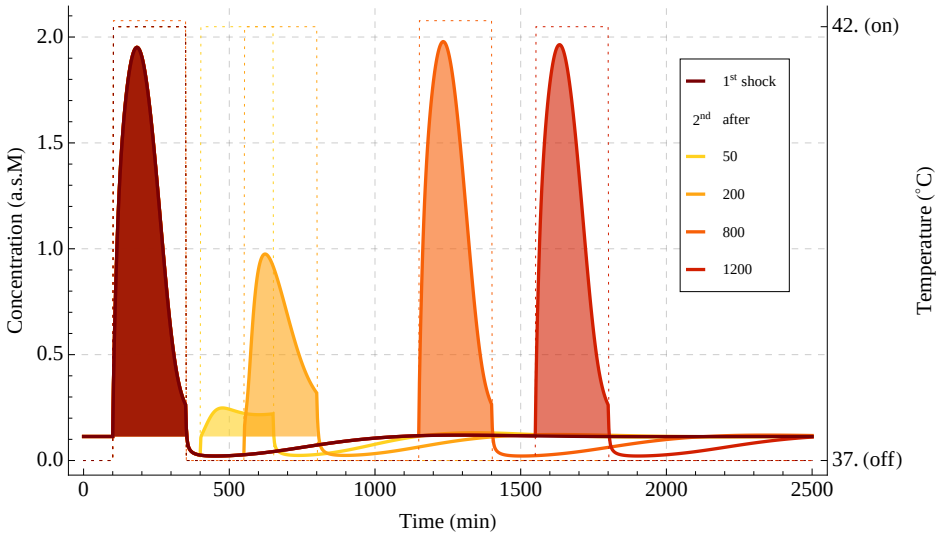

Figure 3.3.6: Thermotolerance in the heat-shock response: the substrate activity (solid) during the two consecutive heat shocks (dotted) of 5°C over the homeostatis level of 37°C. The strength of the intoxication by the substrate (coloured area) depends on the time gap between heat shocks. Interestingly, activity of the substrate in the second shock can be even higher than activity in the first shock, as shown for the time gap of 800 min.

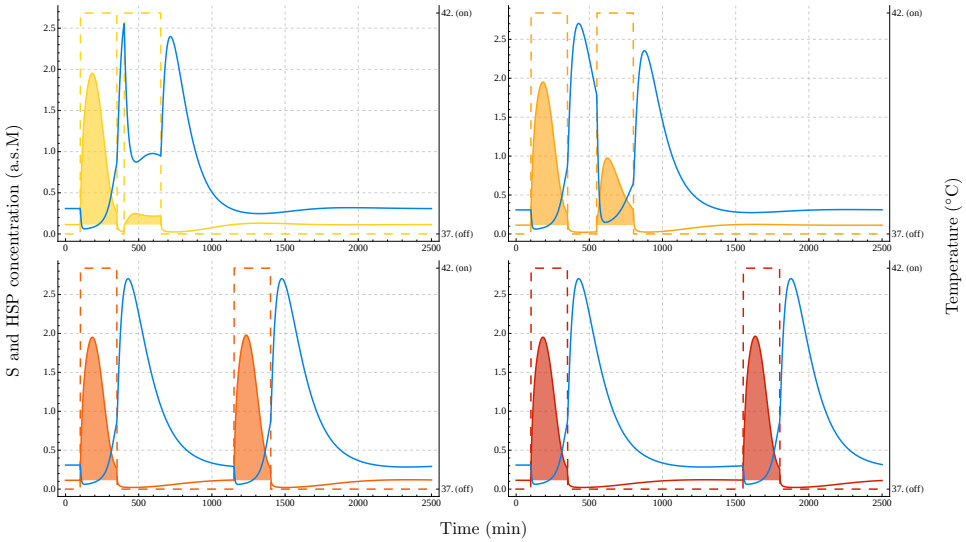

Figure 3.3.7: The substrate (coloured area) and HSP (blue line) response to the two consecutive heat shocks. Duration of the memory of the first temperature perturbation can be tracked by the activity of the free HSP. Its level at the moment when the second heat shock is induced is negatively correlated with the strength of the second response. The second response goes from almost none (upper left), through mediocre (upper right), and even over-dominating the first response (lower left), to exactly the same when the memory is lost (lower right).

We define the notion of the thermotolerance during n-th heat shock ($n > 1$) as the *desensitisation coefficient*:

$$\mathcal{D}_n = 1 - \frac{\mathcal{R}_n}{\mathcal{R}_1}, \tag{3.21}$$

where n-th response $\mathcal{R}_n$ is defined as:

$$\mathcal{R}_n = \max_{t_n < t < t_n + \Delta t_n} \{\#S(t) - \#S^*\}, \tag{3.22}$$

where $\#S^* = \mathbb{E}_\pi(\#S)$ is a mean value in a steady state π, $[t_n, t_n + \Delta t_n]$ is a heat shock duration interval, and the first response, by assumption, satisfies $\mathcal{R}_1 > 0$. Such response measure represents the toxicity of the heat shock: the higher the response the more likely the cell will die. For the deterministic model the species amount is simply a scaled value of ODE variable, corresponding to the stochastic mean value (cf. Eq. (2.6)).

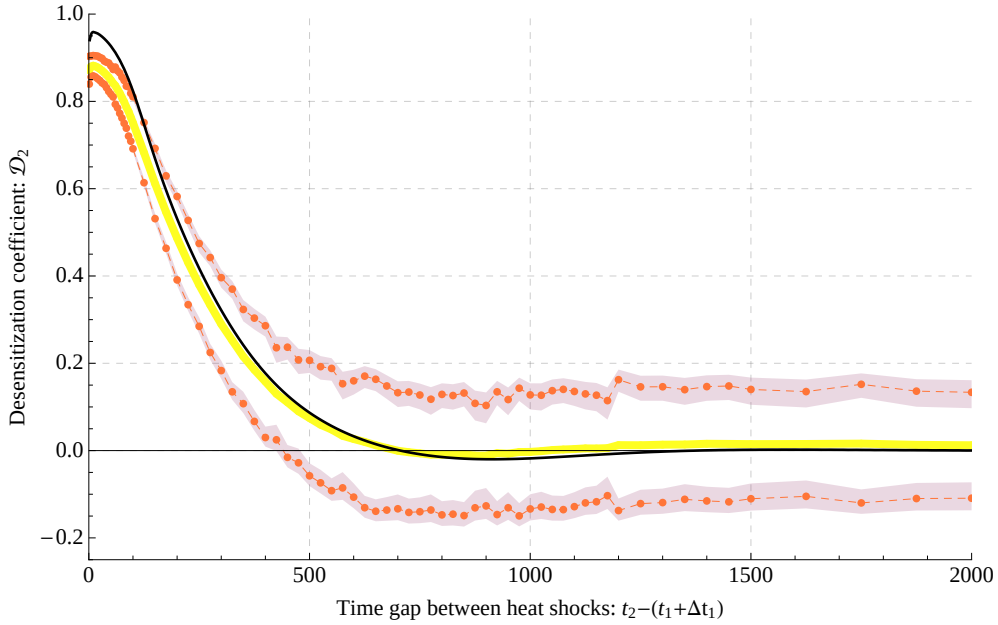

Figure 3.3.8: The desensitisation coefficient $\mathcal{D}_2$ for the substrate in the ODE model (black line) and in the CTMC, plotted against the time gap between end of the first heat shock and the beginning of the second heat shock. Duration of both heat shocks Δt_n $(n = 1, 2)$ is equal to 250 min. Memory of the first heat shock is lost when the desensitisation coefficient value stabilises around 0, which is approximately at 1400 min for both mathematical models. Mean (yellow line) and standard deviation (orange line) of $\mathcal{D}_2$ was calculated at selected time points (dots). Both estimators have a confidence interval with 95% confidence level. In case of the mean value the confidence interval width is less than $5 \cdot 10^{-3}$, whilst for the standard deviation the confidence interval is depicted as a strip. Estimators were calculated using APMC with 10^4 and $5 \cdot 10^4$ independent simulation samples for the first and the second moment respectively (see text for details).

Figure 3.3.8 depicts value of the desensitisation coefficient $\mathcal{D}_2$ for the substrate species, with respect to the time gap between heat shocks. After the first heat shock, at the time gap of the approximated memory loss, i.e. at $t = t_1 + \Delta t_1 + 1400$, system is very close to the homeostasis steady state (data not shown). The slightly positive final level of $\mathcal{D}_2$ in the stochastic model, as well as the overall difference with respect to the deterministic model may be attributed to the stochastic noise (we take maximum amount in Eq. (3.22)). Moreover, the shared initial increase of desensitisation for a time gap under 20 min may be attributed to HSF_3, HSP mRNA and HSP peaks being under 50 min (cf. Figure 3.3.7 and

Figure 3.3.2).

The $\mathcal{D}_2$ mean value for heat shocks time gap $t_1 - (t_1 + \Delta t_1)$ is estimated using the confidence interval APMC method to verify the reward-based property:

$$\phi^i := \mathrm{R}_{\{\mathcal{D}_2^i=?\}}\left(\mathrm{I} = 1.05 \cdot (t_2 + \Delta t_2)\right)$$

where for $i = 1, 2$, first and second moment $\mathcal{D}_2$ rewards are defined as:

```
rewards
    "D_2^1" true: (S_2^max − S*)/(S_1^max − S*);
    "D_2^2" true: ((S_2^max − S*)/(S_1^max − S*))^2;
endrewards
```

Here, $\mathrm{S}_i^{\max}$ is an additional stochastic model variable, which is a witness of the maximum value of the substrate variable S, during the i-th heat shock. Introduction of such variable in PRISM modelling language can be done seamlessly, i.e. without affecting the behaviour of the original CTMC. Finally, we have $\widehat{\mathbb{E}(\mathcal{D}_2)} = 1 - \phi^i$, as $\mathbb{E}(1 - X) = 1 - \mathbb{E}(X)$, and $\widehat{\mathrm{Var}(\mathcal{D}_2)} = \phi^2 - (\phi^1)^2$, as $\mathrm{Var}(1 - X) = \mathrm{Var}(X)$. The unbiased standard deviation estimator $\widehat{\mathrm{SD}(\mathcal{D}_2)} = \sqrt{\widehat{\mathrm{Var}(\mathcal{D}_2)}}$, has the following α level confidence interval:

$$\sqrt{\underline{\mathrm{Var}(X)}} \leq \widehat{\mathrm{SD}(X)} \leq \sqrt{\overline{\mathrm{Var}(X)}},$$

provided that the variance estimator's precision is high enough, i.e. $\underline{\mathrm{Var}(X)} > 0$ (cf. Eq. (3.20)).

Hyperthermia in multimodal oncological strategies

Although hyperthermia exhibits a clear cytotoxic effect its efficacy is not enough to replace any one of the established therapy modalities when applied alone, but, undoubtedly, it is suitable enough to enhance the cell-killing effect of cytotoxic drugs or radiation ("thermal chemosensitisation", "thermal radiosensitisation" Hildebrandt et al., 2002). In order

to improve the efficacy of anti-cancer therapies, it has been recently investigated how to combine different methods of cancer treatment into more effective multimodal oncological strategies. Particular attention has been paid to treatments that involve hyperthermia as an adjuvant protocol for both radio and chemotherapy. A synergistic interaction between hyperthermia and radiotherapy as well as various cytotoxic treatments has already been validated in pre-clinical studies (Wust et al., 2002). Despite clear experimental evidences the precise mechanism of these interactions is not known.

We believe that synergistic effect of hyperthermia and other cancer therapies is caused by the much higher accumulation of denatured proteins (substrate), which are deadly for cell. To give a proof-of-concept we investigate the temperature dependence of the heat-shock response as well as combined temperature and protein refolding inhibition in the deterministic HSR model.

Figure 3.3.9 depicts rate of a change of the level of heat-shock response $\mathcal{R}_1$ with respect to temperature, together with corresponding substrate activity. $\mathcal{R}_1$ is slowly reaching its limit, which is the saturation limit of S, i.e. $\mathrm{P_{tot}}$, minus the base, steady state value of S.

Figure 3.3.10 contains a contour plot of the heat-shock response $\mathcal{R}_1$ values for the combined therapy i.e. hyperthermia and potential chemotherapy. The latter is modelled as the inhibition of protein refolding reaction (r9). More precisely, inhibition is modelled as a linear scaling of the reaction rate constant, i.e. $(1 - x) \cdot k_{10}$ for $x \in [0, 1]$, where x represents inhibition level. When no drug is administrated $x = 0$ whereas in case of full inhibition $x = 1$.

Indeed, when both therapies are applied simultaneously, substrate accumulation reaches higher level than it would be possible with application of only one of the therapies. For example, to reach $\mathcal{R}_1$ level of full inhibition or the over 39.2°C heating, it is enough to heat up cell to ca. 38.5°C and combine it with inhibition of a half of the refolding rate (cf. Figure 3.3.10).

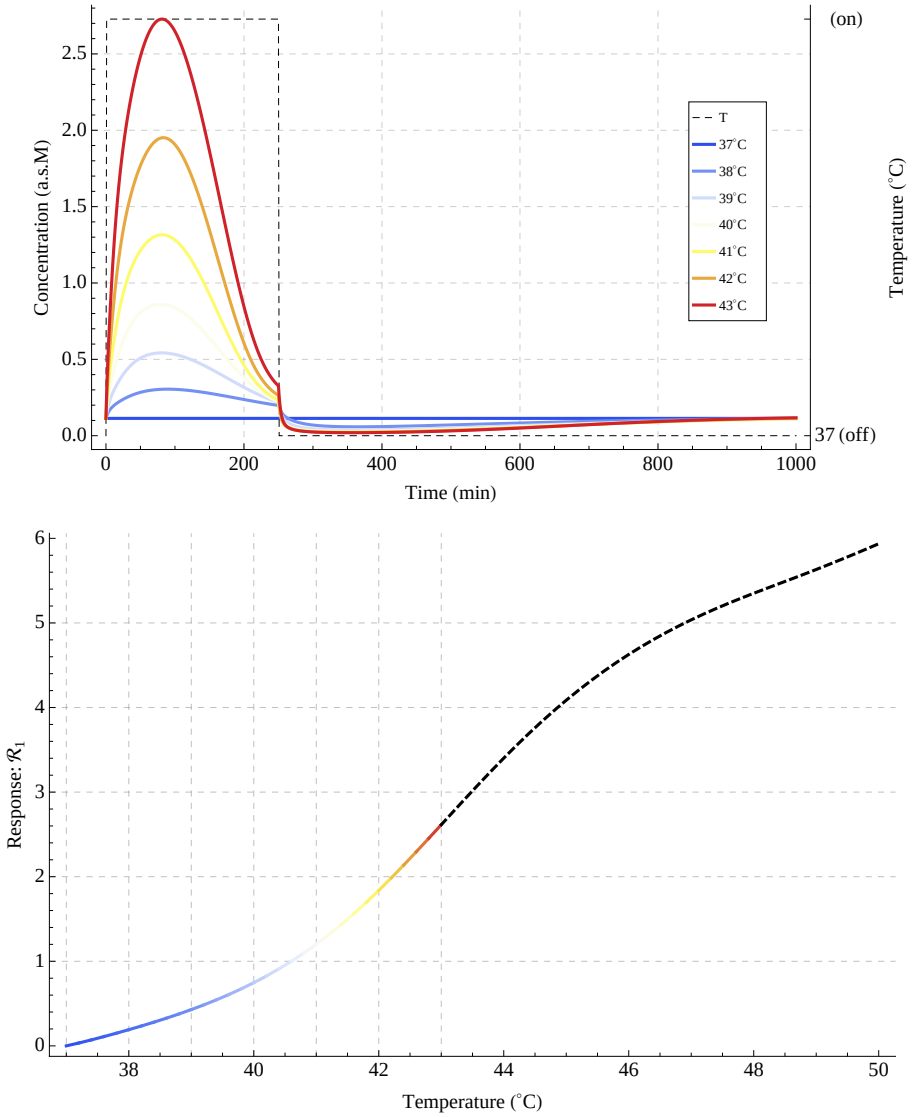

Figure 3.3.9: HSR with respect to temperature. The upper plot depicts RRE trajectory of the substrate, upon 250 min heat shock for $T = 37, \ldots, 43°\mathrm{C}$. The heat-shock response maximal level $\mathcal{R}_1$ with respect to a broader temperature range is depicted in the lower plot.

The rationale behind such a simplified modelling of the drug therapy is that anti-cancer drugs such as bortezomib inhibit proteasome which is responsible for substrate degradation (cf., e.g., Neznanov et al., 2011). Degradation of misfolded proteins is not induced by the temperature and requires assist of HSP (Wagner et al., 1994). Therefore, reaction (r9), in

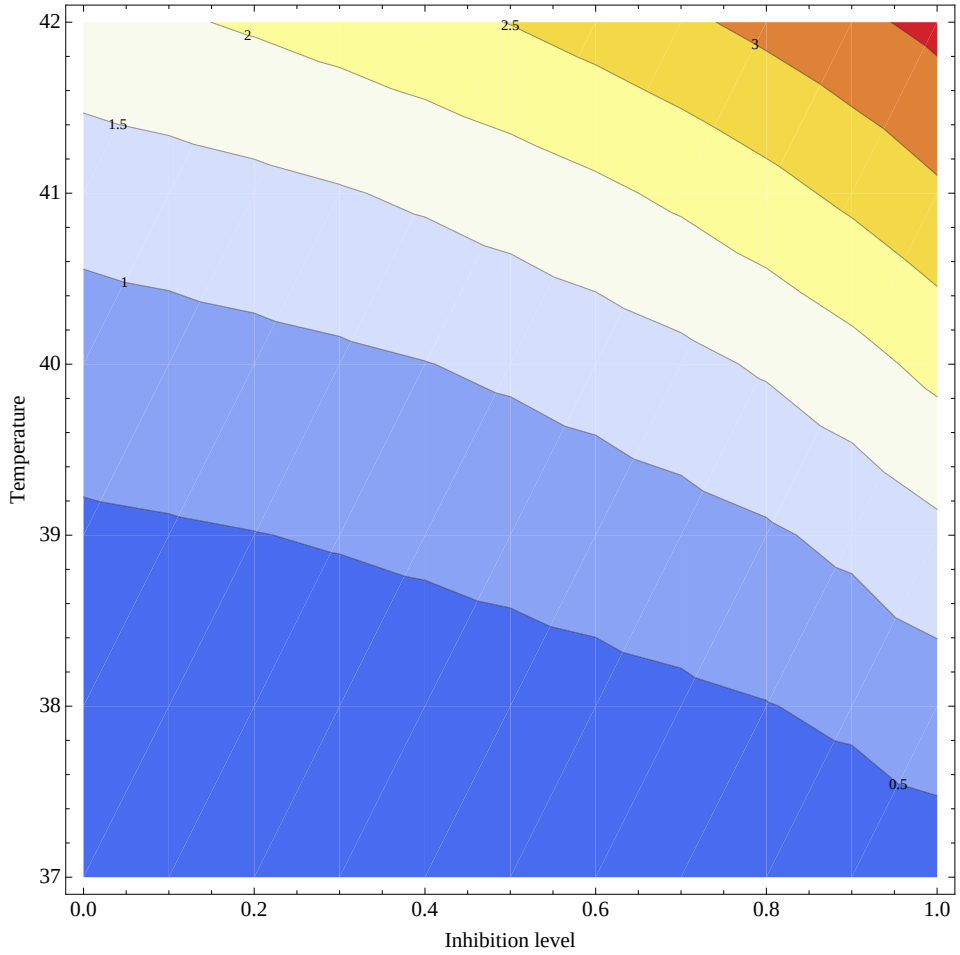

Figure 3.3.10: Contour plot of the heat-shock response level with respect to temperature (vertical axis stands for the applied temperature) and the percentage level of inhibition of the refolding reaction (r9) (horizontal axis; see text for details). Heat shock takes $\Delta t_1 = 250$ min. Level of $\mathcal{R}_1$ (Eq. (3.22)), denoted on the plot by colours from blue (the weakest) to red (the strongest), measures the toxicity of the combined therapy.

fact, represents both the S refolding and the S degradation combined with a production of a new protein P.

3.3.4 Tools and methods

We defined model using the SBML-shorthand notation. The RRE model has been numerically solved using the MathSBML package (Shapiro et al., 2004) of Mathematica software. The latter was used for creation

of most of the plots and for collection of results. To generate the PRISM model, we have used a prototype SBML translator which generates model specification in the PRISM language. Some minor adjustments, such as factorisation of parameters or accounting for mass conservation laws (c1)–(c1), have been done manually. The approximate stochastic perturbation strategy and has also been encoded manually in the PRISM model. All stochastic simulations and the confidence interval-based APMC was done using PRISM.

Success consists of going from failure to failure without loss of enthusiasm.

Winston Churchill

4 Conclusions

Mechanistic modelling is widely used in science and engineering. It provides a powerful intellectual framework for understanding and validation of the modelled phenomena. Developments in modelling of molecular biological systems are driven by the convergence of complementary approaches from many fields of science. However, bringing modelling into the mainstream of biological research still requires the development of modelling theoretical and practical frameworks, that encourage wet-lab experimentation as well as scientific collaboration and communication.

Challenges posed by biological complexity are usually, at least initially, tackled by focusing on the statistical analysis of the phenomenological data alone. Such approach may be ascribed to a general lack of useful relevant mechanistic models or suitable frameworks for their construction and analysis. Moreover, as the experimental technology continues to advance the tendency to simply measure more data to solve the problem at hand becomes more apparent. Such strategy does not enable an explana-

tion of the underlying phenomenon of interest.

Most of the kinetic models of molecular biological systems are known to be incomplete and even though they are accepted as such. It is because even very simplified model will most probably have a great value in advancing towards an understanding of the phenomena that it describes. As such, this model can provide hypothetical, explanatory solutions to the problem under consideration.

In this dissertation we evaluated methods of analysis of spatially homogeneous models of biochemical reactions networks in three case studies, related to the intracellular signalling. More specifically, in the JAK-STAT case study we evaluated usefulness of different model selection methods in a frequently encountered, but not much discussed case of a model of a considerable size, which has several variants differing at peripheries. In such situation, all considered variants can reach nearly perfect agreement with respect to their numerical simulations results and, most often, the sufficient experimental data to test against is not available. We argue that in such an adverse setting, the sensitivity and identifiability analyses, although not directly corresponding to the model selection problem, can be more informative than the representative, generalizability-based approaches to this task. An additional insight into how the responsibility for the network dynamics spreads among model parameters, enables more conscious, expert-mediated choice of the preferred model.

However, parameters sensitivity is strongly dependent on the property under examination (cf. Chen et al., 2009). In the case study of a property-specific sensitivity analysis we supported this statement with a simple example. Moreover, we showed that the marriage of model checking and sensitivity analysis seems promising as it often can yield a better understanding of the dynamics of systems to be analysed. It seems that this approach is well suited for revealing intricate and subtle dependencies in the model that may not be discovered using ODE numerical simulations and error functions based on p-norms. We suppose this technique may have interesting applications, for instance for the probabilistic abstraction, i.e. reduction of the probabilistic model which preserves properties of interest.

We demonstrated feasibility and practical potential of the PMC tech-

nique, more specifically its lesser known approximate variant, in a case study of analysis of the heat-shock response mechanism. We comparatively studied its deterministic and stochastic variants, including the investigation of the thermotolerance phenomenon. Moreover, by mechanistic modelling of HSR we were able to support the common belief that the combined cancer treatment strategies can more effectively increase cytotoxicity of denatured proteins in cancer cells than unimodal strategies.

Finally, we presented implementation of the practical analysis framework — the Tav4SB project. Tav4SB Web service provides a set of integrated tools in the domain for which Web-based applications are still not as widely available as for other areas of computational biology. Moreover, we extended the dedicated hardware base for computationally expensive task of simulating cellular models. Through this project we promote the standardisation of models and experiments as well as accessibility and usability of remote, scientific services, conforming to the "Science as a Service" idea. The main benefit of the availability of the scientific services which implement SaaS idea is that it allows a much broader community to participate in the research process. With knowledge and data distributed widely throughout the global scientific community, and with currently available possibilities to connect and to work together, construction of a rich and comprehensive picture of the machinery of life is more plausible than ever.

Abbreviations

Abbreviation	Meaning
χ^2	chi-squared.
a.s.	arbitrary scale.
AIC	Akaike information criterion.
APMC	approximate probabilistic model checking.
BF	Bayes factor.
BIC	Bayesian information criterion.
BMS	Bayesian model selection.
CME	chemical master equation.
CSL	continuous stochastic logic.
CTMC	continuous-time Markov process.
ECDF	empirical cumulative distribution function.
Epo	Erythropoietin.
FOS	first order sensitivity.
GOF	goodness of fit.
GSA	global sensitivity analysis.
HSE	heat-shock element.
HSF	heat-shock factor.
HSP	heat-shock proteins.
HSR	heat-shock response.
IA	identifiability analysis.
IFN	Interferon.
IL	Interleukin.
JAK	Janus Kinase.

Abbreviation	Meaning
K-S test	Kolmogorov-Smirnov test.
LHS	latin hypercube sampling.
MCF	Monte Carlo filtering.
MCMC	Markov chain Monte Carlo.
MPSA	multi-parameter sensitivity analysis.
NLS	non-linear least squares.
OAT	one-factor-at-a-time.
ODE	ordinary differential equations.
PCTL	probabilistic computation tree logic.
PDF	probability density function.
PIAS	Protein Inhibitor of Activated STAT.
PL	profile likelihood.
PMC	probabilistic model checking.
PMCC	Pearson product-moment correlation coefficient.
PTP	Protein Tyrosine Phosphatases.
RRE	reaction rate equations.
SA	simulated annealing.
SaaS	Science as a Service.
SBML	Systems Biology Markup Language.
SOCS	Supressor of Cytokine Signalling.
SOSlib	SBML ODE Solver.
SRCC	Spearman's rank correlation test.
SSE	sum of squared errors.
STAT	Signal Transducer and Activator of Transcription.
Tav4SB	Taverna services for Systems Biology.
TE	total effects.
TFOS	total FOS.
TTE	total TE.
VMR	variance-to-mean ratio.

Abbreviation	Meaning
WALS	weighted average of local sensitivities.
WS	Web services.

References

Aaronson, D. S., Horvath, C. M., 2002. A road map for those who don't know JAK-STAT, Science, 296, p. 1653.

Akaike, H., 1974. A new look at the statistical model identification, IEEE Transactions on Automatic Control, 19(6), p. 716.

Alberts, B., Johnson, A., Lewis, J., Raff, M., Roberts, K., Walter, P., 2002. Molecular Biology of the Cell, Garland, 4^{th} ed.

Aldridge, B. B., Burke, J. M., Lauffenburger, D. A., Sorger, P. K., 2006. Physicochemical modelling of cell signalling pathways, Nature Cell Biology, 8(11), p. 1195.

Alon, U., 2007. An Introduction to Systems Biology: Design Principles of Biological Circuits, Chapman & Hall/CRC.

Aziz, A., Sanwal, K., Singhal, V., Brayton, R., 1996. Verifying continuous time markov chains, in: Proceedings of the 8th International Conference on Computer Aided Verification (CAV'96), *LNCS*, vol. 1102, Springer, p. 269.

Bachmann, J., Raue, A., Schilling, M., Böhm, M. E., Kreutz, C., Kaschek, D., Busch, H., Gretz, N., Lehmann, W. D., Timmer, J., Klingmüller, U., 2011. Division of labor by dual feedback regulators controls JAK2/STAT5 signaling over broad ligand range, Molecular Systems Biology, 7, p. 516.

Baier, C., Haverkort, B., Hermanns, H., Katoen, J., 2000. Model checking Continuous-Time markov chains by transient analysis, in: Emerson, E., Sistla, A. (Eds.), Computer Aided Verification, *LNCS*, vol. 1855, Springer Berlin / Heidelberg, p. 358.

Banasik, P., 2008. Rozszerzenie funkcjonalności programu Taverna dla biologii systemów, Master's thesis, Faculty of Mathematics, Informatics and Mechanics, University of Warsaw.

Bentele, M., Lavrik, I., Ulrich, M., Stösser, S., Heermann, D. W., Kalthoff, H., Krammer, P. H., Eils, R., 2004. Mathematical modeling reveals threshold mechanism in CD95-induced apoptosis, The Journal of Cell Biology, 166(6), p. 839.

Berg, J. M., Tymoczko, J. L., Stryer, L., 2006. Biochemistry, W. H. Freeman, 6^{th} ed.

Bhagat, J., Tanoh, F., Nzuobontane, E., Laurent, T., Orlowski, J., Roos, M., Wolstencroft, K., Aleksejevs, S., Stevens, R., Pettifer, S., Lopez, R., Goble, C. A., 2010. BioCatalogue: a universal catalogue of web services for the life sciences, Nucleic Acids Research, 38(Web Server issue), p. W689.

Bornstein, B. J., Keating, S. M., Jouraku, A., Hucka, M., 2008. LibSBML: an API library for SBML, Bioinformatics, 24(6), p. 880.

Brysha, M., Zhang, J. G., Bertolino, P., Corbin, J. E., Alexander, W. S., Nicola, N. A., Hilton, D. J., Starr, R., 2001. Suppressor of cytokine signaling-1 attenuates the duration of interferon gamma signal transduction in vitro and in vivo, The Journal of Biological Chemistry, 276(25), p. 22086.

Butcher, J. C., 2008. Numerical Methods for Ordinary Differential Equations, John Wiley & Sons.

Calder, M., Gilmore, S., Hillston, J., Vyshemirsky, V., 2010. Formal methods for biochemical signalling pathways, in: Boca, P., Bowen, J. P., Siddiqi, J. (Eds.), Formal Methods: State of the Art and New Directions, Springer London, p. 185.

Calder, M., Vyshemirsky, V., Gilbert, D., Orton, R., 2006. Analysis of signalling pathways using continuous time Markov chains, in: Priami, C., Plotkin, G. (Eds.), Transactions on Computational Systems Biology VI, *LNCS*, vol. 4220, Springer Berlin / Heidelberg, p. 44.

Charzyńska, A., Nałęcz, A., Rybiński, M., Gambin, A., 2012. Sensitivity analysis of mathematical models of signaling pathways. In press (BioTechnologia).

Chen, W. W., Schoeberl, B., Jasper, P. J., Niepel, M., Nielsen, U. B., Lauffenburger, D. A., Sorger, P. K., 2009. Input-output behavior of ErbB signaling pathways as revealed by a mass action model trained against dynamic data, Molecular Systems Biology, 5, p. 239.

Cho, K.-H., Shin, S.-Y., Kolch, W., Wolkenhauer, O., 2003. Experimental design in systems biology, based on parameter sensitivity analysis using a monte carlo method: A case study for the TNFalpha-mediated NF-kappab signal transduction pathway, SIMULATION, 79, p. 726.

Christensen, E., Curbera, F., Meredith, G., Weerawarana, S., 2001. Web service definition language (WSDL), http://www.w3.org/TR/wsdl (Last accessed: 11 January 2012).

Courtot, M., Juty, N., Knüpfer, C., Waltemath, D., Zhukova, A., Dräger, A., Dumontier, M., Finney, A., Golebiewski, M., Hastings, J., Hoops, S., Keating, S., Kell, D. B., Kerrien, S., Lawson, J., Lister, A., Lu, J., Machne, R., Mendes, P., Pocock, M., Rodriguez, N., Villeger, A., Wilkinson, D. J., Wimalaratne, S., Laibe, C., Hucka, M., Le Novère, N., 2011. Controlled vocabularies and semantics in systems biology, Molecular Systems Biology, 7, p. 543.

Cukier, R. I., Levine, H. B., Shuler, K. E., 1978. Nonlinear sensitivity analysis of multiparameter model systems, Journal of Computational Physics, 26(1), p. 1.

Degasperi, A., Gilmore, S., 2008. Sensitivity analysis of stochastic models of bistable biochemical reactions, in: Proceedings of the 8th International School on Formal Methods for the Design of Computer, Communication, and Software Systems: Computational Systems Biology (SFM'08:Bio), LNCS, Springer-Verlag, Berlin, Heidelberg, p. 1–.

Dräger, A., Rodriguez, N., Dumousseau, M., Dörr, A., Wrzodek, C., Le Novère, N., Zell, A., Hucka, M., 2011. JSBML: a flexible java library for working with SBML, Bioinformatics (Oxford, England), 27(15), p. 2167.

Foster, I., 2005. Service-oriented science, Science (New York, N.Y.), 308(5723), p. 814.

Foster, I., 2006. Globus toolkit version 4: Software for Service-Oriented systems, Journal of Computer Science and Technology, 21(4), p. 513.

Foster, I., 2011. Globus online: Accelerating and democratizing science through Cloud-Based services, Internet Computing, IEEE, 15(3), p. 70.

Fritsche-Guenther, R., Witzel, F., Sieber, A., Herr, R., Schmidt, N., Braun, S., Brummer, T., Sers, C., Blüthgen, N., 2011. Strong negative feedback from erk to raf confers robustness to MAPK signalling, Molecular Systems Biology, 7, p. 489.

Gibson, M. A., Bruck, J., 2000. Efficient exact stochastic simulation of chemical systems with many species and many channels, The Journal of Physical Chemistry A, 104(9), p. 1876.

Gillespie, C. S., Wilkinson, D. J., Proctor, C. J., Shanley, D. P., Boys, R. J., Kirkwood, T. B. L., 2006. Tools for the SBML. community, Bioinformatics (Oxford, England), 22, p. 628.

Gillespie, D. T., 1977. Exact stochastic simulation of coupled chemical reactions, The Journal of Physical Chemistry, 81(25), p. 2340.

Gillespie, D. T., 2000. The chemical Langevin equation, The Journal of Chemical Physics, 113(1), p. 297.

Gillespie, D. T., 2001. Approximate accelerated stochastic simulation of chemically reacting systems, The Journal of Chemical Physics, 115(4), p. 1716.

Gillespie, D. T., 2007. Stochastic simulation of chemical kinetics, Annual Review of Physical Chemistry, 58, p. 35.

Gillespie, D. T., 2009. Deterministic limit of stochastic chemical kinetics, The Journal of Physical Chemistry. B, 113(6), p. 1640.

Goutelle, S., Maurin, M., Rougier, F., Barbaut, X., Bourguignon, L., Ducher, M., Maire, P., 2008. The hill equation: a review of its capabilities in pharmacological modelling, Fundamental & Clinical Pharmacology, 22(6), p. 633.

Goutsias, J., 2007. Classical versus stochastic kinetics modeling of biochemical reaction systems, Biophysical Journal, 92(7), p. 2350.

Grosu, R., Smolka, S. A., 2005. Monte Carlo model checking, in: Proceedings of the 11th International Conference on Tools and Algorithms for the Construction and Analysis of Systems (TACAS'05), *LNCS*, vol. 3440, Springer, p. 271.

Gunawan, R., Cao, Y., Petzold, L., Doyle, F. J., 2005. Sensitivity analysis of discrete stochastic systems, Biophysical Journal, 88(4), p. 2530.

Hansson, H., Jonsson, B., 1994. A logic for reasoning about time and reliability, Formal Aspects of Computing, 6(5), p. 512.

Hapner, M., Burridg, R., Sharma, R., Fialli, J., Stout, K., 2002. Java message service, Specification, version: 1.1, Sun Microsystems, Inc.

Heath, J., Kwiatkowska, M., Norman, G., Parker, D., Tymchyshyn, O., 2008. Probabilistic model checking of complex biological pathways, Theoretical Computer Science, 391(3), p. 239.

Heinrich, R., Neel, B. G., Rapoport, T. A., 2002. Mathematical models of protein kinase signal transduction, Molecular cell, 9(5), p. 957.

Hildebrandt, B., Wust, P., Ahlers, O., Dieing, A., Sreenivasa, G., Kerner, T., Felix, R., Riess, H., 2002. The cellular and molecular basis of hyperthermia, Critical Reviews in Oncology/Hematology, 43(1), p. 33.

Hindmarsh, A. C., Brown, P. N., Grant, K. E., Lee, S. L., Serban, R., Shumaker, D. E., Woodward, C. S., 2005. SUNDIALS: suite of nonlinear and differential/algebraic equation solvers, ACM Transactions on Mathematical Software, 31(3), p. 363.

Hinton, A., Kwiatkowska, M., Norman, G., Parker, D., 2006. PRISM: A tool for automatic verification of probabilistic systems, in: Proceedings of the 12th International Conference on Tools and Algorithms for the Construction and Analysis of Systems (TACAS'06), *LNCS*, vol. 3920, Springer, p. 441.

Hornberger, G. M., Spear, R. C., 1981. An approach to the preliminary analysis of environmental systems, Journal of Environmental Management, 12(1), p. 7.

Huang, C. Y., Ferrell, J. E., 1996. Ultrasensitivity in the mitogen–activated protein kinase cascade, Proceedings of the National Academy of Sciences of the United States of America, 93, p. 10078.

Hucka, M., Finney, A., Sauro, H. M., Bolouri, H., Doyle, J. C., Kitano, H., Arkin, A. P., Bornstein, B. J., Bray, D., Cornish-Bowden, A., Cuellar, A. A., Dronov, S., Gilles, E. D., Ginkel, M., Gor, V., Goryanin, I. I., Hedley, W. J., Hodgman, T. C., Hofmeyr, J.-H., Hunter, P. J., Juty, N. S., Kasberger, J. L., Kremling, A., Kummer, U., Le Novère, N., Loew, L. M., Lucio, D., Mendes, P., Minch, E., Mjolsness, E. D., Nakayama, Y., Nelson, M. R., Nielsen, P. F., Sakurada, T., Schaff, J. C., Shapiro, B. E., Shimizu, T. S., Spence, H. D., Stelling, J., Takahashi, K., Tomita, M., Wagner, J., Wang, J., 2003. The systems biology markup language (sbml): a medium for representation and exchange of biochemical network models, Bioinformatics, 19, p. 524.

Hull, D., Wolstencroft, K., Stevens, R., Goble, C., Pocock, M. R., Li, P., Oinn, T., 2006. Taverna: a tool for building and running workflows of services, Nucleic Acids Research, 34(Web Server issue), p. W729.

Jahnke, T., Huisinga, W., 2007. Solving the chemical master equation for monomolecular reaction systems analytically, Journal of Mathematical Biology, 54(1), p. 1.

Jeffreys, H., 1998. Theory of probability, Oxford University Press.

Kampen, N. G. V., 2007. Stochastic Processes in Physics and Chemistry, Elsevier.

Kass, R. E., Raftery, A. E., 1995. Bayes factors, Journal of the American Statistical Association, 90(430), p. 773.

Keating, S. M., Bornstein, B. J., Finney, A., Hucka, M., 2006. SBMLToolbox: an SBML toolbox for MATLAB users, Bioinformatics (Oxford, England), 22(10), p. 1275.

Kholodenko, B. N., 2000. Negative feedback and ultrasensitivity can bring about oscillations in the mitogen–activated protein kinase cascades, European journal of biochemistry / FEBS, 267, p. 1583.

Kirkpatrick, S., Gelatt, J., C D, Vecchi, M. P., 1983. Optimization by simulated annealing, Science (New York, N.Y.), 220(4598), p. 671.

Kisseleva, T., Bhattacharya, S., Braunstein, J., Schindler, C. W., 2002. Signaling through the JAK/STAT pathway, recent advances and future challenges, Gene, 285(1-2), p. 1.

Kitano, H., 2007. Towards a theory of biological robustness, Molecular Systems Biology, 3, p. 137.

Kitowski, J., Dutka, L., 2010. Status and current achievements of PL-Grid project, in: Bubak, M., Turała, M., Wiatr, K. (Eds.), Proceedings of the Cracow Grid Workshop'09 (CGW'09), ACC CYFRONET AGH, Kraków, p. 295.

Kitowski, J., Mosurska, Z., Pajak, L., R. Dutka, 2011. Recent advancements of national grid initiative in poland (PL-Grid), in: Bubak, M., Turała, M., Wiatr, K. (Eds.), Proceedings of the Cracow Grid Workshop'10 (CGW'10), ACC CYFRONET AGH, Kraków, p. 38.

Klipp, E., Liebermeister, W., Wierling, C., Kowald, A., Lehrach, H., 2009. Systems Biology: A Textbook, Wiley-VCH.

Kloeden, P. E., Platen, E., 1992. Numerical Solution of Stochastic Differential Equations, Springer.

Komorowski, M., Costa, M. J., Rand, D. A., Stumpf, M. P. H., 2011. Sensitivity, robustness, and identifiability in stochastic chemical kinetics models, Proceedings of the National Academy of Sciences of the United States of America, 108(21), p. 8645.

Krause, C. D., Lavnikova, N., Xie, J., Mei, E., Mirochnitchenko, O. V., Jia, Y., Hochstrasser, R. M., Pestka, S., 2006. Preassembly and ligand-induced restructuring of the chains of the ifn-gamma receptor complex: the roles of jak kinases, stat1 and the receptor chains, Cell research, 16, p. 55.

Krause, C. D., Mei, E., Xie, J., Jia, Y., Bopp, M. A., Hochstrasser, R. M., Pestka, S., 2002. Seeing the light: preassembly and ligand-induced changes of the interferon gamma receptor complex in cells, Molecular & Cellular Proteomics, 1, p. 805.

Krishnan, S., Clementi, L., Ren, J., Papadopoulos, P., Li, W., 2009. Design and evaluation of opal2: A toolkit for scientific software as a service, in: Proceedings of the 4th IEEE Congress on Services (SERVICES 2009 - I), IEEE Computer Society, Washington, DC, USA, p. 709.

Kwiatkowska, M., Norman, G., Pacheco, A., 2006. Model checking expected time and expected reward formulae with random time bounds, Computers & Mathematics with Applications, 51(2), p. 305–.

Kwiatkowska, M., Norman, G., Parker, D., 2007. Stochastic model checking, in: Bernardo, M., Hillston, J. (Eds.), Formal Methods for Performance Evaluation, *LNCS*, vol. 4486, Springer Berlin / Heidelberg, p. 220.

Kwiatkowska, M., Norman, G., Parker, D., 2008. Using probabilistic model checking in systems biology, ACM SIGMETRICS Performance Evaluation Review, 35(4), p. 14.

Kwiatkowska, M., Norman, G., Parker, D., 2011. PRISM 4.0: verification of probabilistic real-time systems, in: Proceedings of the 23rd International Conference on Computer Aided Verification (CAV'11), Springer-Verlag, Berlin, Heidelberg, p. 585–591.

Laplante, S., Lassaigne, R., Magniez, F., Peyronnet, S., de Rougemont, M., 2007. Probabilistic abstraction for model checking: An approach based on property testing, ACM Transactions on Computational Logic, 8(4), p. 20/1.

Laurenzi, I. J., 2000. An analytical solution of the stochastic master equation for reversible bimolecular reaction kinetics, The Journal of Chemical Physics, 113(8), p. 3315.

Lee, D., Saha, R., Yusufi, F. N. K., Park, W., Karimi, I. A., 2009. Web-based applications for building, managing and analysing kinetic models of biological systems, Briefings in Bioinformatics, 10(1), p. 65.

Lepock, J. R., Frey, H. E., Ritchie, K. P., 1993. Protein denaturation in intact hepatocytes and isolated cellular organelles during heat shock, The Journal of Cell Biology, 122(6), p. 1267.

Li, C., Donizelli, M., Rodriguez, N., Dharuri, H., Endler, L., Chelliah, V., Li, L., He, E., Henry, A., Stefan, M. I., Snoep, J. L., Hucka, M., Le Novère, N., Laibe, C., 2010. BioModels database: An enhanced, curated and annotated resource for published quantitative kinetic models, BMC Systems Biology, 4, p. 92.

Lula, M., 2009. Rozproszone środowisko dla biologii systemów, Master's thesis, Faculty of Mathematics, Informatics and Mechanics, University of Warsaw.

Lund, E. W., 1965. Guldberg and waage and the law of mass action, Journal of Chemical Education, 42(10), p. 548.

Machné, R., Finney, A., Müller, S., Lu, J., Widder, S., Flamm, C., 2006. The SBML ODE solver library: a native API. for symbolic and fast numerical analysis of reaction networks, Bioinformatics, 22, p. 1406.

Mahdavi, A., Davey, R. E., Bhola, P., Yin, T., Zandstra, P. W., 2007. Sensitivity analysis of intracellular signaling pathway kinetics predicts targets for stem cell fate control, PLoS Computational Biology, 3, p. e130.

Maiwald, T., Schneider, A., Busch, H., Sahle, S., Gretz, N., Weiss, T. S., Kummer, U., Klingmüller, U., 2010. Combining theoretical analysis and experimental data generation reveals IRF9 as a crucial factor for accelerating interferon α-induced early antiviral signalling, The FEBS Journal, 277(22), p. 4741.

Maiwald, T., Timmer, J., 2008. Dynamical modeling and multi-experiment fitting with PottersWheel, Bioinformatics (Oxford, England), 24(18), p. 2037.

McKay, M., Conover, W., Beckman, R., 1979. A comparison of three methods for selecting values of input variables in the analysis of output from a computer code, Technometrics, 21(2), p. 239.

Metropolis, N., Rosenbluth, A. W., Rosenbluth, M. N., Teller, A. H., Teller, E., 1953. Equation of state calculations by fast computing machines, The Journal of Chemical Physics, 21(6), p. 1087.

Miao, H., Xia, X., Perelson, A. S., Wu, H., 2011. On identifiability of nonlinear ode models and applications in viral dynamics, SIAM Review. Society for Industrial and Applied Mathematics, 53(1), p. 3.

Michaelis, L., Menten, M., 1913. Die Kinetik der Invertinwirkung, Biochemische Zeitschrift, 49, p. 333.

Milo, R., Jorgensen, P., Moran, U., Weber, G., Springer, M., 2010. BioNumbers — the database of key numbers in molecular and cell biology, Nucleic Acids Research, 38(Database issue), p. D750.

Mizera, A., Gambin, B., 2010. Stochastic modelling of the eukaryotic heat shock response, Journal of Theoretical Biology, 265(3), p. 455.

Moles, C. G., Mendes, P., Banga, J. R., 2003. Parameter estimation in biochemical pathways: a comparison of global optimization methods, Genome Research, 13(11), p. 2467.

Monteiro, P. T., Ropers, D., Mateescu, R., Freitas, A. T., de Jong, H., 2008. Temporal logic patterns for querying dynamic models of cellular interaction networks, Bioinformatics (Oxford, England), 24(16), p. i227.

Morohashi, M., Winn, A. E., Borisuk, M. T., Bolouri, H., Doyle, J., Kitano, H., 2002. Robustness as a measure of plausibility in models of biochemical networks, Journal of Theoretical Biology, 216(1), p. 19.

Morris, M. D., 1991. Factorial sampling plans for preliminary computational experiments, Technometrics, 33(2), p. 161.

Murphy, S. A., Vaart, A. W. v. d., 2000. On profile likelihood, Journal of the American Statistical Association, 95(450), p. 449.

Myung, J. I., Pitt, M. A., 2004. Model comparison methods, Methods in Enzymology, 383, p. 351.

Myung, J. I., Tang, Y., Pitt, M. A., 2009. Evaluation and comparison of computational models, Methods in Enzymology, 454, p. 287.

Neal, R. M., 2001. Annealed importance sampling, Statistics and Computing, 11(2), p. 125.

Newton, M. A., Raftery, A. E., 1994. Approximate bayesian inference with the weighted likelihood bootstrap, Journal of the Royal Statistical Society. Series B (Methodological), 56(1), p. 3.

Neznanov, N., Komarov, A. P., Neznanova, L., Stanhope-Baker, P., Gudkov, A. V., 2011. Proteotoxic stress targeted therapy (PSTT): induction of protein misfolding enhances the antitumor effect of the proteasome inhibitor bortezomib, Oncotarget, 2(3), p. 209.

Nimal, V., 2010. Statistical Approaches for Probabilistic Model Checking, Master's thesis, Oxford University Computing Laboratory.

Nocedal, J., Wright, S. J., 1999. Numerical Optimization, Springer.

Novère, N. L., Bornstein, B., Broicher, A., Courtot, M., Donizelli, M., Dharuri, H., Li, L., Sauro, H., Schilstra, M., Shapiro, B., Snoep, J. L., Hucka, M., 2006. BioModels database: a free, centralized database of curated, published, quantitative kinetic models of biochemical and cellular systems, Nucleic acids research, 34, p. D689.

OASIS WSRF Technical Committee, 2006. Oasis web services resource framework (wsrf) version 1.2 standard, http://www.oasis-open.org/committees/wsrf/ (Last accessed: 18 May 2012).

Oracle Corporation. Java^{TM} native interface, http://docs.oracle.com/javase/7/docs/technotes/guides/jni/ (Last accessed: 18 May 2012).

Owens, N., Timmis, J., Greensted, A., Tyrrell, A., 2008. Modelling the tunability of early t cell signalling events, in: Bentley, P., Lee, D., Jung, S. (Eds.), Artificial Immune Systems, *LNCS*, vol. 5132, Springer Berlin / Heidelberg, p. 12.

Pahle, J., 2009. Biochemical simulations: stochastic, approximate stochastic and hybrid approaches, Briefings in Bioinformatics, 10(1), p. 53.

Peper, A., Grimbergen, C. A., Spaan, J. A., Souren, J. E., van Wijk, R., 1998. A mathematical model of the hsp70 regulation in the cell, International Journal of Hyperthermia: The Official Journal of European Society for Hyperthermic Oncology, North American Hyperthermia Group, 14(1), p. 97.

Petre, I., Mizera, A., Hyder, C. L., Meinander, A., Mikhailov, A., Morimoto, R. I., Sistonen, L., Eriksson, J. E., Back, R., 2010. A simple mass-action model for the eukaryotic heat shock response and its mathematical validation, Natural Computing, 10(1), p. 595.

Petri, C., Reisig, W., 2008. Petri net, Scholarpedia, 3(4), p. 6477.

Pihur, V., Datta, S., Datta, S., 2007. Weighted rank aggregation of cluster validation measures: a monte carlo cross-entropy approach, Bioinformatics (Oxford, England), 23(13), p. 1607.

Pihur, V., Datta, S., Datta, S., 2009. RankAggreg, an R package for weighted rank aggregation, BMC Bioinformatics, 10, p. 62.

PRISM Web page. PRISM - Probabilistic Symbolic Model Checker, http://www.prismmodelchecker.org/ (Last accessed: 18 May 2012).

Proctor, C. J., Lorimer, I. A. J., 2011. Modelling the role of the Hsp70/Hsp90 system in the maintenance of protein homeostasis, PLoS ONE, 6, p. e22038.

R Development Core Team, 2009. R: A Language and Environment for Statistical Computing, R Foundation for Statistical Computing, Vienna, Austria.

Rabitz, H., Aliş, Ö. F., Shorter, J., Shim, K., 1999. Efficient input—output model representations, Computer Physics Communications, 117(1–2), p. 11.

Ramaswamy, R., González-Segredo, N., Sbalzarini, I. F., 2009. A new class of highly efficient exact stochastic simulation algorithms for chemical reaction networks, The Journal of Chemical Physics, 130(24), p. 244104.

Ramaswamy, R., Sbalzarini, I. F., 2010. A partial-propensity variant of the composition-rejection stochastic simulation algorithm for chemical reaction networks, The Journal of Chemical Physics, 132(4), p. 044102.

Rateitschak, K., Karger, A., Fitzner, B., Lange, F., Wolkenhauer, O., Jaster, R., 2010. Mathematical modelling of interferon-gamma signalling in pancreatic stellate cells reflects and predicts the dynamics of STAT1 pathway activity, Cellular Signalling, 22(1), p. 97.

Raue, A., Kreutz, C., Maiwald, T., Bachmann, J., Schilling, M., Klingmüller, U., Timmer, J., 2009. Structural and practical identifiability analysis of partially observed dynamical models by exploiting the profile likelihood, Bioinformatics (Oxford, England), 25(15), p. 1923.

Raz, R., Lee, C. K., Cannizzaro, L. A., d'Eustachio, P., Levy, D. E., 1999. Essential role of STAT3 for embryonic stem cell pluripotency, Proceedings of the National Academy of Sciences of the United States of America, 96(6), p. 2846.

Ren, J., Williams, N., Clementi, L., Krishnan, S., Li, W. W., 2010. Opal web services for biomedical applications, Nucleic Acids Research, 38(Web Server issue), p. W724.

Rieger, T. R., Morimoto, R. I., Hatzimanikatis, V., 2005. Mathematical modeling of the eukaryotic heat-shock response: dynamics of the hsp70 promoter, Biophysical Journal, 88(3), p. 1646.

Rizk, A., Batt, G., Fages, F., Soliman, S., 2009. A general computational method for robustness analysis with applications to synthetic gene networks, Bioinformatics (Oxford, England), 25(12), p. i169.

Rodriguez-Fernandez, M., Mendes, P., Banga, J. R., 2006. A hybrid approach for efficient and robust parameter estimation in biochemical pathways, Biosystems, 83(2-3), p. 248.

Roper, R. T., Pia Saccomani, M., Vicini, P., 2010. Cellular signaling identifiability analysis: a case study, Journal of Theoretical Biology, 264(2), p. 528.

Rutten, J. J. M. M., Kwiatkowska, M., Norman, G., Parker, D., 2004. Mathematical Techniques for Analyzing Concurrent and Probabilistic Systems, American Mathematical Society, Centre de Recherches Mathematiques.

Rybiński, M., Gambin, A., 2007. Details of the JAK-STAT signalling pathway model, Acta Biochimica Polonica, supplement, 54, p. 63.

Rybiński, M., Gambin, A., 2009. Model selection of the JAK–STAT pathway activation mechanism, Acta Biochimica Polonica, supplement, 56, p. 58.

Rybiński, M., Gambin, A., 2012. Model-based selection of the robust JAK-STAT activation mechanism. In press (Journal of Theoretical Biology).

Rybiński, M., Lula, M., Banasik, P., Lasota, S., Gambin, A., 2012. Tav4SB: integrating tools for analysis of kinetic models of biological systems, BMC Systems Biology, 6(1), p. 25.

Rybiński, M., Lula, M., Lasota, S., Gambin, A., 2011. Tav4SB: grid environment for analysis of kinetic models of biological systems, in: Short Abstracts of the 7th International Symposium on Bioinformatics Research and Applications (ISBRA'11), p. 92.

Saltelli, A., Ratto, M., Andres, T., Campolongo, F., Cariboni, J., Gatelli, D., Saisana, M., Tarantola, S., 2008. Global Sensitivity Analysis: The Primer, Wiley-Interscience.

Saltelli, A., Ratto, M., Tarantola, S., Campolongo, F., 2005. Sensitivity analysis for chemical models, Chemical Reviews, 105, p. 2811.

Saltelli, A., Tarantola, S., Chan, K. P., 1999. A quantitative model-independent method for global sensitivity analysis of model output, Technometrics, 41(1), p. 39.

Schuster, B., Meinert, W., Rose-John, S., Kallen, K.-J., 2003. The human interleukin-6 (IL-6) receptor exists as a preformed dimer in the plasma membrane, FEBS letters, 538, p. 113.

Schwarz, G., 1978. Estimating the dimension of a model, The Annals of Statistics, 6(2), p. 461.

Senger, M., Rice, P., Bleasby, A., Oinn, T., Uludag, M., 2008. Soaplab2: more reliable sesame door to bioinformatics programs, in: The 9th Annual Bioinformatics Open Source Conference, Toronto, Canada. http://soaplab.sourceforge.net/soaplab2/ (Last accessed: 14 March 2012).

Shankaran, H., Wiley, H. S., Resat, H., 2006. Modeling the effects of HER/ErbB1-3 coexpression on receptor dimerization and biological response, Biophysical Journal, 90(11), p. 3993.

Shapiro, B. E., Hucka, M., Finney, A., Doyle, J., 2004. MathSBML: a package for manipulating SBML-based biological models, Bioinformatics (Oxford, England), 20(16), p. 2829.

Shudo, E., Yang, J., Yoshimura, A., Iwasa, Y., 2007. Robustness of the signal transduction system of the mammalian JAK/STAT. pathway and dimerization steps, Journal of Theoretical Biology, 246, p. 1.

Sivakumaran, S., Hariharaputran, S., Mishra, J., Bhalla, U. S., 2003. The database of quantitative cellular signaling: management and analysis of chemical kinetic models of signaling networks, Bioinformatics (Oxford, England), 19(3), p. 408.

Sjöberg, P., Lötstedt, P., Elf, J., 2009. Fokker-Planck approximation of the master equation in molecular biology, Computing and Visualization in Science, 12(1), p. 37.

Smieja, J., Jamaluddin, M., Brasier, A. R., Kimmel, M., 2008. Model-based analysis of interferon-beta induced signaling pathway, Bioinformatics (Oxford, England), 24(20), p. 2363.

Sobol, I. M., 1993. Sensitivity analysis for nonlinear mathematical models, Mathematical Modeling and Computational Experiment, 1, p. 407.

Sobol, I. M., 2001. Global sensitivity indices for nonlinear mathematical models and their Monte Carlo estimates, Mathematics and Computers in Simulation, 55(1–3), p. 271.

Srinath, S., Gunawan, R., 2010. Parameter identifiability of power-law biochemical system models, Journal of Biotechnology, 149(3), p. 132.

Stelling, J., Sauer, U., Szallasi, Z., Doyle, r., Francis J, Doyle, J., 2004. Robustness of cellular functions, Cell, 118(6), p. 675.

Swameye, I., Muller, T. G., Timmer, J., Sandra, O., Klingmuller, U., 2003. Identification of nucleocytoplasmic cycling as a remote sensor in cellular signaling by databased modeling, Proceedings of the National Academy of Sciences of the United States of America, 100, p. 1028.

Szymańska, Z., Żylicz, M., 2009. Mathematical modeling of heat shock protein synthesis in response to temperature change, Journal of Theoretical Biology, 259(3), p. 562.

The MathWorks Inc., 2011. MATLAB: Version 7.12.0 (R2011a), The MathWorks Inc., Natick, Massachusetts.

The World Wide Web Consortium, 2002. Web services activity, http://www.w3.org/2002/ws/ (Last accessed: 17 May 2012).

The World Wide Web Consortium, 2007. SOAP version 1.2, http://www.w3.org/TR/soap12/ (Last accessed: 18 May 2012).

The World Wide Web Consortium, 2008. Extensible markup language (XML) 1.0 (fifth edition), http://www.w3.org/TR/xml/ (Last accessed: 18 May 2012).

Toni, T., Stumpf, M. P. H., 2010. Simulation-based model selection for dynamical systems in systems and population biology, Bioinformatics (Oxford, England), 26(1), p. 104.

Černý, V., 1985. Thermodynamical approach to the traveling salesman problem: An efficient simulation algorithm, Journal of Optimization Theory and Applications, 45(1), p. 41.

Vera, J., Bachmann, J., Pfeifer, A. C., Becker, V., Hormiga, J. A., Darias, N. V. T., Timmer, J., Klingmüller, U., Wolkenhauer, O., 2008. A systems biology approach to analyse amplification in the JAK2-STAT5 signalling pathway, BMC Systems Biology, 2, p. 38.

Vera, J., Rateitschak, K., Lange, F., Kossow, C., Wolkenhauer, O., Jaster, R., 2011. Systems biology of JAK-STAT signalling in human malignancies, Progress in Biophysics and Molecular Biology, 106(2), p. 426.

Vyshemirsky, V., Girolami, M., 2008a. BioBayes: a software package for bayesian inference in systems biology, Bioinformatics (Oxford, England), 24(17), p. 1933.

Vyshemirsky, V., Girolami, M. A., 2008b. Bayesian ranking of biochemical system models, Bioinformatics (Oxford, England), 24(6), p. 833.

Wagner, I., Arlt, H., van Dyck, L., Langer, T., Neupert, W., 1994. Molecular chaperones cooperate with PIM1 protease in the degradation of misfolded proteins in mitochondria, The EMBO Journal, 13(21), p. 5135.

Wegele, H., Müller, L., Buchner, J., 2004. Hsp70 and hsp90–a relay team for protein folding, Reviews of Physiology, Biochemistry and Pharmacology, 151, p. 1.

Wilkinson, D. J., 2011. Stochastic Modelling for Systems Biology, CRC Press.

Wilkinson, M. D., Senger, M., Kawas, E., Bruskiewich, R., Gouzy, J., Noirot, C., Bardou, P., Ng, A., Haase, D., Saiz, E. d. A., Wang, D., Gibbons, F., Gordon, P. M. K., Sensen, C. W., Carrasco, J. M. R., Fernández, J. M., Shen, L., Links, M., Ng, M., Opushneva, N., Neerincx, P. B. T., Leunissen, J. A. M., Ernst, R., Twigger, S., Usadel, B., Good, B., Wong, Y., Stein, L., Crosby, W., Karlsson, J., Royo, R., Párraga, I., Ramírez, S., Gelpi, J. L., Trelles, O., Pisano, D. G., Jimenez, N., Kerhornou, A., Rosset, R., Zamacola, L., Tarraga, J., Huerta-Cepas, J., Carazo, J. M., Dopazo, J., Guigo, R., Navarro, A., Orozco, M., Valencia, A., Claros, M. G., Pérez, A. J., Aldana, J., Rojano, M. M., Fernandez-Santa Cruz, R., Navas, I., Schiltz, G., Farmer, A., Gessler, D., Schoof, H., Groscurth, A., 2008. Interoperability with Moby 1.0–it's better than sharing your toothbrush!, Briefings in Bioinformatics, 9(3), p. 220.

Wolfram Research, Inc., 2008. Mathematica Edition: Version 7.0, Wolfram Research, Inc., Champaign, Illinois.

Wolkenhauer, O., Ullah, M., Kolch, W., Cho, K., 2004. Modeling and simulation of intracellular dynamics: choosing an appropriate framework, IEEE Transactions on Nanobioscience, 3(3), p. 200.

Wolkenhauer, O., Wellstead, P. E., Cho, K., 2008. Systems Biology, Portland Press.

Wust, P., Hildebrandt, B., Sreenivasa, G., Rau, B., Gellermann, J., Riess, H., Felix, R., Schlag, P. M., 2002. Hyperthermia in combined treatment of cancer, The Lancet Oncology, 3(8), p. 487.

Yamada, S., Shiono, S., Joo, A., Yoshimura, A., 2003. Control mechanism of JAK/STAT. signal transduction pathway, FEBS letters, 534, p. 190.

Young, P. C., Spear, R. C., Hornberger, G. M., 1978. Modeling badly defined systems: some further thoughts, in: Proceedings of the Simulation Special Interest Group Conference (SIMSIG-78), Australian National University, Canberra, p. 24.

Yu, H., Jove, R., 2004. The STATs of cancer–new molecular targets come of age, Nature reviews. Cancer, 4, p. 97.

Yue, H., Brown, M., He, F., Jia, J., Kell, D., 2008. Sensitivity analysis and robust experimental design of a signal transduction pathway system, International Journal of Chemical Kinetics, 40(11), p. 730.

Zi, Z., Cho, K.-H., Sung, M.-H., Xia, X., Zheng, J., Sun, Z., 2005. In silico identification of the key components and steps in ifn-gamma induced JAK-STAT. signaling pathway, FEBS letters, 579, p. 1101.

Zi, Z., Zheng, Y., Rundell, A. E., Klipp, E., 2008. SBML-SAT: a systems biology markup language (SBML) based sensitivity analysis tool, BMC Bioinformatics, 9, p. 342.